

Spatially Averaged Physics of the
Snowmelt Process

By

FEDERICO ERNESTO HORNE

Agronomic Eng. (Universidad Nacional del Sur, Argentina) 1975

M.Sc. Water Resources Planning (CIDIAT, ULA, Venezuela) 1980

DISSERTATION

Submitted in partial satisfaction of the requirements for the degree of

DOCTOR OF PHILOSOPHY

in

Civil Engineering

in the

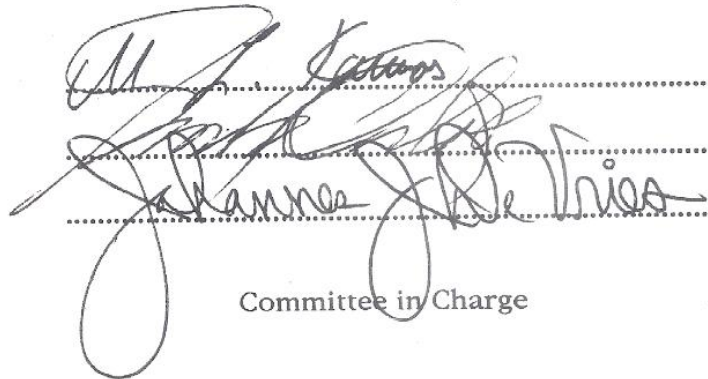
GRADUATE DIVISION

of the

UNIVERSITY OF CALIFORNIA

DAVIS

Approved:



The image shows three handwritten signatures in black ink, each written over a horizontal dotted line. The signatures are cursive and somewhat stylized. The first signature is at the top, the second is in the middle, and the third is at the bottom. The lines are evenly spaced and extend across the width of the signatures.

Committee in Charge

1993

*To my father,
Federico Jorge Horne*

ABSTRACT

It has been recognized that snowmelt models developed in the past 50 years do not fully meet current prediction requirements. Part of the reason is because either they do not represent the physics involved in the snowmelt process or they do not reflect the spatial dynamics of this process. Most of the physics-based distributed models for catchment scale are based on point location equations. The hypothesis behind this study is that physically-based **spatial** models describe the snowmelt dynamics over an area better than distributed, **point** location, physics-based models.

As a first step, energy and mass continuity equations that govern the snowmelt dynamics at a point location were averaged over the snowpack depth, resulting in depth averaged equations (DAE). In this averaging, it is assumed that the snowpack has two layers.

Then, the point location DAE were averaged over the snowcover area. In order to develop the areally averaged equations of the snowmelt physics, we made the fundamental assumption that snowmelt process was spatially ergodic. Furthermore, the snow temperature and the snow density were considered stochastic variables. The expectation of the terms in the areally averaged snowmelt equations were obtained through Taylor series expansion. Only the first two moments of the series were considered. A numerical solution scheme (Runge-Kutta) was then applied in order to solve the resulting system of ordinary differential equations. This equation system was solved for the areal averaged mean and variance of snow temperature and snow density and for the areal mean of snowmelt.

The validation of the developed model was achieved by using Scott Valley (Siskiyou County, California) snowmelt and meteorological data. The observed areal averaged snowmelt data were simulated with the developed model. The performance of the model in simulating the observed data was quite satisfactory. The methodology introduced in this study can be a promising tool for describing other spatial hydrologic processes besides snowmelt.

TABLE OF CONTENTS

	<u>Page</u>
ACKNOWLEDGMENTS	vi
LIST OF SYMBOLS	1
<i>CHAPTER I.</i>	
1. INTRODUCTION	3
1.2. Snowmelt Models	5
1.2.1. Point Models.....	5
1.2.2. Catchment Models.....	8
1.3. Aim of the Dissertation	10
1.4. Organization of the Dissertation.....	10
<i>CHAPTER II.</i>	
2. PHYSICS OF SNOWMELT	12
2.1. Snow Cover Energy Exchange	13
2.2.1. Radiant Energy Exchange	14
2.2.1.1. Solar Radiation	15
2.2.1.1.1. Incoming Short Wave Radiation	17
2.2.1.1.2. Long Wave or Thermal Radiation	20
2.2.2. Turbulent Transfers	22
2.2.3. Ground Heat Flux and Heat Transfer by Rain	25
2.3. Simplified Expression of the Energy Balance	26
2.4. Processes Within the Snowpack	28
2.4.1. Properties of the Snowpack	30
2.4.1.1. Snow Density	33
<i>CHAPTER III.</i>	
3. DEPTH AVERAGING OF THE GOVERNING EQUATIONS	
3.1. Point Equations	36
3.2. Snowpack Model	37
3.3. Snowpack Depth Averaging	39
3.4. Density Changes in the Snowpack	45
3.5. Depth Average of the Mass Balance Equation	46

CHAPTER IV.

4. SPATIAL AVERAGING	49
4.1. Spatial Averaging of the DAE	50
4.1.1. Equation for the Spatial Mean	51
4.1.2. Equation for the Spatial Variance	53
4.1.3. Equation for the Spatial Covariance	55
4.1.4. Freezing Depth	57
4.2. Solution to the Mass Equation	58
4.3. Model Formulation	59
4.3.1. Model Algorithm	59
4.3.1.1. Numerical Solution for the Equation System	60

CHAPTER V.

5. MODEL TESTING	63
5.1. Study Area Characteristics	64
5.2.1. Snow Water Equivalent Information	64
5.2.2. Hydrometeorological Data	66
5.2.3. Solar Radiation	66
5.3. Case 1: Point Location Simulation	66
5.3.1. Simulation Results	67
5.4. Case 2: Theoretical Application	70
5.5. Case 3: Spatially Averaged Estimations at Scott Valley	80
5.5.1. Results	82
5.5.1.1. Contribution to the Spatial Temperature Variation	93

CHAPTER VI.

6. CONCLUDING REMARKS	98
REFERENCES	102
APPENDIX A	110
APPENDIX B	115
APPENDIX C	120

ACKNOWLEDGMENTS

I would like to thank professor M. L. Kavvas for his fundamental guidance in this research and his advise during my doctoral program. I am grateful to him and to professors G. Orlob and J. De Vries for reviewing this dissertation, for their valuable comments and constructive criticism during this study. Particular thanks and sincere recognition goes to professor Joe De Vries for supporting me when I most needed it. I enjoyed and learned working with Joe.

I am also very grateful to the Fulbright Commission and the Argentinean institutions Universidad del Comahue, Conicet and Hidronor that supported my doctoral program.

I would like very much to thank professors, friends and fellows of UC-Davis for the clarifying discussions about this research and their valuable collaboration in the editing of this dissertation. I am specially grateful to my friends Gokmen Tayfur and Joyce and Mel Trujillo.

Finally, let me offer the warmest thank to my family for their tolerance and for providing a delightful atmosphere at home.

LIST OF SYMBOLS

<u>Symbol</u>	<u>Description</u>
α	Albedo
η_d	Atmospheric anisotropy for diffuse radiation
ϵ	Atmospheric emissivity
ϕ_m, ϕ_h, ϕ_e	Atmospheric stability parameters
ϕ	Capillary tension
λ_e	Effective thermal conductivity of snow
η	Snow viscosity coefficient
κ	Soil thermal conductivity
σ	Stephan-Boltzmann constant
λ	Wavelength
a	Extinction coefficient
$\text{cov}(\rho, T)$	Areal snow covariance of density with temperature
C_p	Specific heat
D	Snowpack depth
D_e, D_h	Atmospheric bulk transfer coefficients
D_0	Diffuse sky radiation
d_n	Day of the year
D_r	Reflected diffuse radiation
e	Vapor pressure
E_v	Evaporation flux
H	Sensible heat exchanged with atmosphere
H	Hour angle
h	Specific enthalpy
I	Radiation intensity
I_0	Solar constant
I_d	Clear sky radiation
I_h	Direct solar radiation on a horizontal plane
I_t	Extraterrestrial radiation on a horizontal surface
$I_{\downarrow}, I_{\uparrow}$	Long wave or thermal radiation
K	Eddy diffusivity coefficient
k	von Karman constant
L_{kj}	Latent heat released by a phase change j to k

LE	Latent heat of evaporation
M	Snowmelt energy
M_{kj}	Mass transfer from phase j to k
Mr	Water from snowmelt
Mv	Momentum transferred vertically to the atmosphere
p^m	Atmospheric attenuation of S
Pr	Rainfall
Qg	Heat flux exchanged with the soil
Qn	Net radiation
Qp	Heat flux convected by rain
$\langle \bar{\rho} \rangle$	Areal mean snowpack density
$\bar{\rho}$	Depth average density
r	Mean distance earth-sun
S	Incident short wave radiation
S	Sun's position
sw	Net short wave radiation
T	Temperature
T_a	Air temperature
T_s	Snow temperature
t	Time
$\langle \bar{T} \rangle$	Areal mean snowpack temperature
\bar{T}	Depth average temperature
U	Internal energy
U^*	Friction velocity
v	Velocity
Var(ρ)	Snow density areal variance
Var(T)	Snow temperature areal variance
Vd	View factor
w_s	Weight of snow
W, θ	Snow water content
X	Unit vector normal to the plane of the slope
Z	Snowpack freezing depth
z	Depth within the snowpack

CHAPTER I.

1. INTRODUCTION

Snow constitutes an important part of the water resources in many countries. Because it accumulates during the winter and melts in the spring, it is a strategic resource for irrigated agriculture. Therefore, it is critical to have accurate runoff estimates. Snowmelt runoff estimation is also needed for flood warning, reservoir management, and hydroelectricity power planning.

A variety of models have been developed in the past 50 years as a result of the operational needs for forecast. It is now recognized that these models do not fully meet current prediction requirements. Bloschl et al. (1991) pointed out, that most of these models are spatially lumped and hence, they do not represent the underlying physical processes (WMO, 1986). When these models are calibrated to a catchment with long observational records, they generally produce good results. However, these models do not work well in applications such as ungauged catchments, evaluation of land use impacts, climate change investigations, or extreme event simulations. These situations require realistic, physics-based, spatially distributed models.

Spatial representation of the snow cover is at the present a matter of discussion. Although the physics of the snow cover at a point scale is well understood (Anderson, 1976; Dunne et al., 1976; Male and Gray, 1981; Morris, 1983; Kondo and Yamazaki, 1990) very few studies deal with spatially distributed snowmelt models. This observation was made by Dozier (1987) who emphasized the need for research in the area of spatially distributed models.

The lack of a methodology that represents spatially the physical processes occurring in the snow cover, has lead to a scale related problem. In order to simulate runoff, the snowmelt routines have to be integrated with other processes in a more general hydrologic model. However, conceptual difficulties are found in matching processes that are physically described at different scales. This becomes a critical issue in climate change investigations when land surface-atmosphere interactions are modeled. Wood (1991) points this out very clearly:

"The inadequate representation reflects the recognition that the well-known physical relationships, which are well described at small scales, result in different relationships when presented at the scale used in climate models. Understanding this transition in the mathematical relationships with increased space-time scales appears to be very difficult"

From another field: satellite technology is attempting to provide direct observations of snow properties such as water equivalent, snow depth and snow cover area . These direct observations can be used to avoid important problems in the mathematical modeling of snow cover. However, passive microwave observations of snow cover, that is weather independent, have not been sufficient to break through a barrier; the size of the "pixel" representing the domain of influence is of the order of 100 km².

A combination of low and high frequency observations in the microwave range can be used to estimate the snow water equivalent and snow depth. However, estimations of snow water equivalent require *a priori* information about grain size. Similarly, estimation of snow depth would require *a priori* knowledge of snow density. But at a pixel scale, estimation of grain size and snow density for the snow cover is subject to many uncertainties.

Vegetation cover is an additional complicating factor. According to Choudhury (1991) there could be errors in the estimated snow water equivalent from multifrequency microwave data originated from grain size and vegetation; the magnitude of these errors is uncertain.

It is clear from the above discussion that snowmelt estimations still need to be based on mathematical modeling. In addition, present needs require that these models be physics-based, spatially distributed, and if possible, scale independent. The approach presented in this dissertation is a contribution to these needs and to the understanding of the snowmelt processes at varying spatial scales.

1.2. SNOWMELT MODELS

To visualize the limitations of the existing methodologies for simulating spatially varying snow processes, it is convenient to discuss some of the assumptions in which the current models are based.

A large number of methods have evolved for forecasting purposes. Each makes use of empirical formulae and various approximations to describe melt, transmission and runoff processes. Some authors classified the models based on their applications as operational or research-oriented. Other classifications are based on the method of estimating the energy flux to snow. For our purpose, it is convenient to discuss the contrast between point location models and catchment models.

1.2.1 POINT LOCATION MODELS

The simplest model of all is the empirically based regression model in which linear equations relate input and output variables. The water production at the base of the pack is usually expressed as a function of one or more meteorological variables. In these models the internal physical process and boundary fluxes are not considered in any way but the general nature of the governing physical processes is taken into account by choosing the input variables. According to Zuzel and Cox (1975), air temperature is the best choice if only one variable is used. The best combination of variables is vapor pressure, wind velocity and net radiation.

Regression models are in common usage, and references to them can be found everywhere. However, a large record of data of the study area is required to establish an accurate statistical relationship. They are also site specific. In order to produce snowmelt models which are more widely applicable it is necessary to add more detail of the physical processes involved (Morris, 1985).

Conceptual models try to represent all the physical processes occurring within the snowpack. These models are classified by the degree of complexity of the physical description. In general the equations relate the internal thermodynamics processes with the energy exchanged across the

boundaries (energy continuity). In a similar way, internal mass transport is related to mass fluxes exchanged with the surroundings.

The equations can be integrated over the snow depth resulting in a lumped conceptual model. These models deal only with the mean properties of the snowpack at a point location of the snow cover. Two important assumptions are usually made in these models:

1. Snow exists in two possible states depending upon its temperature: $T=0^{\circ}\text{C}$ and $T<0^{\circ}\text{C}$, for wet isothermal conditions and for dry snow respectively. Wet snow can hold a certain amount of water in the pores before flow begins.
2. Melt water plus rainfall less evaporation, is instantly released at the bottom of the pack.

Lumped equations may also be applied to different layers of the pack when vertical differentiation of snow layers is required. A classical example is the model developed by Anderson (1976) in which the energy balance equation for each layer is expressed in implicit finite-difference form.

The distributed (in depth) models are based on the same mass and energy equations. However, they consider the details of the process occurring within the pack. An equation of state or constitutive relation is needed for the solution of the system. One possibility is to adopt assumptions 1 and 2, mentioned above, and find a solution to the energy equation under dry snow hypothesis (no water, $T<0^{\circ}\text{C}$) and a solution to the mass equation for wet snow (isothermal). Examples of these models are given by Yen (1962), Colbeck (1972), Wankiewicz (1978), Oblad and Rose (1977). The problem with this approach is that it does not deal with the transition between the two equations, especially when the wet front moves through time and space.

Morris (1983) proposed a model based on Colbeck's (1975) analysis of thermodynamics in which there is no transition between cold and ripe snow. It assumes a single phase in which the water content θ , and capillary tension ϕ , are associated by a given empirical "characteristic" equation. A second empirical equation relates capillary tension with grain size. Grain diameter increases with the amount of water that freezes. A model with a constant number and equal size of ice grains is assumed. A relation between snow temperature T , and ϕ must be specified to close the system. This last relationship is expressed by two equations specified for wet and dry snow

conditions. The velocity of the water in the ice matrix is given by Darcy's Law in which hydraulic conductivity is a function of grain diameter, capillary tension, water content and density. This model is part of the Systeme Hydrologique Europeen (Abbot et al, 19878) that simulates the entire land phase of the hydrological cycle.

The energy input at the upper boundary in both lumped or distributed representation can be estimated in many different ways. There are several different models based upon which components of the energy input are measured and upon which technique is used to estimate the other components.

The simplest model uses an index equation for the energy captured by the snowpack. This model is based on one or more variables that reflect the energy budget of the pack. Air temperature is the most commonly used parameter because it is a reasonably good measure of energy flux. At the same time, it is easy to measure, extrapolate and forecast. A classical example of this family of models is the degree-day factor model that uses the product of number of days and daily average air temperature (Martinec and Rango, 1986)

More accurate results are obtained when the energy input at the upper boundary is estimated by accounting for each term in the energy balance. This constitutes the classical energy budget model that will be detailed in the next chapter. Temperature index models do not necessarily reflect the short wave incoming radiation and the turbulent mechanism of energy transfer to the atmosphere. Consequently, energy budget models give better results when they are applied to an open environment with varying climatic conditions during snowmelt. In places with forests, wind and solar radiation are attenuated. Therefore, infrared waves are dominant in the exchange of energy at the snow-air boundary. In these particular cases, a very high correlation is found between energy exchanged and temperature. These circumstances favor the use of temperature index models, as pointed out by Anderson (1976) . The choice between these two estimation techniques is usually a matter of data availability. When enough meteorological information is available, the energy budget method appears to be much more precise.

Point location lumped and multilayer models have been investigated and compared in many studies (Obled and Rosse, 1977; Bauwens, 1988; Bloschl and Kirnbauer, 1991). Both models perform adequately during melt conditions.

However, in situations dominated by prolonged frost and freeze-thaw cycles, the multilayer models produce better results.

In general, physics based point location models produce accurate estimates of snowmelt, snow temperature or snow depth. These models have been usually tested in small experimental plots or under laboratory conditions. However, less accurate results are obtained when these models are applied to a hillslope or a basin. At this scale of application, the established point location physical relationships are not valid anymore.

1.2.2. CATCHMENT MODELS

Catchment models are classified in the same way as point location models: regression type, conceptual lumped and conceptual distributed (over the area). Regression models are subject to same restrictions as the analogous point location models, and are not of interest in this study.

Morris(1985), pointed out that many of the equations used in basin scale models have the same form as those used in point location models. The difference is that catchment models use mean areal inputs and, there is a general belief, that they give mean areal results. However, they do not. In these models, the physical relationships among point variables are assumed to remain the same when they are applied to spatially averaged variables.

Lumped and distributed (in area) catchment snowmelt models are both based on point location physics. The mean value of snowmelt for the whole catchment can be estimated by a lumped model or separate values of snowmelt may be calculated for different zones. In either case the aim of the model is to predict average behavior of the snowmelt over an area that is larger than the small plots used to test the point models.

Consequently, up to the present catchment models have represented point location dynamics of snow processes. They are applied to one or more locations in the basin which makes the difference between lumped and distributed. These locations are represented by mean areal (or spatial) values.

One problem with the distributed approach is that a large amount of information must be available in the study area. This type of model, based on physics of the process at a point location is validated in small plots or laboratory scale experiments. Therefore, the grid size of the application has to be the smallest possible. Accordingly, average spatial data have to be provided

for each of these "plot" size partitions, which is virtually impossible in most cases. An important line of hydrological models attempts to solve this problem by parameterizing the required inputs. Input variables are expressed as functions of other parameters for which "continuous" spatial data are provided. Thus, data from GIS, satellite images, aerial photographic patterns and remote sensing can provide detailed data of topography, snow cover area, aspect, slope and vegetation. A distributed model following this line was presented by Bloschl et al. (1991).

However, difficulty is found in matching the scale of the input values and the scale at which the physical process are described. Additionally, the parameterization is achieved using the data available, and is often not very faithful to the physical representation of the processes, which may be misleading.

The second problem is a conceptual one. There are important implicit assumptions in using point location models with mean areal values. For the sake of clarity, one can hypothesize that the output dependent variable X is given by the input variables Y and Z according to the point model relationship (1):

$$X = YZ + Y^2 \quad (1)$$

A spatial averaging (indicated by brackets) over a fixed area will lead to:

$$\langle X \rangle = \langle Y \rangle \langle Z \rangle + \text{Cov}(Y, Z) + \langle Y \rangle^2 + \text{Var}(Y) \quad (2)$$

In order to apply the point equation (1) to an area using the mean areal values $\langle Y \rangle$ and $\langle Z \rangle$ we have to neglect the covariance and variance terms in (2). If the covariance term is zero we assume that there is no interaction, or that there is independence between Y and Z . If the variance is zero we assume no spatial variability of Y . However, neither one of these assumptions are true for variables describing most hydrologic processes. These assumptions are potential sources of errors. Therefore, even knowing the mean input values corresponding to an area, there is an error involved in the procedure when point location models are used for spatial estimations. Calibration of this type of models is usually achieved by adjusting one or more physical parameters in

order to match observed data. This may lead to parameter values adjusted to compensate for "scale" errors, e.g., disregarding variance and covariance, distorting the physical meaning of these parameters.

Additionally, we can expect different values for the variance and covariance terms for the different sizes of the area represented. In a dynamic model values will also change with time. That may be a reason why models calibrated to a certain scale have to be recalibrated when the size of the area (or time scale) is changed.

Our research is anchored on the hypothesis that these variance and covariance terms exemplified in equation (2) can not be ignored in a spatial formulation of snowmelt physics.

The problem of scale is also present in other disciplines. Non-linear relationships that govern point scale models are usually applied to large control volumes. However, at changing spatial scales, variables do not associate in the same way as they do in the point location physics case.

1.3. AIM OF THE DISSERTATION

The purpose of this dissertation is to develop a physics based spatial representation of the processes occurring in the snow cover. The model can be used to simulate the mean spatial snowmelt produced in a snow covered area.

The emphasis of our study is on the spatial averaging procedure of point location equations. Less attention is given to the parameterization and parameter values, particularly in the energy flux estimations. We use parameter values reported in the literature. In any case these elements can be changed without altering the final structure.

The procedure used is adequate for use in any other field. Other hydrological processes can be spatially averaged if the physical relationships at a point location are well known.

1.4. ORGANIZATION OF THE DISSERTATION

Chapter I discusses the limitations in current snowmelt models for representing the spatially varying dynamics that take place in the snow cover. The developed spatially averaged snowmelt model, the objective of our research, is presented in the framework of present needs.

Chapter II describes the point location physics of the snowmelt process. The first part deals with the energy exchanged by the snowpack, the nature of the fluxes, and estimation techniques. The second part describes the processes that take place within the snowpack. The main properties and parameters involved in the melt dynamics are also discussed. An expression for energy budget estimation is derived and is also included.

In Chapter III the point location equations that govern the energy and mass fluxes are described. Then, these equations are integrated over the snow depth in order to obtain depth averaged equations (DAE). In order to integrate the point equations, an active layer model is adopted in which a dry and a wet portion of the pack are considered.

In Chapter IV, the point location DAE are averaged over the snow cover area obtaining the spatially averaged expression that governs the processes occurring in the snow cover under ergodicity assumptions. This was accomplished by considering snow temperature and snow density as stochastic spatial variables. A moment solution technique is applied, leading to a deterministic ordinary differential equation system. Then, the procedure used to solve the system of ordinary differential equations is presented.

In Chapter V, the validation of the developed model, based primarily on the data from the Scott Valley Basin area, is presented. Several tests are performed in order to evaluate the performance of the model as a point location model and as a spatially averaged model. As a point location model, the results are compared with observed data at the Scott Mountain site and with results from another model which was also applied to the same location. The results of our spatially averaged model are compared with observed areal average snowmelt. Plots showing the good performance of the developed model, are also included.

In Chapter VI, several conclusions about the model performance are presented. Additionally, suggestions for future work are formulated, based on the results obtained and on inferences drawn from the research.

CHAPTER II.

2. PHYSICS OF SNOWMELT

The snowmelt is governed by the energy transferred by radiation, convection and conduction. Part of the convection of heat is caused by the mass fluxes transported across the boundaries. These mass fluxes may be in either solid, liquid or vapor phases. According to Male (1980), the energy balance in a control volume takes the form:

$$\frac{dU}{dt} = \sum_k (m h)_k + \sum_k Q_k \quad (2.1)$$

On the left hand side (LHS) of (2.1), $\frac{dU}{dt}$ is the change in the internal energy of a pack. The distribution of the internal energy is controlled by the thermal properties of the snow and by the phase changes that take place within the pack, inducing the transfer of mass and energy. However, difficulties have been found in describing the transport processes in a medium whose structure is in a permanent state of change.

The right hand side (RHS) of (2.1) refers to the energy exchange with the surroundings. $\sum_k (m h)_k$ is the energy transferred due to mass exchange of each phase k where h is the specific enthalpy of each phase determined by the temperature. $\sum_k Q_k$ is the energy flux due to radiation, sensible and latent heat transfer (convection) and heat transfer from lower layers.

The first part of this chapter is reserved for the description of the energy fluxes transferred through the boundaries of the snowpack. Since these fluxes are treated in detail in the literature, only a brief description of each of them will be given here in order to obtain a simplified mathematical expression for the energy balance. This simplification will allow us to accomplish the spatial average of the snowmelt physics.

The second part is reserved for the discussion of the thermal and physical properties of the snowpack and how these properties relate to the internal structure of the snow (i.e, by the shape and disposition of the grains).

2.1. SNOW COVER ENERGY EXCHANGE

The actual heat expenditure M of melting snow can be determined by the energy balance applied to a unit area of the snow cover limited by the air and soil interfaces and may be written as:

$$M = H + LE + sw + Lw + Qg + Qp - dU/dt \quad (2.2)$$

in which terms are given in cal/cm². H is the heat flux exchange with the atmosphere by turbulent convection; LE is the heat flux induced by evaporation/condensation; sw is the short wave radiant heat flux; Lw is the long wave portion of the radiant heat flux exchange; Qg represents the flux exchange with the soil; Qp is the heat flux convected across the upper boundary by the rain, and dU/dt , already defined, is the rate of change of internal energy per unit area of snow cover. Depending on the condition of the heat exchange and the state of the snow cover, either the temperature will change within it, or the snow will melt, with expenditure of quantities M and dU/dt .

Male and Gray (1981) showed the extent of the various energy fluxes during the snowmelt period on clear days at Bad Lake, where there was no vegetation above the snow cover (Table 2.1).

Date	sw	Lw	H	LE	Qg
11-4-75	194	-151	4.4	-20.42	-1
12-4-75	230	-202	18.6	0.6	-0.5
14-4-75	294	-225	0.3	-9.43	-0.09
17-3-76	110	-107	43.7	13.2	1.5
27-3-76	172	-184	36.3	-5	-5.6
28-3-76	186	-170	1.6	-4.8	-2.6
29-3-76	217	-182	12.7	-1.43	-4.3

Table 2.1 Daily Energy Flux Transfer (cal/cm²) at Bad Lake, Saskatchewan.

The heat sources enumerated above have qualitatively different effects on the snow cover. Solar radiation s_w may penetrate at a perceptible rate to a depth of 30-70 cm heating or melting the snow. Long wave radiation exchange with the atmosphere is marked by the emission of a flux of thermal radiation controlled by the snow surface temperature, and by the absorption of a flux of atmospheric counter radiation at the uppermost layer of the snowpack.

Similar to L_w , the heat flux exchange due to turbulent convection H , and condensation-evaporation LE , act only directly on the uppermost snow layer or active layer. As a result, the heat received on the snow surface has to be transferred to deeper layers by conduction through the snowpack. There is a great difference between the rate at which heat is transmitted depending on whether it is by conduction or by radiation. While the latter is practically instantaneous, the transmission of the former may take hours. Consequently, heat conduction by snow can be viewed as a kind of regulator of the fluxes L_w , H , LE . This is because the absolute values of these fluxes depend largely on the temperature of the active surface of snow.

It can be said that except for the short wave radiant flux, the surface temperature of snow is critically important for determining all of the other sources of energy that contribute to snowmelt (Kuz'min 1961).

2.2.1. RADIANT ENERGY EXCHANGE

Radiation is the transfer of energy by the rapid oscillation of the magnetic field. All bodies possessing energy ($T > 0$ K) emit radiation in proportion to their absolute temperature following the Stefan-Boltzmann Law. The relation between the amount of radiation and its wavelength is given by the Planck's Law.

The sun- earth system can be characterized by the different temperatures prevailing in each component. Typical wavelengths for solar radiation (6000 K) extend from 0.15 μm (ultra-violet) to 3.0 μm (near infra-red), whereas the earth-atmosphere system (~ 300 K) wavelengths extend from 3.0 to 100 μm . In fact, the difference between the two radiation regimes is very distinct because 99% of the total energy emitted by the two planets lies within

these limits. On this basis atmospheric scientists have designated these two wavelength ranges as short-wave, or solar radiation, and long-wave radiation.

2.2.1.1. SOLAR RADIATION, *sw*

Snow and ice have characteristics that allow some transmission of short wave radiation, meaning that incident radiation can be transmitted, reflected, or absorbed within the snowpack. This penetration of radiation has little effect on deep packs, but may affect the melting process in a shallow snow cover.

The decay of the flux with penetration into the snow follows an exponential curve so that the amount of short wave radiation S_z reaching any depth z is expressed as:

$$S_z = S_0 e^{-az} \quad (2.3)$$

where S_0 is the incident short wave radiation absorbed on the top of the snowpack and a is the extinction coefficient (m^{-1}). Equation (2.3) is known as Beer's Law and is applicable only to the transmission of individual wavelengths in a homogeneous medium, but it has been used with success for fairly wide wave bands in snowmelt applications.

The magnitude of the extinction coefficient "a" depends on factors such as wavelength, size of particles, snow density and impurities. The long wave portion is quickly absorbed, but the short-wave radiation penetrates to much greater depth. Values ranging from 10-70 cm of penetration have been reported by investigators based on experiments performed under different snow conditions. Manz (1974) has shown that the radiation penetration process is very sensitive to impurities such as dust and organic matter.

Integrating equation (2.3) over the snow depth D and considering only the short-wave portion that is not reflected by the snow surface, the amount of short-wave radiant energy captured by the snowpack can be expressed as:

$$sw = (1 - \alpha) S (1 - e^{-aD}) \quad (2.4)$$

where α is the albedo and S is the incoming short wave radiation at the ground level that will be discussed later.

Albedo is the ratio of the reflected radiation to the incident radiation. This reflective property of the snow depends on the wavelength λ of the incident radiation. However, the usual approach is to define it as the integrated reflectance of light over the short wavelength spectrum:

$$\alpha = \frac{\int_{\lambda_1}^{\lambda_2} r(\lambda) I(\lambda) d\lambda}{\int_{\lambda_1}^{\lambda_2} I(\lambda) d\lambda} \quad (2.5)$$

where $r(\lambda)$ and $I(\lambda)$ are the reflected and incident monochromatic intensities, respectively. The mean reflectance or albedo governs the amount of radiant energy absorbed by a snow cover and hence it is important in determining the rate of melting. The albedo of snow may vary from 0.95 for compact, dry and clean snow to 0.30 for dirty saturated snow.

Due to the penetration of the short-wave radiation into the snow, the albedo is the result of both the internal structure of the pack contributing to the reflection and the surface snow layer reflectivity. It has been recognized by Mellor (1977) who reviewed and compared different experimental results, that reflectance decreases with increasing wavelengths, that wet snow is less reflective than dry snow, and that albedo decreases with the age of snow. However, an analytical approach that relates all of these factors to the variation of the snow albedo has not yet been found. Expressions that relate albedo to the square root of grain size have been reported by Bohren and Barkstrom (1974), Anderson (1976) and Dozier, et al. (1987). Estimation of albedo from density was proposed by Anderson (1976) who empirically related grain size to snow density.

The decay of albedo during the melting period is a result of the increases in grain size and age of the snow. Kondo and Yamazaki (1990) proposed an exponential decay of albedo from the moment of the snowfall in which a maximum value for the albedo $\alpha(0)$ is assumed:

$$\alpha(n) = \alpha(\min) + [\alpha(0) - \alpha(\min)] e^{(-n/k)} \quad (2.6)$$

where n is the time in days, $\alpha(\min)$ is the converged value of albedo, and k is a parameter for the rate of decrease.

2.2.1.1.1. INCOMING SHORT WAVE RADIATION, S

Short wave radiation reaching the earth surface has two components: a direct beam component and a diffused component scattered by the atmosphere, but with the main flux coming from the direction of the sun.

The direct solar radiation is attenuated as it passes through the atmosphere by absorption and scattering processes. This attenuation is due to three factors: molecular scattering, scattering by large particles and selective absorption. Scattering by large particles such as dust, liquid and solid water causes more attenuation than molecular scattering (Rayleigh scattering). Direct radiation is absorbed by ozone in wavelengths from 0.20 to 0.29 μm and by oxygen in wavelengths shorter than 0.20 μm . The attenuation suffered by short wave radiation is proportional to the mass of air through which the rays have to pass.

Garnier and Ohmura (1970) have presented an expression for clear sky radiation I_d , falling upon a slope as:

$$I_d = \frac{I_0}{r^2} \int P^m \cos(X \wedge S) dH \quad (2.7)$$

The value I_0 is related to the mean distance r between earth and sun and is called solar constant. r is the sun-earth distance expressed in terms of the mean terrestrial orbital distance. Obled and Harder (1979) found an approximation for r^2 as function of the day of the year d_n :

$$r^2 = \bar{r}^2 (0.01676 \cos(\pi - 0.0172615(d_n - 3)) + 1)^2$$

The correction factor P^m accounts for the attenuation of the solar radiation in the atmosphere. P is the mean transmissivity of the atmosphere along the zenith path and m is the optical air mass which is the ratio of the

distance sun's ray travel through the atmosphere to the depth of the atmosphere along the zenith path.

The term $\cos (X \wedge S)$ is the projection of the sun's rays unit vector on the slope. X is the unit vector normal to the plane of the slope and S is the unit vector showing the sun's position. The vector product is indicated by \wedge . H is the hour angle measured from solar noon, the integral taken over the duration of the sunlight on the slope.

The sun position S , can be expressed as function of latitude, day of the year and hour angle by applying spherical trigonometric relationships. Similarly, X may be related to slope and aspect..

Lately, models that give a better estimation of the attenuation process in the atmosphere have been developed by Suckling and Hay (1976) and Dozier (1979). In these models, separate transmission functions are defined for each atmospheric component such as ozone, water vapor, oxygen, carbon dioxide, methane and nitrous oxide.

Diffuse or sky radiation is that portion of the solar radiation that reaches the earth's surface after having been scattered by molecules and suspended particles in the atmosphere. In cloudy conditions it also includes the portion of the short wave radiation which is reflected by the clouds. It is the incoming short wave radiation in shade. Before sunrise and after sunset, all short wave radiation is in diffused form. The ratio of diffuse to total incoming short wave radiation varies daily, seasonally, and with the latitude. In mid latitudes it constitutes 30-40% of the total incoming solar radiation. Cloudiness greatly increases the ratio of diffuse to total solar radiation. Estimation of D_0 , the diffuse radiation flux on a horizontal surface under cloudless and isotropic conditions, is given by the expression presented by List (1968):

$$D_0 = 0.5 ((1 - a_w - a_0) I_t - I_d) \quad (2.8)$$

where:

a_w is the radiation absorbed by water vapor (approx. 7%)

a_0 is the radiation absorbed by ozone (approx. 2%)

I_t extraterrestrial radiation on a horizontal surface

The radiation I_t , is calculated by:

$$I_t = \frac{I_0}{r^2} \int \cos z_s dH \quad (2.9)$$

where z_s is the sun zenith distance, which can be written as a function of latitude, day and hour angle. The factor 0.5 in (2.8) is based on the assumption that half of the direct solar beam is scattered toward the surface and half is scattered away from it. To use this model it is necessary to estimate or measure the total short wave received on a horizontal surface.

A different method, not based on the estimation of diffuse radiation as a part of the total radiation, was presented by Dozier (1979). The radiation scattered initially out of the beam is estimated by wavelength-dependent coefficients for aerosol, Rayleigh scattering, and for ozone and water vapor absorption. A requirement in this model is information on the distribution of each component with altitude, which is not often available.

The diffuse sky radiation on a horizontal plane D_0 , is subjected to correction due to three different effects: the slope of the terrain, the portion of the overlying hemisphere that is visible to the point and the anisotropy of the diffuse radiation. The view factor is a correction factor for D_0 ranging from 0 to 1, that includes these three effects and was presented by Dozier, et al.(1987) as:

$$V_d = \int_0^{2\pi} \int_0^{H_0} \eta_d(\theta, \phi) \sin \theta \cos \theta_s d\theta d\phi \quad (2.10)$$

where $\eta_d(\theta, \phi)$ accounts for the anisotropy for any azimuth direction ϕ and for any horizon angle H_0 as defined by Dozier. The terrain point is characterized by its solar incidence angle θ_s and aspect θ .

Diffuse radiation is also received from the obscured part of the sky dome by reflection from the surrounding terrain.

$$D_r = (1 - V_d) \alpha (D_0 + I_h) \quad (2.11)$$

where α is the average reflectance coefficient or albedo of the surroundings. D_0 and I_h are the diffuse and direct solar radiation calculated over an

horizontal plane. Diffuse radiation is anisotropic because it is not perfectly diffused. The sky diffuse radiation is maximum around the sun and at the horizon. Reflected diffuse radiation is anisotropic due to the variation of the albedo values of the surrounding terrain and due to the variation of the ray's incidence angle on that terrain. However, assumption of isotropy of D_r in most of the models is often made as a result of the difficulties in the analytical description of the process and lack of cloud distribution data. Models that account for the anisotropy of the radiation were developed by Obled and Harder (1979) and Dozier, et al.(1987).

Clouds affect direct and diffuse short-wave radiation. Although scatter is the dominant process occurring with the presence of clouds, a second important effect is the multiple reflections between the snow surface and the clouds, increasing the radiation received at the snow surface. Type and altitude of clouds and extent of cloud cover are important factors in the estimation of radiation. Several models with different levels of complexity have been proposed in order to evaluate the cloud effects on the incoming short wave radiation. However, empirical models based only on hours of sunshine, such as Angstrom (1924), or approaches including multiple levels of cloud and transmissivity coefficients for each of them, such as Davies and Idso (1979), have shown disparity with measured radiation. It appears that since cloud fields change dramatically with time, surface-based cloud observations are not adequate for radiation estimates on a time scale of hours (van der Heydt, 1991).

In summary, short wave incoming radiation can be written by combining (2.7), (2.8), (2.10) and (2.11), as:

$$S = I_d + D_0 V_d + D_r \quad (2.12)$$

Expression (2.12) can be used with (2.4) for the calculation of the total short-wave radiation energy captured by the snowpack.

2.2.1.2. LONG WAVE or THERMAL RADIATION

The balance of long wave radiation of the snow's active surface is given by the difference between the outgoing thermal radiation of the active

surface and the incoming radiation from the atmosphere. This difference is usually positive and some heat (effective radiation) is lost by the snow cover.

Downward radiation $I\downarrow$ is originated under clear sky mainly in the lower 100 m of atmosphere (Geiger, 1961). Ozone emits approximately 2% of the total, carbon dioxide 17% and water vapor 81%. Variations in $I\downarrow$ are largely due to variations in the amount and temperature of water vapor (Male and Gray, 1981). The atmospheric downward long-wave radiation can be expressed as:

$$I\downarrow = \epsilon_a \sigma T_a^4 \quad (2.13)$$

where ϵ_a is atmospheric emissivity, σ is the Stefan-Boltzmann constant and T_a is the temperature of the air. Several approximations have been developed for ϵ_a based on empirical correlation with air temperature and/or vapor pressure as shown in Table 2.2.

Brunt (1952) suggested a correlation that is frequently used, as function of air temperature and vapor pressure e , where a and b are empirical coefficients. Kuz'min (1961) reported values of 0.62 and 0.005 for a and b , respectively from measurements in the Russian plains, while Male and Granger (1979) obtained values of 0.68 and 0.005 for prairie environments.

Investigator	Date	Equation
Brunt	1952	$\epsilon_a = a + b \sqrt{e}$
Brutsaert	1975	$\epsilon_a = (0.642/\sigma) (\frac{e}{T_a})^{1/7}$
Satterlund	1979	$\epsilon_a = 1.08 (1 - \exp(-e^{T_a/2.01} / 6))$
Swinbank	1963	$\epsilon_a = 0.92 \cdot 10^{-5} T_a^2$

Table 2.2 Air emissivity equations

Brutsaert's (1975) equation is physically based and was derived by assuming a linear temperature decrease with height. Marks (1979) modified this equation for alpine areas, assuming constant humidity variation with height. Swinbank's (1963) formula has the advantage of depending only on air temperature, but according to Paltridge and Platt (1976), it may over-estimate radiation during the daytime.

A comparative analysis of these equations was made by Aese and Idso (1978). In general, the accuracy of these equations depends on the range of air temperature prevailing during the application. Applying Swinbank (1963) estimation for ϵ_a the incoming long wave radiation may be written as:

$$I\downarrow = 0.92 \cdot 10^{-5} \sigma T_a^6 \quad (2.14)$$

Long-wave radiation from the snow surface is easier to estimate because the snow acts practically as a perfect radiator or "blackbody" for wavelengths above 2.5 μm . whose reflectance is nearly zero. Using the Stefan-Boltzmann Law, upward long-wave radiation $I\uparrow$ can be written as:

$$I\uparrow = \epsilon_s \sigma T_s^4 \quad (2.15)$$

where the emissivity of the snow ϵ_s , takes values between 0.97-1.0 (Kondratyev, 1969; Anderson, 1976).

The net long wave radiation can be corrected for the effect of clouds. By means of empirical regressions several formulas have been found. These can be applied as a factor of the effective long-wave radiation. These approaches also consider the clouds as a black body in the long-wave range. A typical expression is presented by Unsworth and Moneith (1975) as:

$$F_c = 1 - a m_c^b \quad (2.16)$$

where m_c is the fractional snow cover and a,b are empirical constants.

2.2.2. TURBULENT TRANSFERS H AND LE

Heat and moisture transfers above snow occur as a consequence of the turbulent mixing of air layers. Therefore, it can be considered that this transfer process is governed by mechanical convection in the presence of

wind, and thermal convection when dominated by buoyancy effects. In comparison, molecular heat conduction and heat diffusion are of minor importance. The exchange process mainly occurs in the lower 2 or 3 meters of atmosphere and the fluxes, if air density is considered constant, can be expressed as:

$$H = C_p \rho \overline{T'w'} \quad (2.17)$$

$$L_v E = L_v \rho \overline{q'w'} \quad (2.18)$$

where q' , T' and w' are the departures from the mean values of specific humidity, air temperature and vertical wind component respectively. One way of estimating these fluxes is to measure $\overline{T'w'}$ and $\overline{q'w'}$, the covariances of the respective variables. The eddy correlation method is essentially a direct monitoring of the upward and downward fluxes of the quantities of interest with a set of fixed instruments. The most stringent requirement is that sensors respond to all scales of motion responsible for the fluxes, which involves complex instrumentation. Furthermore, it is difficult to find flat places in the snow area suitable for these types of measurements.

A second approach is to compute these fluxes from measurements of the wind, temperature and humidity profiles in a layer above the snow surface. Within this layer (~30m), vertical fluxes are considered as constant, although the thickness changes with the strength of the wind, temperature gradient and terrain type. Prandtl (1932) developed the equations for the fluxes as:

$$M_v = -\rho K_m \frac{\partial U}{\partial z} \quad (2.19)$$

$$H = -C_p \rho K_h \frac{\partial T_a}{\partial z} \quad (2.20)$$

$$L_v E = -L_v \rho K_e \frac{\partial q}{\partial z} \quad (2.21)$$

where M_v is shear stress or momentum transferred vertically, K_m , K_h and K_e are the eddy diffusivities for momentum, convective and latent energy transfers, respectively, in [m^2/sec]. U is the mean horizontal wind speed in the same units.

If the temperature profile is equal to the adiabatic lapse rate (0.01°C/m), Munn (1966) shows that:

$$\frac{\partial U}{\partial z} = \frac{U^*}{k z} \quad \text{and} \quad K_m = U^* \cdot k z \quad (2.22)$$

where $U^* = \left(\frac{M_0}{\rho}\right)^{1/2}$ is the friction velocity, M_0 is the value of M_v at the surface and k is the von Karman constant's (0.4). Substituting equations (2.22) into equations (2.20) and (2.21), then integrating between heights z_1 and z_2 and considering the constant flux layer $M_v = M_0$, the following expressions are obtained:

$$H = C_p \rho k^2 \frac{K_h}{K_m} \frac{(U_2 - U_1) (T_{a2} - T_{a1})}{(\ln z_2/z_1)^2} \quad (2.23)$$

$$L_v E = L_v \rho k^2 \frac{K_e}{K_m} \frac{(U_2 - U_1) (q_2 - q_1)}{(\ln z_2/z_1)^2} \quad (2.24)$$

Under neutral conditions of the atmosphere, that is, when mechanical convection predominates, K_e/K_m and K_h/K_m can be considered as equal to unity. Under unstable conditions these relationships are calculated using the Monin-Obukhov (1954) similarity theory in which they are put as functions of a dimensionless ratio z/L . The Monin Obukhov length L is an index of the atmospheric stability (shear versus buoyant production of turbulence).

$$\frac{K_h}{K_m} = \frac{\phi_m(z/L)}{\phi_h(z/L)} \quad \text{and} \quad \frac{K_e}{K_m} = \frac{\phi_m(z/L)}{\phi_e(z/L)} \quad (2.25)$$

where ϕ_m , ϕ_h and ϕ_e are unique functions of the stability parameter z/L . Equation (2.25) has been found experimentally (Businger et al., 1971).

The most common application of equations (2.23) and (2.24), also called aerodynamic technique, requires detailed measurements at a minimum of two different heights. For measurements available at one height only, we can apply these equations between the snow surface and the elevation of the observation point. Considering that at the surface, $z=z_0$, the roughness length

of snow (~ 0.001 m), $U=0$, $T=T_s$, and $q=q(T_s)$, equations (2.23) and (2.24) can be written as:

$$H = D_h U_z (T_a - T_s) \quad (2.26)$$

$$L_v E = D_e U_z (e_{(T_a)} - e_{(T_s)}) \quad (2.27)$$

where:

$$D_h = \frac{C_p \rho k^2}{(\ln z_2/z_1)^2} \frac{K_h}{K_m} \quad \text{and} \quad D_e = \frac{0.622 L_v \rho k^2}{P (\ln z_2/z_1)^2} \frac{K_e}{K_m} \quad (2.28)$$

In equation (2.28), $e_{(T)}$ the vapor pressure at temperature T , is related to q by $e_{(T)} = q P / 0.622$, where P is the atmospheric pressure. D_h and D_e are bulk transfer coefficients for convected heat and for latent heat transfer, respectively. Values for D_h and D_e have been reported by various investigators. These values are obtained by measuring air temperature, wind velocity and humidity at a unique height, assuming exponential variation with elevation. A comparison of these values was presented by Male and Gray (1981), showing significant differences between them. Instrumental errors and differences in the height of observation, atmospheric stability conditions, terrain cover and topography are considered to be the possible causes of the gap among values.

2.2.3. GROUND HEAT FLUX and HEAT TRANSFER BY RAIN

The very low conductivity and diffusivity of snow, especially when fresh, makes snow an effective insulating cover for the ground beneath. Even when snow surface temperature drops by 10°C during the night, the soil surface temperature may change by only about 1°C for a 10 cm depth of snowpack (Oke and Hannell, 1966). However, the snow not only protects the soil by moving the "active" layer upwards, but it also conserves the latent heat released. The soil surface is habitually near 0°C with an almost isothermal profile in the upper layers. In this situation, the water in the pores is close to freezing. However, when freezing occurs latent heat is released. This warms

the surrounding area and slows down the freezing process. Therefore, until all the water changes to ice there is a self equilibrating process which keeps temperatures hovering near 0°C . A similar situation prevails during the fusion process in which the latent heat is taken from the soil when the ice in the pore melts. Consequently, with a small temperature gradient the heat exchanged with the soil $Q_g = -\kappa_g \frac{\partial T_g}{\partial z}$ is usually small for seasonal snow cover and frequently neglected in snowmelt models.

Heat convected by rainfall can be expressed by the difference of heat content in the rain before reaching the surface and the heat content in equilibrium with the pack temperature. It is usually calculated as:

$$Q_p = \rho_w C_p (T_r - T_s) P_r$$

where P_r is the rainfall. The magnitude of this flux is relatively low. In fact, for operational purposes, it is usually assumed that T_s is 0°C and T_r is equal to the air temperature (Male and Gray, 1981). When the snow temperature is below 0°C the situation is more complicated because part of the rain freezes, releasing latent heat. The distribution of this heat is controlled by the way the water moves within the pack. The transmission properties are in turn governed by the internal structure of the pack, which changes by the percolating water. However, under freezing conditions snowfall is expected. In this case the heat is not convected across the boundary since the new snow rests on top of the pack.

2.3. SIMPLIFIED EXPRESSION OF THE ENERGY BALANCE

From equations (2.14) and (2.15) the net long wave radiation can be written as:

$$I_n = 0.92 \cdot 10^{-5} \sigma T_a^6 - \epsilon_s \sigma T_s^4$$

Applying the Taylor series, we can expand I_n around T_a :

$$I_n = 0.92 \cdot 10^{-5} \sigma T_a^6 - \epsilon_s \sigma T_a^4 - 4 \epsilon_s \sigma T_a^3 (T_s - T_a) \quad (2.29)$$

The latent heat transfer to the atmosphere (2.27) can be expressed as a function of temperature and relative humidity. The saturated vapor pressure $e_{(T)}^*$ can be calculated as a function of temperature using the Clausius-Clapeyron equation:

$$e_{(T)}^* = 6984.5 + T(-188.9 + T(2.133 + T(-1.289 \cdot 10^{-2} + T(4.39 \cdot 10^{-5} + T(-8.024 \cdot 10^{-8} + 6.137 \cdot 10^{-2} T)))))) \quad (2.30)$$

On the snow surface, the vapor pressure is considered the pressure of saturation and calculated using (2.30) for the temperature of snow at the surface. The air vapor pressure can also be written as a function of the air saturated vapor pressure if h , the relative humidity, and T_a are known:

$$e_{(T_a)} = e_{(T_a)}^* h \quad (2.31)$$

Applying (2.30) to the snow surface and expanding around T_a we obtain:

$$e_{(T_s)}^* = e_{(T_a)}^* + \left(\frac{\partial e_{(T)}^*}{\partial T} \right)_{T_a} (T_s - T_a) \quad (2.32)$$

and substituting (2.31) and (2.32) in (2.27) yields:

$$L_v E = D_e U_z \left[e_{(T_a)}^* (1-h) + \left(\frac{\partial e_{(T)}^*}{\partial T} \right)_{T_a} (T_s - T_a) \right] \quad (2.33)$$

Equations (2.26), (2.29) and (2.33) are linear expressions of the snow temperature T_s , therefore the long wave radiation and turbulent transfer terms, labeled G_1 , can be simplified to the expression:

$$I_n + H + L_v E = G_1 = A + B T_s \quad (2.34)$$

where:

$$\begin{aligned}
A = & 3.80859 \cdot 10^9 \sigma + 8.37052 \cdot 10^7 \text{Ta} \sigma + 766531. \text{Ta}^2 \sigma + \\
& 3743.74 \text{Ta}^3 \sigma + 10.285 \text{Ta}^4 \sigma + 0.0150696 \text{Ta}^5 \sigma + \\
& 9.2 \cdot 10^{-6} \text{Ta}^6 \sigma - 5554571841.0 \epsilon_s \sigma + 447174 \text{Ta}^2 \epsilon_s \sigma + \\
& 2184.0 \text{Ta}^3 \epsilon_s \sigma + 3 \text{Ta}^4 \epsilon_s \sigma + 83.3938 \text{De} u + \text{Dh} \text{Ta} u + \\
& 0.0122117 \text{De} \text{Ta}^2 u + 0.000527205 \text{De} \text{Ta}^3 u + \\
& 0.00000906021 \text{De} \text{Ta}^4 u + 8.11362 \cdot 10^{-8} \text{De} \text{Ta}^5 u + \\
& 3.0685 \cdot 10^{-10} \text{De} \text{Ta}^6 u - 83.3938 \text{De} h u - 0.362288 \text{De} \text{Ta}^* h^* u + \\
& 0.0122117 \text{De} \text{Ta}^2 h u + 0.000263603 \text{De} \text{Ta}^3 h u + \\
& 3.02007 \cdot 10^{-6} \text{De} \text{Ta}^4 h u + 2.02841 \cdot 10^{-8} \text{De} \text{Ta}^5 h u + \\
& 6.137 \cdot 10^{-11} \text{De} \text{Ta}^6 h u
\end{aligned}$$

and

$$\begin{aligned}
B = & -162771336 \epsilon_s \sigma - 1788696 \text{Ta} \epsilon_s \sigma - 6552 \text{Ta}^2 \epsilon_s \sigma - \\
& 8 \text{Ta}^3 \epsilon_s \sigma + 0.724575 \text{De} u - 2 \text{Dh} u - 0.0488467 \text{De} \text{Ta} u - \\
& 0.00158162 \text{De} \text{Ta}^2 u - 0.0000241606 \text{De} \text{Ta}^3 u - \\
& 2.02841 \cdot 10^{-7} \text{De} \text{Ta}^4 u - 7.3644 \cdot 10^{-10} \text{De} \text{Ta}^5 u
\end{aligned}$$

If Q_p and Q_g are neglected, equation (2.2) for the energy balance of the snowpack can now be written as:

$$dU/dt = G1 + sw + M \quad (2.35)$$

2.4. PROCESSES WITHIN THE SNOWPACK

The snow pack is made of non-homogeneous material whose constitutive characteristics depend at any time on the thermal history of the snow cover from the time of its deposition. This makes snow a difficult study material. As Mellor (1975) states, "...there is no material of broad engineering

significance that under normal conditions display the bewildering complexities found in snow".

The melting of snow depends strongly on the transfer of heat and mass (water and vapor phase) within the pack. In turn, the redistribution of mass and heat creates the conditions for a rapid metamorphism in the crystal structure, i.e. size, shape and bonds between ice grains. Finally, the changes in the crystalline structure that take place in the ice matrix control the transport process. Integration of these processes is at present an unsolved problem. Moreover, there are limitations in describing each individual process in terms of bulk properties of the snow pack.

Research on dry snow has shown different metamorphic characteristics under conditions of uniform temperature and those occurring under a constant temperature gradient. Different physical processes take place under these two idealized conditions.

The metamorphism in snow is governed by the movement of vapor within the snowpack. The shape of ice particles and bonds result from the sublimation of water vapor on the grain surface and/or the condensation of vapor coming through the void spaces between particles. The vapor pressure gradient required for transportation of heat through pores may be driven either by the temperature gradient (temperature gradient metamorphism) or by the curvature of grain surfaces, and surface stress when temperature remains constant (equitemperature metamorphism).

Vapor diffusion seems to be the key to the understanding of snow metamorphism. Several basic structural models of snow have been adopted in an attempt to explain the vapor transport and the change in snow density. However, a comprehensive theory of the processes has yet to be achieved. Fortunately, the thermal effects due to vapor movement in the snowpack is accounted for in practice through the use of the "effective" thermal conductivity, as will be explained latter. Nevertheless, an overview of metamorphism is presented herein in order to clarify the equations used.

The changes experienced by crystals in a uniform temperature field have been carefully documented by Bader et al. (1939) and Yosida et al. (1955). A sign of equitemperature metamorphism is the rounding of sharp corners in the snow grains and the decreases in thickness at the bases of individual branches (Male,1980). When grains are close to each other formation of bonds at the points of contact takes place. Grains then become larger and more

nearly spherical. This metamorphic process can be viewed as the movement of snow grains toward a state of equilibrium in which the free energy tends to be minimal. Since the surface is important on the scale of individual crystals, they move in the direction which decreases both the surface energy per unit area and the surface area per unit volume (Male, 1980). Experimental evidence reported by Yosida (1955), Hobbs and Masson (1964), Hobbs and Radke (1967) suggests that the movement of water vapor is responsible for these changes in the crystal structure. The vapor transport is caused by differences in vapor pressure in the vicinity of the grains given by the curvature of grain surface, local surface stress and crystal structure. Based on Fick's law, Yosida (1955) developed an equation for the vapor flux as a function of the grain surface curvature and the vapor diffusion coefficient. Later de Quervain (1973) presented an expression for the saturated vapor pressure as a function of temperature. This expression applies to the range of temperatures encountered in the seasonal snow cover. Perla (1978) derived the equation for the diffusion coefficient based on a normalized diffusion value measured at specified conditions of pressure and temperature.

Dozier (1987) pointed out that the rounded forms associated with the so-called equi-temperature metamorphism apparently required a small temperature gradient to occur. He said that under true equi-temperature conditions, metamorphism is very slow. Consequently, temperature gradient metamorphism and equi-temperature metamorphism are terms that poorly describe the process (Colbeck, 1986).

Under a temperature gradient maintained at a constant value for a sufficiently long period, distinctive crystal shapes will grow on the snow cover depending on the magnitude of the gradient, the grain size, and density of the original snow. Typically "deep hoar" and "skeleton" type crystal as classified by Akitaya (1975) are found under the above conditions. The primary mechanism responsible for the formation of these types of crystal is the vapor transport due to the temperature gradient. Since vapor pressure is temperature dependent, temperature gradients produce associated vapor pressure gradients, which cause water vapor to diffuse from warmer to colder parts of the snowpack. The understanding of temperature gradient mechanisms is due primarily to the works of Yosida et al. (1955), Giddings and La Chapelle (1962) and de Quervain (1973).

Yosida assumed that if the grains at a deeper layer have a higher temperature, water will sublimate from the top of these grains, move across the voids and condense on the grain immediately above. The heat of condensation gained by the upper grains will cause the repetition of the process. This "hand to hand" process will last as long as the temperature gradient exists. In this way, mass and heat are transported by temperature gradients in the pores and sublimation-condensation processes in the grains. Therefore, the engine that runs this mechanism is the temperature gradient in the pores which is larger than the average temperature gradient of the snow pack. Temperature gradient in the pores is larger because the thermal conductivity in the ice is one hundred times that of the air and convection currents in the air spaces are improbable (Akitaya 1975).

The vapor diffusion coefficient is the proportionality constant of Fick's law applied to vapor diffusion. This is a fundamental parameter in many problems of heat and mass flow. However it is very difficult to quantify the vapor diffusion coefficient in porous media containing water or ice because of two effects which counteract each other (Colbeck 1993). First, the blocking effect of the solid particles reduce the area available for flow, and so increase the flow path length. Second, the ice-water phases system acts as a source and/or sink of water vapor, increasing the flow. The flow path is shortened when a coupled source-sink drives the flow directly across the pore. Consequently, attempts to determine the diffusion coefficient in snow have led to contradictory results depending on the approach taken.

The vapor diffusion coefficient must be determined under large temperature gradients over a large period of time because the equations apply to a steady state regime. These conditions can only be maintained in laboratory experiments. However, steady state regime is difficult to reach without significant changes in crystal structure. It is important to note that enough time has to be allowed in order to reach equilibrium, not only in the temperature profile, but also in the snow mass redistribution.

2.4.1. PROPERTIES OF THE SNOWPACK

The discussion in the preceding sections has emphasized the various processes of metamorphism. These processes control the bulk properties of snow. Thermal properties that depend only on density such as specific heat

and latent heat, are well defined. However, those that depend on thermal conductivity or intrinsic permeability of the snowpack are affected by size, shape and structure of crystals. The accuracy with which the various properties can be determined is directly related to their dependence on the metamorphic processes and our understanding of these processes.

The latent heat of fusion of snow per unit mass is equivalent to that of ice. The latent heat of fusion for ice at 0°C and atmospheric pressure is 79.8 cal/gr (Dorsey, 1940). This value decreases approximately 0.6% per degree drop in temperature. The latent heat of sublimation is also temperature dependent as shown in table 2.3 .

T °C	Lat. Heat cal/gr
0	677.20
-10	677.80
-20	678.09
-30	678.20
-40	678.21

Table 2.3 Latent heat of sublimation

The thermal conductivity of snow, defined as the proportionality constant in the Furrier equation, depends on factors such as density, temperature and micro-structure of snow. As it was explained above, temperature gradient could induce a transfer of vapor and subsequent release of latent heat of vaporization. Mellor (1977) pointed out that in dry snow the heat transfer process involves conduction of heat in the network of ice grains and bonds, conduction across the air spaces, convection and radiation across pores (probably negligible), and vapor diffusion through pores. Yosida (1955) suggested that the movement of water vapor contributes 37 percent to the "apparent" thermal conductivity of snow density of 100 Kg/m³, but only 8 percent at a density of 500 Kg/m³. Because of the complexities of the heat transfer process the thermal conductivity is taken as "apparent" or "effective" conductivity λ_e in order to embrace all the heat transferred. Measured values

of λ_e as reported in the literature are dependent on the method of measurement (transient, steady) and on the morphic state of the snow. Mellor (1977) shows the variability in the relationship between λ_e and density ρ as reported by different scientists (Table 2.3). As Langham(1981) pointed out, considerable care should be exercised in applying these relationships, since it is difficult to determine whether the thermal regime encountered in the field problem will correspond to the regime under which the curve is developed. Snow density ρ_s , is defined as the density of the solid (ice) portion of the snow cover, and is expressed in gr/cm³ in Table 2.3.

Investigator	Expression	Density range
Abels (1984)	$\lambda_e=0.0068\rho_s^2$	$0.14 < \rho_s < 0.34$
Janson (1901)	$\lambda_e=0.00005+0.001\rho_s^2+0.006\rho_s^4$	$0.08 < \rho_s < 0.5$
Van Dusen (1929)	$\lambda_e=0.00005+0.001\rho_s^2+0.0052\rho_s^4$	
DeVaux (1933)	$\lambda_e=0.00007+0.007\rho_s^2$	$0.10 < \rho_s < 0.6$
Kondra'eva (1945)	$\lambda_e=0.0085\rho_s^2$	$0.35 < \rho_s < 0.5$
Bracht (1949)	$\lambda_e=0.0049\rho_s^2$	$0.19 < \rho_s < 0.35$
Sulakvelidze (1958)	$\lambda_e=0.00122\rho_s^2$	$\rho_s < 0.35$
Yen (1965)	$\lambda_e=0.0077\rho_s^2$	$0.52 < \rho_s < 0.59$

Table 2.3. Effective thermal conductivity of snow - cal/(cm sec K).

2.4.1.1. SNOW DENSITY

The laws that describe transfer processes within the pack are related to the physical characteristics of the snow that is dictated by the density and metamorphic state. The relationships with the metamorphic state of the snow are not precisely defined, and grain size, shape and crystal structure are not commonly measured for hydrologic purposes. Thus, density is used as the major indicator of the physical structure of the snow cover (Anderson, 1976).

Snow deforms elastically when subject to small loads for short periods of time, but it also deforms continuously and permanently if loads are applied for longer periods. One of the most commonly observed characteristics of snow, and the principal mechanical process occurring in snow deposited on

relatively flat terrain is the settlement or densification of a given layer under the action of the overburden pressure (Male, 1980).

The seasonal compacting of snow has been studied by several investigators such as Yosida (1955), but Bader (1953) was the first to suggest that this process could be characterized by the compacting viscosity η to be determined from field observations:

$$\frac{1}{\rho_s} \frac{d\rho}{dt} = \frac{w_s}{\eta}$$

where:

w_s : weight of snow above the layer for which the density change is being computed in water equivalent [cm].

η : viscosity coefficient, a constant for a given density, temperature and snow density [cm. hr].

The viscosity coefficient η can be calculated as the result of two different multiplicative effects, compacting and temperature changes:

$$\frac{1}{\rho_s} \frac{d\rho}{dt} = \frac{w_s}{\eta_c \cdot \eta_t} \quad (2.36)$$

Kojima (1967) obtained from experimental measurements an expression for η_c :

$$\eta_c = \eta_{c0} \cdot \exp(k_0 \cdot \rho_s) \quad (2.37)$$

where η_{c0} is the viscosity when ρ_s is reduced to zero [cm.hr] and k_0 is a constant value from 15-38 [cm³/gr].

Mellor(1975), based on observations of natural snow in polar regions, developed an equation for the viscosity coefficient η_t . This expression included the temperature gradient effect:

$$\frac{\eta_t}{\eta_{t0}} = \exp \left[\frac{A}{R} \left(\frac{T_c - T}{T \cdot T_c} \right) \right] \quad (2.38)$$

where: A is the activation energy of snow 10^4 [cal/mol]

R is the gas constant, 2[cal/mol K]

T_c is critical temperature, 0°C

η_{t0} is η_t at 0°C

For the temperature normally experienced in areas with seasonal snow cover ($\frac{A}{R.T.T_c}$) could be about 0.08K^{-1} , according to Anderson (1976).

Substituting (2.37) and (3.38) in equation (2.36) we obtain:

$$\frac{1}{\rho_s} \frac{d\rho}{dt} = \frac{w_s}{\eta_o} \exp[-0.08 (T_c - T)] \exp[-k_0 \rho_s] \quad (2.39)$$

where η_o is the viscosity coefficient at 0°C and zero density. This expression has been also presented by Kutchment et al. (1983) and Motovilov (1986).

CHAPTER III

3. DEPTH AVERAGING OF GOVERNING EQUATIONS

3.1. POINT EQUATIONS

Snow is a three phase system composed of a mixture of water (gas, liquid and ice) and air in proportions that depend on the energy balance. Source energy is provided internally by latent heat due to phase change and externally by heat exchange with the atmosphere and by solar radiation. Energy is stored as heat in each phase and is subject to advection within the snowpack.

Equations for the conservation of mass and energy were formulated by Morris(1982,1983). Subscripts i,w and v are used to denote ice, water and vapor. The mass continuity equation for the component k is:

$$\frac{\partial}{\partial t} (\rho_k \theta_k) + \frac{\partial}{\partial z} (\rho_k \theta_k v_k) = \sum_j M_{kj} \quad (3.1)$$

The equation for the conservation of energy is:

$$\sum_k \left[\rho_k \theta_k (Cp)_k \frac{\partial T}{\partial t} + \rho_k \theta_k v_k (Cp)_k \frac{\partial T}{\partial z} \right] = \frac{\partial}{\partial z} \left(\kappa \frac{\partial T}{\partial z} \right) + M_{wv} L_{wv} + M_{iw} L_{iw} + M_{iv} L_{iv} + \frac{\partial Q_n}{\partial z} \quad (3.2)$$

where:

- ρ_k = density of component k [gr/cm³];
- θ_k = volume per unit volume of snow;
- v_k = velocity in the vertical direction [cm/hr];
- t = time [hr];
- M_{kj} = mass of component k produced per unit volume per unit time by a phase change from component j [gr/(cm³ hr)];
- $(Cp)_k$ = specific heat at constant pressure [cal/(gr °C)];
- T = temperature of the mixture [°C];

κ = thermal conductivity [cal/(hr cm °C)];

Q_n = net radiation energy [cal/cm²];

L_{kj} = latent heat released by transformation M_{kj} , in [cal/gr]

Every term in the mass equation is given in gr/(cm³ hr). In the energy equation (3.2) terms are in cal/cm³ hr.

Several assumptions are often made in order to simplify these equations. It is usually assumed that the ice matrix is at rest i.e. $v_i = 0$. Therefore, melting or snowfall do not involve a movement of the ice grains in the snowpack. Additionally, the heat capacity of the gaseous phase is very small compared to those of ice and water and may be ignored. Also, the pressure of the moist air can be considered constant. With these assumptions, the equation for energy (3.2) now becomes:

$$\begin{aligned} & (\rho_i \theta_i (Cp)_i + \rho_w \theta_w (Cp)_w) \frac{\partial T}{\partial t} + \rho_w \theta_w v_w (Cp)_w \frac{\partial T}{\partial z} = \\ & \frac{\partial}{\partial z} \left(\kappa \frac{\partial T}{\partial z} \right) + M_{wv} L_{wv} + M_{iw} L_{iw} + M_{iv} L_{iv} + \frac{\partial Q_n}{\partial z} \end{aligned} \quad (3.3)$$

Distributed models consider the details of the process occurring within the pack and are based on the conservation equations which relate density, specific volumes, velocities and temperatures. However, to solve the system, an equation of state is needed which expresses the constitutive properties of the material. Morris and Godfrey (1975) and Morris (1983) have used Colbeck's (1975) analysis of thermodynamics of wet snow to develop a single phase approximation model, approaching the problem as in soil physics. This formulation is based on several assumptions (mentioned in section 1.), resulting in a complex system.

In this study, the problem is approached by integrating the energy equation over the snow depth in which two distinct layers of dry and wet snow are considered.

3.2. SNOWPACK MODEL

In order to average the energy equation over the snow depth, an active layer model is adopted. It is assumed that the vertical temperature of the

snow varies linearly with the depth until the freezing level Z is reached (Kondo and Yamazaki, 1990). Below that, the temperature remains constant at 0°C . The freezing depth layer will move vertically responding to the energy balance. It is assumed that the water content W of the snowpack is null above Z and that it takes a constant value W_0 below Z as shown in figure (3.1). The linear relation between T and Z allow us to write the average snow depth temperature of the snowpack \bar{T} , as $\bar{T} = \frac{1}{2}T_s$.

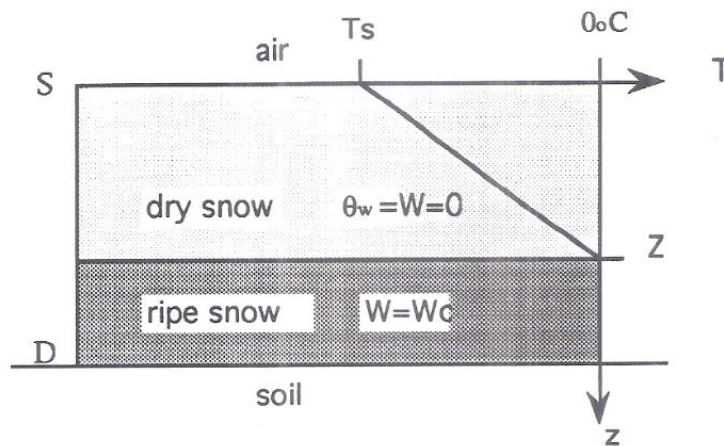


Figure 3.1. Snowpack Model

The constitutive relation can be expressed by the following equation of state of the snowpack:

$$\begin{aligned} W &= 0 & \text{for } T < 0^\circ\text{C} \\ W &= W_0 & \text{for } T = 0^\circ\text{C} \end{aligned} \quad (3.4)$$

W_0 is the gravitational water content of the snow defined as the ratio of mass of liquid water to the mass of wet snow. Since θ_w is a volume relation, it can be said that:

$$\theta_w \rho_w = W_0 \rho_s \quad (3.5)$$

If the air mass in the snow is ignored, it can be assumed for dry snow that the mass of ice is equal to the mass of snow.

$$\theta_i \rho_i = \rho_s \quad (3.6)$$

A positive energy balance will result in a shallower freezing depth Z by which fusion heat will be used to produce water from a dry snow. When the whole snow profile D reaches a saturation state ($Z=0$ and $T=0^\circ\text{C}$.) any additional heat surplus M will yield snowmelt contributing to the runoff. Kuz'min (1961) called M the snowmelt energy. The relationship between the snowmelt energy M and the water production by the snowpack M_r can be written:

$$M_r = \frac{M}{[L_f \rho_w (1-W_0)]} \quad \left[\frac{\text{cm}^3}{\text{cm}^3 \text{ hr}} \right] \quad (3.7)$$

where $(1-W_0)$ is defined by DeVries and Franke (1988) as the thermal quality of the snow. It represents the heat necessary to produce a given amount of melt water from the existing snow, to the same quantity of melt from pure ice.

3.3. SNOWPACK DEPTH AVERAGING

Usually averaged equations over the snow depth deal only with the mean properties of the snowpack and do not consider spatial variability occurring within the pack. However, by considering two layers, the main properties of the snow are captured.

Integration of the energy equation (3.3) is performed in two steps: (1) from $z=0$ (surface) to $z=Z(t)$, and (2) from $z=Z(t)$ to $z=D$, the snowpack depth. Given that one of the integration limits is changing with time, the Liebnitz rule was used. In the first term of (3.3) $(Cp)_i$ is a constant. Considering (3.6) and assuming a mean vertical density $\bar{\rho}_s$ for the snow cover profile, we obtain:

$$\int_0^D \rho_i \theta_i (Cp)_i \frac{\partial T}{\partial t} dz = \bar{\rho}_s (Cp)_i \int_0^{Z(t)} \frac{\partial T}{\partial t} dz + \bar{\rho}_s (Cp)_i \int_{Z(t)}^D \frac{\partial T}{\partial t} dz \quad (3.8)$$

Since there is no temperature change in the lower layer (0°C), the second integral on the RHS of (3.8) is zero. The first term of (3.8) leads to:

$$\int_0^{z_0} \frac{\partial T}{\partial t} dz = \frac{d}{dt} \int_0^{z_0} T dz - T_z \frac{dz}{dt} + T_s \frac{dS}{dt} \quad (3.9)$$

where $T_z = 0^{\circ}\text{C}$ and $\frac{dS}{dt} = 0$. Based on the relation $T_s = 2\bar{T}$, the integral term of the RHS of (3.9) can be expressed in terms of \bar{T} as $\frac{d}{dt} [Z\bar{T}]$. Substituting back (3.9) in (3.8) result in:

$$\int_0^D \rho_i \theta_i (Cp)_i \frac{\partial T}{\partial t} dz = \bar{\rho}_s (Cp)_i \left[\bar{T} \frac{dZ}{dt} + Z \frac{d\bar{T}}{dt} \right] \quad (3.10)$$

The second term of equation (3.3) is written as:

$$\int_0^D \rho_w \theta_w (Cp)_w \frac{\partial T}{\partial t} dz = \int_0^{z_0} \rho_w \theta_w (Cp)_w \frac{\partial T}{\partial t} dz + \int_{z_0}^D \rho_w \theta_w (Cp)_w \frac{\partial T}{\partial t} dz \quad (3.11)$$

From the model adopted it can be seen that $\theta_w = 0$ in the upper layer nullifies the first integral of the RHS of (3.11). The second integral is also nullified because the lower layer is assumed under isothermal 0°C conditions. Therefore there it is not necessary to apply Leibnitz rule to (3.11) and one can simply state it as:

$$\int_0^D \rho_w \theta_w (Cp)_w \frac{\partial T}{\partial t} dz = 0 \quad (3.12)$$

The integral of the third term of equation (3.3) is expressing the flow of heat contained in the water carried across the upper and lower boundaries of the snowpack with a velocity v_w . These flows are the result of the incoming precipitation and the melt water leaving the pack:

$$\int_0^D \rho_w \theta_w v_w (Cp)_w \frac{\partial T}{\partial z} dz = M - Q_p \quad (3.13)$$

where M was already defined as the energy required to produce snowmelt and Q_p is the heat convected to the pack by precipitation. The heat content of snowfall is not carried across the boundaries since the new snow rests on the old surface of the pack.

Integration of the first term on the right hand side of equation (3.3) gives the heat flows across the boundaries controlled by a temperature gradient at the interface:

$$\int_0^D \frac{\partial}{\partial z} \left(\kappa \frac{\partial T}{\partial z} \right) dz = -Q_g + H \quad (3.14)$$

Q_g is the heat exchange with the soil (negative downward) and H is the sensible heat exchange with the atmosphere by turbulent transfer.

The term $M_{iw} L_{iw}$ of (3.3) is related to the fusion heat of the snowpack. Considering that M_{iw} is the mass of water per unit time produced by a unit volume of snow when a phase change takes place, then it can be assumed that $M_{iw} = \rho_s \frac{\partial w}{\partial t}$. In this case:

$$\int_0^D M_{iw} L_{iw} dz = L_f \bar{\rho}_s \int_0^{z^{(i)}} \frac{\partial w}{\partial t} dz + L_f \bar{\rho}_s \int_{z^{(i)}}^D \frac{\partial w}{\partial t} dz \quad (3.15)$$

By using the Leibnitz rule of differentiation on the first integral of the RHS of (3.15) we can write:

$$\int_0^{z^{(i)}} \frac{\partial w}{\partial t} dz = \frac{d}{dt} \int_0^{z^{(i)}} w dz - W_z \frac{dz}{dt} + W_s \frac{ds}{dt} \quad (3.16)$$

Since in the upper "dry" layer $W = 0$ (and obviously $\bar{W} = 0$), (3.16) becomes:

$$\int_0^{Z(t)} \frac{\partial w}{\partial t} dz = 0 \quad (3.17)$$

The second integral of the RHS of (3.15) may be treated in a similar way:

$$\int_{Z(t)}^D \frac{\partial w}{\partial t} dz = \frac{d}{dt} \int_{Z(t)}^D W dz - W_D \frac{dD}{dt} + W_Z \frac{dZ}{dt} \quad (3.18)$$

where it is assumed $\frac{dD}{dt} = 0$ in a small computational time increment. In fact, the relative velocity of $Z(t)$, [~ 1 m/hr], compared to the velocity of $D(t)$, [~ 1 mm/hr], allow us to neglect $\frac{dD}{dt}$ for the integration of the energy conservation equation. Since water content W takes only two values 0 or W_0 which are constant for the upper and lower layer respectively, equation (3.18) leads to:

$$\int_{Z(t)}^D \frac{\partial w}{\partial t} dz = \frac{d}{dt} [W_0 (D - Z)] = -W_0 \frac{dZ}{dt} \quad (3.19)$$

Considering that L_{iw} by definition of (3.2) is equal to $-L_f$, the latent heat of fusion, expressions (3.17) and (3.19) can be substitute in (3.15) to obtain:

$$\int_0^D M_{iw} L_{iw} dz = L_f \bar{\rho}_s W_0 \frac{dZ}{dt} \quad (3.20)$$

Note that the change in the amount of liquid water content is a source of heat when the freezing layer moves downward, increasing z .

If the latent heat of sublimation/solidification is neglected by assuming $M_{iv} L_{iv} = 0$, then the latent heat of vaporization/sublimation can be expressed in terms of the evaporation transferred to the atmosphere as follow:

$$\int_0^D M_{wv} L_{wv} dz = \bar{M}_{wv} L_{wv} D = -L_v E_v \quad (3.21)$$

Finally, the solar radiation, which is positive downward by micro meteorological convention, becomes:

$$\int_0^D \frac{\partial Q_n}{\partial z} dz = Q_{n0} - Q_{nz} = Q_n \quad (3.22)$$

Q_n includes the short-wave incoming radiation sw , and the net long wave radiation:

$$Q_n = sw_0 - sw_D + I_{in} + I_{out} \quad (3.23)$$

Expressions (3.10), (3.12-14) and (3.20-21) can be substituted in (3.3) in order to obtain a depth averaged energy equation for the snowpack.

$$\bar{\rho}_s (Cp)_i Z \frac{d\bar{T}}{dt} + \bar{\rho}_s [(Cp)_i \bar{T} - L_f W_0] \frac{dZ}{dt} = sw_0 - sw_D + I_{in} + I_{out} + H - L_v E_v - M + Q_p - Q_g \quad (3.24)$$

It is difficult to estimate the heat Q_p convected by the rain. Kondo and Yamazaki (1989) consider that it is small enough to be ignored, i.e. 10 mm of rain at 10°C can melt only 1 mm/d in water equivalent. The heat exchanged with the ground is even less except in early winter (Kojima and Motoyama, 1985). Their values agreed with experimental results presented by Kuz'min (1961) in which the calculated heat exchange never exceeds 10 cal/cm² d. Morris (1985) also indicates that the heat exchange with the ground by solid conduction is very small compared to the energy fluxes at the upper boundary. He suggest the use of a constant value of 0 -10 cal/cm² d. Similar conclusions were found by Smith (1974). Neglecting the rain and ground heat exchanges equation (3.24) becomes:

$$\bar{\rho}_s (Cp)_i Z \frac{d\bar{T}}{dt} + \bar{\rho}_s [(Cp)_i \bar{T} - L_f W_0] \frac{dZ}{dt} = sw + G_1 - M \quad (3.25)$$

where:

sw = the net short wave radiation component absorbed by the pack.

$$G_1 = I_{in} + I_{out} + H - L_v E_v$$

G_1 is the incoming energy across the upper boundary excluding the net incoming short-wave radiation. As described in Chapter II, G_1 can be approximated by a linear function of the surface snow temperature:

$$G_1 = A + B T_s .$$

The right hand side of (3.25) includes the driving force terms that represent the energy exchanged by the snowpack. This energy may increase the temperature of the upper layer of the pack (first LHS term) and/or raise the freezing depth layer (second LHS term) by melting dry snow. The snowmelt energy M is zero except when $\bar{T}=0^\circ\text{C}$ and $Z=0$ according to the equation of state:

$$\begin{array}{llll} W=0 & \text{and} & M=0 & \text{for} & \bar{T} <= 0^\circ\text{C} \\ W=W_0 & \text{and} & M=-(sw+G_1) & \text{for} & \bar{T} = 0^\circ\text{C} \end{array} \quad (3.26)$$

A relationship between T and Z can be obtained from the heat flow balance in the surface layer as shown in Figure 3.2

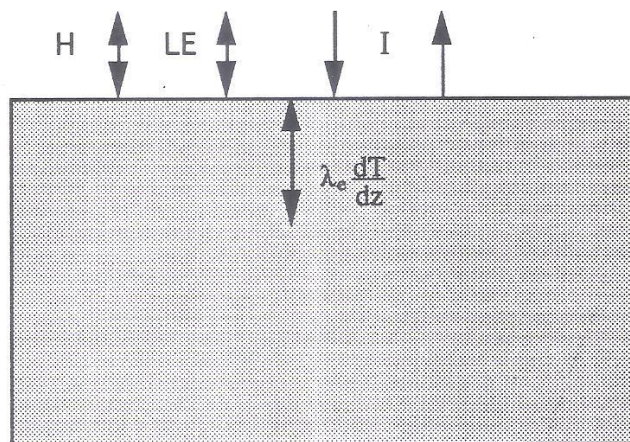


Figure 3.2 Flows exchanged at the snow surface

If a heat balance is performed on an infinitesimally thin snow layer according to Figure 3.2 we can state that (Kondo and Yamazaki 1990):

$$\lambda_e \frac{dT}{dz} = G_1 \quad (3.27)$$

It should be noted that the short-wave radiation is not included. In fact, sw radiation is either transmitted or reflected in this "thickless" layer.

The effective thermal conductivity is used in place of the thermal conductivity to allow the thermal effect of the transport of water to be taken into account indirectly. This term captures most of the heat transferred due to the vapor carried by a temperature gradient. On the other hand, since it is virtually impossible to separate the effects of the conduction and diffusion processes, it is customary to express the measured value as an effective conductivity of the snowpack.

Since the temperature gradient is assumed to be linear in the adopted snowpack model, the snow surface temperature T_s is expressed as $T_s = 2\bar{T}$ (Figure 3.1). Therefore, equation (3.27) can be written in term of \bar{T} as:

$$\frac{-2\bar{\lambda}_e (T_c - \bar{T})}{Z} = G_1 \quad (3.28)$$

Although λ_e depends on the state of the crystalline structure of the snow, most of the experimental determination of λ_e has been correlated solely with snow density ρ_s . A quadratic relation of the form:

$$\bar{\lambda}_e = k_1 + k_2 \bar{\rho}_s^2 \quad (3.29)$$

can be adopted based on the experimental results obtained by several investigators and presented in Table 2.3.

3.4. DENSITY CHANGES IN THE SNOWPACK

Since the changes in the density that are controlled by metamorphic processes are not fully understood, only changes due to compacting and temperature

gradient processes are considered. These two processes have been precisely quantified and validated in the last 40 years by Bader et al. (1939), Kojima (1967), Mellor (1964), Anderson (1976) and others.

As mentioned in Chapter 2, variations of the snow cover density with time is expressed in equation (2.37). Integration of equation (2.37) over the snow depth can be approximated by considering $\bar{\rho}_s$ as the density corresponding to the point located at $2D/3$, D being the snowpack depth (van der Heydt, 1991). Equation (2.37) becomes:

$$\frac{d\bar{\rho}_s}{dt} = \left(\frac{2}{3}D\right) \bar{\rho}_s^2 \eta_o^{-1} \exp[-0.08(T_c - \bar{T})] \exp[-k_0 \bar{\rho}_s] \quad (3.30)$$

3.5. DEPTH AVERAGE OF THE MASS BALANCE EQUATION

The conservation of mass equation (3.1) is simplified assuming that the snow composition remains constant. This assumption is commonly made in lumped (in depth) models. Neglecting the mass exchanged between ice and vapor phases ($M_{iv} = 0$), equation (3.1) can be written:

$$\begin{aligned} \frac{\partial}{\partial t} (\bar{\rho}_i \theta_i) + \frac{\partial}{\partial z} (\bar{\rho}_i \theta_i v_i) &= M_{iw} \\ \frac{\partial}{\partial z} (\bar{\rho}_w \theta_w v_w) &= M_{wi} + M_{wv} \\ \frac{\partial}{\partial z} (\bar{\rho}_v \theta_v v_v) &= M_{vw} \end{aligned} \quad (3.31)$$

These equations are integrated over the snowpack depth D assuming that the ice matrix is at rest ($v_i=0$). Substituting water velocities across the boundaries by M and P_t , vapor fluxes by E_v and considering (3.6), the system can be written as:

$$\int_0^D \frac{\partial}{\partial t} \rho_s dz = D \bar{M}_{iw} \quad (3.32a)$$

$$\rho_w (M - P_t) = D \bar{M}_{wv} - D \bar{M}_{iw} \quad (3.32b)$$

$$\rho_w E_v = -D M_{wv} \quad (3.32c)$$

Introducing (3.32a) and (3.32c) into equation (3.32b), and rearranging:

$$\int_0^D \frac{\partial}{\partial t} \rho_s dz = \rho_w (P_t - E - M_r) \quad (3.33)$$

Considering that D may vary with time, the integration has to be performed by using the Liebnitz rule:

$$\int_0^D \frac{\partial}{\partial t} \rho_s dz = \frac{d}{dt} \int_0^D \rho_s dz - \left[\rho_s \frac{dz}{dt} \right]_0^D \quad (3.34)$$

$$\int_0^D \frac{\partial}{\partial t} \rho_s dz = D \frac{d\bar{\rho}_s}{dt} - \bar{\rho}_s \frac{dD}{dt} \quad (3.35)$$

Introducing (3.35) in (3.33) the mass balance equation becomes:

$$D \frac{d}{dt} \bar{\rho}_s - \bar{\rho}_s \frac{dD}{dt} = \rho_w (P_t - E - M_r) \quad (3.36)$$

In summary, a point location on the snow cover area may be represented by the developed equation system. This system describes the averaged physical processes at this point location occurring in a vertical axis through the snowpack. The laws that govern the energy and mass continuity in the snowpack can be characterized by the system of equations (3.25-26), (3.28-30) and (3.36):

Energy Equations:

$$\bar{\rho}_s (C_p)_i Z \frac{d\bar{T}}{dt} + \bar{\rho}_s [(C_p)_i \bar{T} - L_f W_0] \frac{dZ}{dt} = sw + G_1 - M \quad (3.37.a)$$

$$\frac{2 \bar{\lambda}_e \bar{T}}{Z} = G_1 \quad (3.37.b)$$

$$\bar{\lambda}_e = k_1 + k_2 \bar{\rho}_s^2 \quad (3.37.c)$$

$$\frac{d\bar{\rho}_s}{dt} = \bar{\rho}_s^2 D \eta_0^{-1} \exp[0.08 \bar{T}] \exp[-k_0 \bar{\rho}_s] \quad (3.37.d)$$

Mass equation:

$$D \frac{d}{dt} \bar{\rho}_s - \bar{\rho}_s \frac{dD}{dt} = \rho_w (P_t - E - M_r) \quad (3.37.e)$$

Equation of state:

$$\begin{aligned} M &= 0 & \text{for } \bar{T} < 0^\circ\text{C} \\ M &= -(sw + G_1) & \text{for } \bar{T} = 0^\circ\text{C} \end{aligned} \quad (3.37.f)$$

CHAPTER IV.

4. SPATIAL AVERAGING

The equation system (3.37) describes the energy and mass continuity of the snowpack. These equations represent the snowmelt dynamics at a point location in the snow cover area and characterize the depth averaged properties and processes within the pack at that point. Although they are actually depth averaged equations, we can consider them as point location equations in relation to the snow cover area.

The averaging of differential equations over time or space has been traditionally performed by using the Leibnitz rule of differentiation. The Leibnitz rule was applied in Chapter II in order to obtain depth averaged equations from the equations that describe the snowmelt physics at a point location. Similarly, the Leibnitz rule can be applied in order to develop a spatial average system. However, when the point location differential equation is non-linear as in (3.37.a) the averaging process introduces covariance terms that result in a non-closed system which eliminates the possibility of finding a solution to the conservation equations. Additionally, a drawback of the Leibnitz rule of differentiation is that it requires the specifications of the boundary conditions at the integration limits which are very difficult to specify in certain physical cases (Chen and Chow, 1971).

A second frequent approach is to write the point location equations in a way that state variables are expressed as departures from the spatial means. In a problem arising from the physics there are often good reasons to choose a certain variable as the perturbation parameter, although there are usually other possible choices. According to Murdock (1991) "the creation of good perturbation problems is an art rather than a science, requiring the understanding both of the subject area from which the problem arises, and the mathematical theory behind the solution". A classical application of this techniques is the well known averaging of Navier-Stokes equation that govern turbulence. An expression for the momentum of the mean flow is achieved by perturbing point velocities around the mean. However, the non-linear nature of the point equations results in a non-closed problem, yet it depends on the covariance of the velocities.

The approach that is applied here is based on the perturbation of the "snowmelt physics" rather than single variable perturbations. We can consider the

point location equation as a perturbed mean equation. This perturbation is due to the separation from the areal mean of some of the variables that describe the snowmelt physics. With the use of the expansion theory and some mathematical manipulations we can obtain an approximate closed system depending on spatial statistical parameters of the snowmelt process. However, in order to apply the ensemble averaging methodology to develop the areally-averaged equations of the snowmelt physics, we make the fundamental assumption that snowmelt process is spatially ergodic.

4.1 SPATIAL AVERAGING OF THE DEPTH AVERAGED EQUATIONS (DAE)

It is convenient as a first step to reduce the equation system (3.37). Solving (3.37.b) for Z and substituting in (3.37.a) one obtains,

$$\bar{\rho}_s (Cp)_i \left(\frac{2 \lambda_e \bar{T}}{G_1} \right) \frac{d\bar{T}}{dt} + \bar{\rho}_s [(Cp)_i \bar{T} - L_f W_0] \frac{d \left(\frac{2 \lambda_e \bar{T}}{G_1} \right)}{dt} = sw + G_1 - M \quad (4.0)$$

Replacing $\bar{\lambda}_e$ by the RHS of (3.37.c) and rearranging, we can condense equations (3.37.a-c) into a single equation:

$$\frac{d\bar{T}}{dt} = \frac{1}{b} (sw + G_1 - M) \quad (4.1)$$

where:

$$b = [2 A (Cp)_i \bar{T} - L_f W_0 A + B (Cp)_i \bar{T}^2] \left[\frac{2 k_1 \bar{\rho}_s + 2 k_2 \bar{\rho}_s^3}{G_1^2} \right]$$

The energy conservation equation can now be described by (4.1) and (3.37.d). In these equations, sw is given, $G_1 = A + B T$, where A and B are calculated from the meteorological data (equation 2.34), M is unknown and \bar{T} and $\bar{\rho}_s$ are independent variables.

In an extended area, we can consider that $\bar{T}(t, \dot{x})$ and $\bar{\rho}(t, \dot{x})$ are also functions of the point location \dot{x} in the snow cover. In the spatial averaging

procedure, the equations will be expanded around the ensemble mean of these two variables, hypothesizing that the spatial variability of the snowmelt process is mainly given by the spatial variability of $\bar{T}(t, \mathbf{x})$ and $\bar{\rho}(t, \mathbf{x})$. We have discussed already in Chapter II the importance of these two variables in the melting processes. In a broad sense, it can be said that snow temperature dictates the direction and magnitude of most energy fluxes across the boundaries, and snow density is the bulk parameter that best describes the internal properties and physical state of the snowpack.

4.1.1. EQUATION FOR THE SPATIAL MEAN

In order to simplify the procedure we can denote equation (4.1) and (3.37.d) in the forms:

$$\frac{d\bar{T}}{dt} = a(T, \rho) \quad \text{and} \quad \frac{d\bar{\rho}}{dt} = b(T, \rho)$$

The depth averaged rate of the snow temperature \bar{T} can be written in terms of Taylor expansion series around the spatial average (under the ergodic assumption) $\langle \bar{T} \rangle$ and $\langle \bar{\rho}_s \rangle$ as:

$$\begin{aligned} \frac{d\bar{T}}{dt} = & [a(T, \rho)]_{(o)} + \left[\frac{\partial (a(T, \rho))}{\partial T} \right]_{(o)} (\bar{T} - \langle \bar{T} \rangle) + \left[\frac{\partial (a(T, \rho))}{\partial \rho} \right]_{(o)} (\bar{\rho} - \langle \bar{\rho} \rangle) + \\ & \frac{1}{2} \left[\frac{\partial^2 (a(T, \rho))}{\partial T^2} \right]_{(o)} (\bar{T} - \langle \bar{T} \rangle)^2 + \frac{1}{2} \left[\frac{\partial^2 (a(T, \rho))}{\partial \rho^2} \right]_{(o)} (\bar{\rho} - \langle \bar{\rho} \rangle)^2 + \\ & \left[\frac{\partial^2 (a(T, \rho))}{\partial T \partial \rho} \right]_{(o)} (\bar{T} - \langle \bar{T} \rangle) (\bar{\rho} - \langle \bar{\rho} \rangle) + O [(\bar{T} - \langle \bar{T} \rangle)^3, (\bar{\rho} - \langle \bar{\rho} \rangle)^3] \end{aligned} \quad (4.4)$$

where the sub index (o) refers to the function within the brackets evaluated at the mean values ($\bar{T} = \langle \bar{T} \rangle$, $\bar{\rho}_s = \langle \bar{\rho}_s \rangle$), and $O []$ indicates the truncation error which is of the order of the first omitted term.

Taking the expectations on both sides of (4.4) we obtain the expected rate of temperature that a point location in the snow cover will experience, i.e. the spatially averaged snow temperature rate. First, analyzing the left hand side of (4.4):

$$\left\langle \frac{d\bar{T}}{dt} \right\rangle = \frac{1}{A_s} \int_{A_s} \frac{\partial \bar{T}}{\partial t} dA \quad (4.5)$$

Applying the Leibnitz rule to the integral, (4.5) becomes:

$$\left\langle \frac{d\bar{T}}{dt} \right\rangle = \frac{1}{A_s} \frac{d}{dt} \int_{A_s} \bar{T} dA - \left[\bar{T} \frac{dA_s}{dt} \right]_{A_{s1}}^{A_{s2}}$$

If the averaging is performed over a region within the snow cover area we can state that:

$$\left\langle \frac{d\bar{T}}{dt} \right\rangle = \frac{d \langle \bar{T} \rangle}{dt} \quad (4.6)$$

The expectation on the right hand side of (4.4) can be analyzed as follows: In the second term the function within the brackets takes a deterministic value when evaluated at (o). Hence:

$$\left\langle \left[\frac{\partial (a(\tau, \rho))}{\partial T} \right]_{(o)} (\bar{T} - \langle \bar{T} \rangle) \right\rangle = \left[\frac{\partial (a(\tau, \rho))}{\partial T} \right]_{(o)} \langle (\bar{T} - \langle \bar{T} \rangle) \rangle$$

But, $\langle (\bar{T} - \langle \bar{T} \rangle) \rangle = 0$ and $\langle (\bar{\rho} - \langle \bar{\rho} \rangle) \rangle = 0$ under ergodicity. Using the same reasoning in the fourth and fifth terms of (4.4), it can be seen that the expected values of the square of the deviations are the corresponding spatial variances, and the product of deviations in the sixth term becomes the spatial covariance between \bar{T} and $\bar{\rho}_s$. According to (4.6) and with the above considerations, equation (4.4) can be written as:

$$\frac{d\langle\bar{T}\rangle}{dt} = [a_{(T,\rho)}]_{(o)} + \frac{1}{2} \left[\frac{\partial^2 (a_{(T,\rho)})}{\partial T^2} \right]_{(o)} \text{Var}(\bar{T}) + \frac{1}{2} \left[\frac{\partial^2 (a_{(T,\rho)})}{\partial \rho^2} \right]_{(o)} \text{Var}(\bar{\rho}) + \left[\frac{\partial^2 (a_{(T,\rho)})}{\partial T \partial \rho} \right]_{(o)} \text{cov}(\bar{T}, \bar{\rho}) \quad (4.7)$$

The error involved in the approximation is of the order of the third moment of \bar{T} and $\bar{\rho}_s$. Following the same procedure for the equation (depth averaged) describing the rate of change in snow density, a second spatially averaged equation can be obtained:

$$\frac{d\langle\bar{\rho}_s\rangle}{dt} = [b_{(T,\rho)}]_{(o)} + \frac{1}{2} \left[\frac{\partial^2 (b_{(T,\rho)})}{\partial T^2} \right]_{(o)} \text{Var}(\bar{T}) + \frac{1}{2} \left[\frac{\partial^2 (b_{(T,\rho)})}{\partial \rho^2} \right]_{(o)} \text{Var}(\bar{\rho}_s) + \left[\frac{\partial^2 (b_{(T,\rho)})}{\partial T \partial \rho} \right]_{(o)} \text{Cov}(\bar{T}, \bar{\rho}) \quad (4.8)$$

It may be noticed that equations (4.7) and (4.8) depend on the spatial parameters $\langle\bar{T}\rangle$, $\langle\bar{\rho}_s\rangle$, $\text{Var}(\bar{T})$, $\text{Var}(\bar{\rho}_s)$ and $\text{Cov}(\bar{T}, \bar{\rho}_s)$. Therefore, in order to close the system we need to develop equations for the variance and covariance terms.

4.1.2. EQUATION FOR THE SPATIAL VARIANCES

Applying the definition of the variance,

$$\frac{d\text{Var}(\bar{T})}{dt} = \frac{d}{dt} (\langle\bar{T}^2\rangle - \langle\bar{T}\rangle^2) \quad (4.9)$$

and operating on the RHS of (4.9) and considering (4.6) one obtains:

$$\langle 2\bar{T} \frac{d\bar{T}}{dt} \rangle - 2\langle\bar{T}\rangle \langle \frac{d\bar{T}}{dt} \rangle = 2 \left\langle (\bar{T} - \langle\bar{T}\rangle) \left(\frac{d\bar{T}}{dt} \right) \right\rangle$$

Denoting by $f = (\bar{T} - \langle\bar{T}\rangle)$ and by $a_{(T,\rho)} = \frac{d\bar{T}}{dt}$, equation (4.9) can be written as:

$$\frac{d\text{Var}(\bar{T})}{dt} = 2 \langle f a_{(T,\rho)} \rangle \quad (4.10)$$

In order to obtain an expression for the variance, $\langle f a_{(T,\rho)} \rangle$ can be expanded around $\langle \bar{T} \rangle$ and $\langle \bar{\rho} \rangle$:

$$\begin{aligned} \langle f a_{(T,\rho)} \rangle = & \left\langle [f a_{(T,\rho)}]_{(o)} + \left[\frac{\partial (f a_{(T,\rho)})}{\partial \bar{T}} \right]_{(o)} (\bar{T} - \langle \bar{T} \rangle) + \left[\frac{\partial (f a_{(T,\rho)})}{\partial \bar{\rho}} \right]_{(o)} (\bar{\rho} - \langle \bar{\rho} \rangle) \right\rangle + \\ & \left\langle \frac{1}{2} \left[\frac{\partial^2 (f a_{(T,\rho)})}{\partial \bar{T}^2} \right]_{(o)} (\bar{T} - \langle \bar{T} \rangle)^2 + \frac{1}{2} \left[\frac{\partial^2 (f a_{(T,\rho)})}{\partial \bar{\rho}^2} \right]_{(o)} (\bar{\rho} - \langle \bar{\rho} \rangle)^2 \right\rangle + \\ & \left\langle \left[\frac{\partial^2 (f a_{(T,\rho)})}{\partial \bar{T} \partial \bar{\rho}} \right]_{(o)} (\bar{T} - \langle \bar{T} \rangle) (\bar{\rho} - \langle \bar{\rho} \rangle) + O [(\bar{T} - \langle \bar{T} \rangle)^3, (\bar{\rho} - \langle \bar{\rho} \rangle)^3] \right\rangle \end{aligned} \quad (4.11)$$

Note that:

$$[f]_{(o)} = 0, \quad \frac{\partial f}{\partial \bar{T}} = 1, \quad \frac{\partial f}{\partial \bar{\rho}} = 0$$

After expanding all the derivative expressions, and not including the error term of (4.11), there results:

$$\begin{aligned} \langle f a_{(T,\rho)} \rangle = & [a_{(T,\rho)}]_{(o)} \langle (\bar{T} - \langle \bar{T} \rangle) \rangle + \left[\frac{\partial (a_{(T,\rho)})}{\partial \bar{T}} \right]_{(o)} \langle (\bar{T} - \langle \bar{T} \rangle)^2 \rangle + \\ & \left[\frac{\partial (a_{(T,\rho)})}{\partial \bar{\rho}} \right]_{(o)} \langle (\bar{\rho} - \langle \bar{\rho} \rangle) (\bar{T} - \langle \bar{T} \rangle) \rangle \end{aligned}$$

Substituting $\langle f a_{(T,\rho)} \rangle$ in (4.10) gives

$$\frac{d\text{Var}(\bar{T})}{dt} = 2 \text{Var}(\bar{T}) \left[\frac{\partial (a_{(T,\rho)})}{\partial \bar{T}} \right]_{(o)} + 2 \text{Cov}(\bar{T}, \bar{\rho}) \left[\frac{\partial (a_{(T,\rho)})}{\partial \bar{\rho}} \right]_{(o)} \quad (4.12)$$

Which is a nice expression for the variance as a function of the first derivative of the point location equation. A similar procedure can be applied to the variance of the snow density. This can be expressed as:

$$\frac{d\text{Var}(\bar{\rho})}{dt} = 2 \left\langle (\bar{\rho} - \langle \bar{\rho} \rangle) \left(\frac{d\bar{\rho}}{dt} \right) \right\rangle$$

Now, by denoting $g = (\bar{\rho} - \langle \bar{\rho} \rangle)$ and $b_{(\tau, \rho)} = \frac{d\bar{\rho}_s}{dt}$, the expected product can be expanded in Taylor series around the spatial means. Simplifications due to the fact that $[g]_{(0)} = 0$, $\frac{\partial g}{\partial \bar{\rho}} = 1$ and $\frac{\partial g}{\partial \bar{T}} = 0$, will produce the following relationship:

$$\frac{d\text{Var}(\bar{\rho})}{dt} = 2 \text{Var}(\bar{\rho}) \left[\frac{\partial (b_{(\tau, \rho)})}{\partial \bar{\rho}} \right]_{(0)} + 2 \text{Cov}(\bar{T}, \bar{\rho}) \left[\frac{\partial (b_{(\tau, \rho)})}{\partial \bar{T}} \right]_{(0)} \quad (4.13)$$

4.1.3. EQUATION FOR THE SPATIAL COVARIANCE

By definition, the covariance can be written as,

$$\frac{d \text{Cov}(\bar{T}, \bar{\rho})}{dt} = \frac{d}{dt} \langle (\bar{\rho} - \langle \bar{\rho} \rangle) (\bar{T} - \langle \bar{T} \rangle) \rangle \quad (4.14)$$

Operating on the RHS of (4.14) one can write,

$$\frac{d}{dt} [\langle \bar{T} \bar{\rho} \rangle - \langle \bar{T} \rangle \langle \bar{\rho} \rangle] = \left\langle (\bar{T} - \langle \bar{T} \rangle) \frac{d\bar{\rho}}{dt} \right\rangle + \left\langle (\bar{\rho} - \langle \bar{\rho} \rangle) \frac{d\bar{T}}{dt} \right\rangle$$

Let us call $f = (\bar{T} - \langle \bar{T} \rangle)$, $g = (\bar{\rho} - \langle \bar{\rho} \rangle)$, $a_{(\tau, \rho)} = \frac{d\bar{T}}{dt}$ and $b_{(\tau, \rho)} = \frac{d\bar{\rho}_s}{dt}$, then (4.14) can be expressed as:

$$\frac{d \text{Cov}(\bar{T}, \bar{\rho})}{dt} = \langle f b_{(\tau, \rho)} \rangle + \langle g a_{(\tau, \rho)} \rangle \quad (4.15)$$

By expanding each of the terms on the RHS of (4.15) around the spatial mean values, there results,

$$\begin{aligned} \langle f b_{(\tau, \rho)} \rangle = & \left\langle \left[f b_{(\tau, \rho)} \right]_{(o)} + \left[\frac{\partial (f b_{(\tau, \rho)})}{\partial \bar{T}} \right]_{(o)} (\bar{T} - \langle \bar{T} \rangle) + \left[\frac{\partial (f b_{(\tau, \rho)})}{\partial \bar{\rho}} \right]_{(o)} (\bar{\rho} - \langle \bar{\rho} \rangle) \right\rangle + \\ & \left\langle \frac{1}{2} \left[\frac{\partial^2 (f b_{(\tau, \rho)})}{\partial \bar{T}^2} \right]_{(o)} (\bar{T} - \langle \bar{T} \rangle)^2 + \frac{1}{2} \left[\frac{\partial^2 (f b_{(\tau, \rho)})}{\partial \bar{\rho}^2} \right]_{(o)} (\bar{\rho} - \langle \bar{\rho} \rangle)^2 \right\rangle + \\ & \left\langle \left[\frac{\partial^2 (f b_{(\tau, \rho)})}{\partial \bar{T} \partial \bar{\rho}} \right]_{(o)} (\bar{T} - \langle \bar{T} \rangle) (\bar{\rho} - \langle \bar{\rho} \rangle) + O \left[(\bar{T} - \langle \bar{T} \rangle)^3, (\bar{\rho} - \langle \bar{\rho} \rangle)^3 \right] \right\rangle \end{aligned}$$

Applying the same considerations used in (4.11) yields:

$$\begin{aligned} \langle f b_{(\tau, \rho)} \rangle = & \left[b_{(\tau, \rho)} \right]_{(o)} \langle (\bar{T} - \langle \bar{T} \rangle) \rangle + \left[\frac{\partial (b_{(\tau, \rho)})}{\partial \bar{T}} \right]_{(o)} \langle (\bar{T} - \langle \bar{T} \rangle)^2 \rangle + \\ & \left[\frac{\partial (b_{(\tau, \rho)})}{\partial \bar{\rho}} \right]_{(o)} \langle (\bar{T} - \langle \bar{T} \rangle) (\bar{\rho} - \langle \bar{\rho} \rangle) \rangle \end{aligned}$$

which leads us to the relationship:

$$\langle f b_{(\tau, \rho)} \rangle = \text{Var}(\bar{T}) \left[\frac{\partial (b_{(\tau, \rho)})}{\partial \bar{T}} \right]_{(o)} + \text{Cov}(\bar{T}, \bar{\rho}) \left[\frac{\partial (b_{(\tau, \rho)})}{\partial \bar{\rho}} \right]_{(o)} \quad (4.16)$$

In a similar manner, the second term on the RHS of (4.15) may be expanded around the same mean spatial values:

$$\langle g a_{(\tau, \rho)} \rangle = \left\langle \left[g a_{(\tau, \rho)} \right]_{(o)} + \left[\frac{\partial (g a_{(\tau, \rho)})}{\partial \bar{T}} \right]_{(o)} (\bar{T} - \langle \bar{T} \rangle) + \left[\frac{\partial (g a_{(\tau, \rho)})}{\partial \bar{\rho}} \right]_{(o)} (\bar{\rho} - \langle \bar{\rho} \rangle) \right\rangle +$$

$$\left\langle \frac{1}{2} \left[\frac{\partial^2 (g a_{(T,\rho)})}{\partial \bar{T}^2} \right]_{(o)} (\bar{T} - \langle \bar{T} \rangle)^2 + \frac{1}{2} \left[\frac{\partial^2 (g a_{(T,\rho)})}{\partial \bar{\rho}^2} \right]_{(o)} (\bar{\rho} - \langle \bar{\rho} \rangle)^2 \right\rangle +$$

$$\left\langle \left[\frac{\partial^2 (g a_{(T,\rho)})}{\partial \bar{T} \partial \bar{\rho}} \right]_{(o)} (\bar{T} - \langle \bar{T} \rangle) (\bar{\rho} - \langle \bar{\rho} \rangle) + O [(\bar{T} - \langle \bar{T} \rangle)^3, (\bar{\rho} - \langle \bar{\rho} \rangle)^3] \right\rangle$$

Using the same arguments that allowed us to simplify the above equations, results in

$$\langle g a_{(T,\rho)} \rangle = \text{Var} (\bar{\rho}) \left[\frac{\partial (a_{(T,\rho)})}{\partial \bar{\rho}} \right]_{(o)} + \text{Cov} (\bar{T}, \bar{\rho}) \left[\frac{\partial (a_{(T,\rho)})}{\partial \bar{T}} \right]_{(o)} \quad (4.17)$$

Substituting (4.16) and (4.17) into (4.15), a relationship for the spatial covariance leads to:

$$\frac{d \text{Cov} (\bar{T}, \bar{\rho})}{dt} = \text{Var} (\bar{T}) \left[\frac{\partial (b_{(T,\rho)})}{\partial \bar{T}} \right]_{(o)} + \text{Var} (\bar{\rho}) \left[\frac{\partial (a_{(T,\rho)})}{\partial \bar{\rho}} \right]_{(o)} +$$

$$\text{Cov} (\bar{T}, \bar{\rho}) \left[\frac{\partial (a_{(T,\rho)})}{\partial \bar{T}} + \frac{\partial (b_{(T,\rho)})}{\partial \bar{\rho}} \right]_{(o)} \quad (4.18)$$

The set of ordinary differential equations (4.7) , (4.8) , (4.12) , (4.13), (4.18) constitutes a closed system depending on spatially averaged parameters. This system of equations was originated from the dynamics of snowmelt expressed as a point location process.

4.1.4. FREEZING DEPTH

The freezing depth Z can be averaged over the snow cover area using the same expansion method. Combining equation (3.37.c) and (3.37.d), the expression for Z can be written as:

$$Z = \frac{2 (k_1 + k_2 \bar{\rho}_s^2) \bar{T}}{G_1} = c_{(T,\rho)} \quad (4.19)$$

Expanding Z around the spatial means:

$$\begin{aligned} \langle Z \rangle = & \left\langle [c_{(T,\rho)}]_{(o)} + \left[\frac{\partial (c_{(T,\rho)})}{\partial \bar{T}} \right]_{(o)} (\bar{T} - \langle \bar{T} \rangle) + \left[\frac{\partial (c_{(T,\rho)})}{\partial \bar{\rho}} \right]_{(o)} (\bar{\rho} - \langle \bar{\rho} \rangle) \right\rangle + \\ & \left\langle \frac{1}{2} \left[\frac{\partial^2 (c_{(T,\rho)})}{\partial \bar{T}^2} \right]_{(o)} (\bar{T} - \langle \bar{T} \rangle)^2 + \frac{1}{2} \left[\frac{\partial^2 (c_{(T,\rho)})}{\partial \bar{\rho}^2} \right]_{(o)} (\bar{\rho} - \langle \bar{\rho} \rangle)^2 \right\rangle + \\ & \left\langle \left[\frac{\partial^2 (c_{(T,\rho)})}{\partial \bar{T} \partial \bar{\rho}} \right]_{(o)} (\bar{T} - \langle \bar{T} \rangle) (\bar{\rho} - \langle \bar{\rho} \rangle) + O [(\bar{T} - \langle \bar{T} \rangle)^3, (\bar{\rho} - \langle \bar{\rho} \rangle)^3] \right\rangle \end{aligned}$$

That will give us the relationship:

$$\begin{aligned} \langle Z \rangle = & [c_{(T,\rho)}]_{(o)} + \frac{1}{2} \text{Var}(\bar{T}) \left[\frac{\partial^2 (c_{(T,\rho)})}{\partial \bar{T}^2} \right]_{(o)} + \frac{1}{2} \text{Var}(\bar{\rho}) \left[\frac{\partial^2 (c_{(T,\rho)})}{\partial \bar{\rho}^2} \right]_{(o)} + \\ & \text{Cov}(\bar{T}, \bar{\rho}) \left[\frac{\partial^2 (c_{(T,\rho)})}{\partial \bar{T} \partial \bar{\rho}} \right]_{(o)} \end{aligned} \quad (4.20)$$

4.2. SOLUTION TO THE MASS EQUATION

If there is no snowmelt, i.e., whenever $\langle \bar{T} \rangle < 0^\circ\text{C}$, the equations (4.7, 4.8, 4.12, 4.13, 4.18) can be solved for: $\langle \bar{T} \rangle$, $\langle \bar{\rho}_s \rangle$, $\text{Var}(\bar{T})$, $\text{Var}(\bar{\rho}_s)$ and $\text{Cov}(\bar{T}, \bar{\rho}_s)$. Once $\langle \bar{\rho}_s \rangle$ is known at the beginning and end of the time interval, the mass equation (3.37.e) then becomes linear with respect to the spatially averaged depth of the snowpack, $\langle D \rangle$:

$$D > \frac{d}{dt} \langle \bar{\rho}_s \rangle + \langle \bar{\rho}_s \rangle \frac{d\langle D \rangle}{dt} = \rho_w (\langle P_t \rangle - \langle E \rangle - \langle M_f \rangle) \quad (4.21)$$

Expressing (4.21) in finite differences, it can be solved for $\langle D \rangle$ at the end of the interval. If the solution of the equation system (4.7, 4.8, 4.12, 4.13, 4.18) results

in $\langle \bar{T} \rangle \geq 0^\circ\text{C}$, then the snowmelt $\langle M \rangle$ is calculated from this equation system for $\langle \bar{T} \rangle = 0$. The algorithm used in these calculations will be described later.

4.3. MODEL FORMULATION

The final formulation of the spatial approach is obtained taking derivatives of $a_{(T,\rho)}$, $b_{(T,\rho)}$ and $c_{(T,\rho)}$ with respect to \bar{T} and $\bar{\rho}$ and substituting these derivatives into equations (4.7), (4.8), (4.12), (4.13), (4.18), (4.20). These operations lead to large algebraic expressions. The equations obtained are presented in Appendix A.

It can be noticed that the point location equations are a particular case of the spatially averaged equations system. In a point location situation the variances and covariances are zero and the mean spatial parameters take the point values. Consequently, the averaged system of equations is reduced to the system given by equations (3.37) representing a point location process. On the other hand, when the application is extended over an area, the spatial parameters $\langle \bar{T} \rangle$, $\langle \bar{\rho}_s \rangle$, $\text{Var}(\bar{T})$, $\text{Var}(\bar{\rho}_s)$ and $\text{Cov}(\bar{T}, \bar{\rho}_s)$, will adjust to the scale of the process by taking values dictated by the fluctuations in time of the input meteorological variables and by how these spatial parameters are related in the physics of the melt process.

4.3.1. MODEL ALGORITHM

The calculation procedure is schematized in the flow chart of Figure (4.1). The initial conditions are specified for $\langle \bar{T} \rangle$, $\langle \bar{\rho}_s \rangle$, $\langle D \rangle$, $\text{Var}(\bar{T})$, $\text{Var}(\bar{\rho}_s)$ and $\text{Cov}(\bar{T}, \bar{\rho}_s)$. The energy balance is calculated using spatially averaged meteorological data. This information may come from point location observations or from any other means such as satellite information or mesoscale climatic models.

The system of equations is solved using a Runge-Kutta numerical method for each time interval. It is assumed beforehand that $\langle M \rangle = 0$. If the spatial snow temperature results in a positive value, then according to the equation of state, $\langle \bar{T} \rangle$ is fixed to 0°C and the equation system is solved again for $\langle \bar{\rho}_s \rangle$, $\text{Var}(\bar{T})$, $\text{Var}(\bar{\rho}_s)$, $\text{Cov}(\bar{T}, \bar{\rho}_s)$ and $\langle M \rangle$.

Using equation(4.20), the average snow freezing depth $\langle Z \rangle$ is calculated . If $\langle Z \rangle$ is out of the interval ($0 < \langle Z \rangle < \langle D \rangle$) then $\langle Z \rangle$ is forced to take the

extreme admissible value of the interval, and $\langle \bar{T} \rangle$ is recalculated by Newton method applied to (4.20). This new value of $\langle \bar{T} \rangle$ is used to solve the equation system for the final values of the spatial parameters in the time interval. Finally, (4.21) is solved for $\langle D \rangle$ at the next time step $(t+1)$.

Note that considering (4.6), $\langle M \rangle$ applies to the mean depth of SWE corresponding to the area cover by snow.

4.3.1.1. NUMERICAL SOLUTION FOR THE EQUATION SYSTEM

Most of the methods used for solving ordinary differential equations are based on the Taylor series approximation which implies the differentiation of the function.

However, the Runge-Kutta method succeeds in approximating the Taylor polynomial, without taking derivatives. The basic idea is that functional values at different values of time can be substituted for derivative values. Various exploratory steps are taken from the current time location $t = t_j$ and solution estimates $T = T_j$, and the function $\frac{dT}{dt} = f(T, t)$ is evaluated at these nearby locations. These estimates are combined in such a fashion that the sum must agree with the Taylor's expansion of the solution, up to a certain power in step size h . The successor estimate T_{j+1} is computed recursively from T_j , $(j= 0, 1, \dots)$ by the formula:

$$T_{j+1} = T_j + h \left(\sum_{i=1}^s \alpha_i k_i \right)$$

where the terms k_i are computed recursively according to:

$$k_1 = f(t_j, T_j) \quad \text{and} \quad k_i = f \left(t_j + h \beta_i, h \left(\sum_{m=1}^{i-1} \lambda_{im} k_m \right) \right) \quad \text{for } i= 2, \dots, s$$

The stage number of the rule is determined by s that was chosen to be 4 which gives a global error on the order of h^4 . The parameters α_i , β_i , λ_{im} were chosen following the classical fourth order approach that gives the relations:

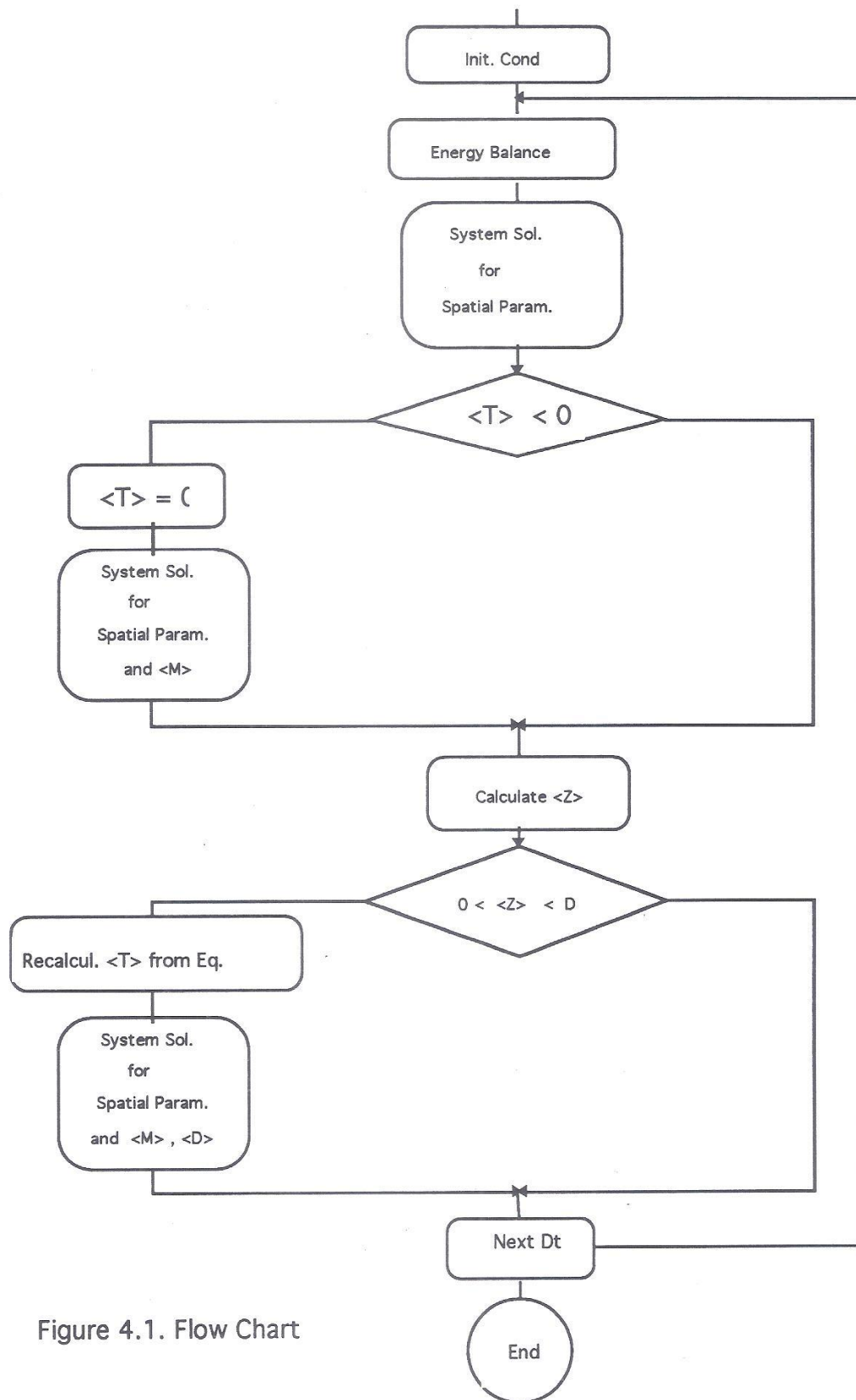


Figure 4.1. Flow Chart

$$\begin{aligned}k_1 &= f(t_j, T_j) \\k_2 &= f\left(t_j + \frac{1}{2}h, T_j + \frac{1}{2}h k_1\right) \\k_3 &= f\left(t_j + \frac{1}{2}h, T_j + \frac{1}{2}h k_2\right) \\k_4 &= f\left(t_j + h, T_j + \frac{1}{2}h k_3\right) \\T_{j+1} &= T_j + \frac{h}{6} (k_1 + 2k_2 + 2k_3 + k_4)\end{aligned}$$

The obvious vector generalization of the univariate technique is adequate and effective for solving simultaneous differential equation problems. Therefore the methodology explained for a single equation was applied simultaneously for our 5 differential equations system. The evaluation of the time derivative functions is supplied by an external function program.

CHAPTER V.

5. MODEL TESTING

The main difficulty in testing a spatial model is acquiring spatially distributed data records. Meteorological data of air temperature, relative humidity, radiation and wind velocity are required at several sites of the area. The areal average of these values are the inputs of the spatial model. Additionally, distributed observations of snowmelt, snow temperature and snow density should be available in order to compare with the results obtained by the spatial model ($\langle T \rangle$, $\text{Var}(T)$, $\langle \rho \rangle$, $\text{Var}(\rho)$ and $\langle M \rangle$). However, some of these variables are not routinely observed. As a consequence, the model developed in this study had to be tested with the regular information available for a typical snow covered catchment.

The area selected for model testing was Scott Valley Basin. Most of the information and data required from Scott Valley Basin were already compiled in a previous study of the region by van der Heydt (1991). A careful analysis, selection and screening of the observed data were performed in this study with the aim of applying a point location snowmelt model to Scott Valley Basin (it will be called Model L). The use of this set of data in the present research for some of the model tests has facilitated the data collection task. Results obtained by van der Heydt (1991) also provided valuable information used for comparison purposes with the presently developed model.

The study carried out by van der Heydt (1991) is based on the Kondo and Yamazaki(1990) snowpack model. In this point location model, the entire snowpack is treated as one homogeneous layer with average properties of density, thermal conductivity and water holding capacity. Governing differential equations are approximated by finite differences. The resulting quadratic equations are solved analytically. The energy exchange estimations are based on the energy budget approach.

The fact that the model developed in this study had to be tested by data from few observation point location, forced us to prepare three different test cases. The first one was directed to evaluate the model developed only as a point location model. Since the point location model is a special case of the spatial model, a point site simulation was made. The result from the developed model

was compared with observed snowmelt and also with the snowmelt and snow temperature predicted by van der Heydt (1991).

The second case is a hypothetical one. Snow temperature and snowmelt were generated at three sites of the Scott Valley Basin. The data generated was utilized to calculate the arithmetical mean and variance of snowmelt and snow temperature. These values were compared with the results of the spatial model developed in this study.

The third case was an application of the developed spatial snowmelt model to the entire Scott Valley Basin area. All the information available in the catchment and near the catchment were used to obtain the required input. The snowmelt predicted by the spatial model was compared with observations from five stations representatives of the area.

Although the validation of the methodology may not be conclusive, by these three tests, an insight into model performance was obtained.

A brief description of the location and data are described below. The detailed information can be obtained from van der Heydt (1991).

5.1. STUDY AREA CHARACTERISTICS

The Scott Valley watershed is a 1600 square kilometer basin located in the northern California (Figure 5.1). The topography of the region is rugged, having elevations of 2500 m at the peaks to 500 m at the basin outlets. Snow accumulation occurs by storms coming from the Pacific during the winter season. Snowmelt takes place during interstorm periods and in the spring season.

5.2.1. SNOW WATER EQUIVALENT INFORMATION (SWE)

There are two snow pillow sites within the basin at the southern end of the watershed, namely Middle Boulder 3 and Scott Mountain. In addition a group of three observation point sites at Peterson Flat, Mumbo and Big Flat are out of the basin, but close enough to provide valid information for the study area. At these five stations cumulative precipitation are also recorded. Data are registered by sensors that transmit the signal at periodic intervals via the Geostationary Operational Environmental Satellite to a central computer facility in Sacramento (Suits, 1986).

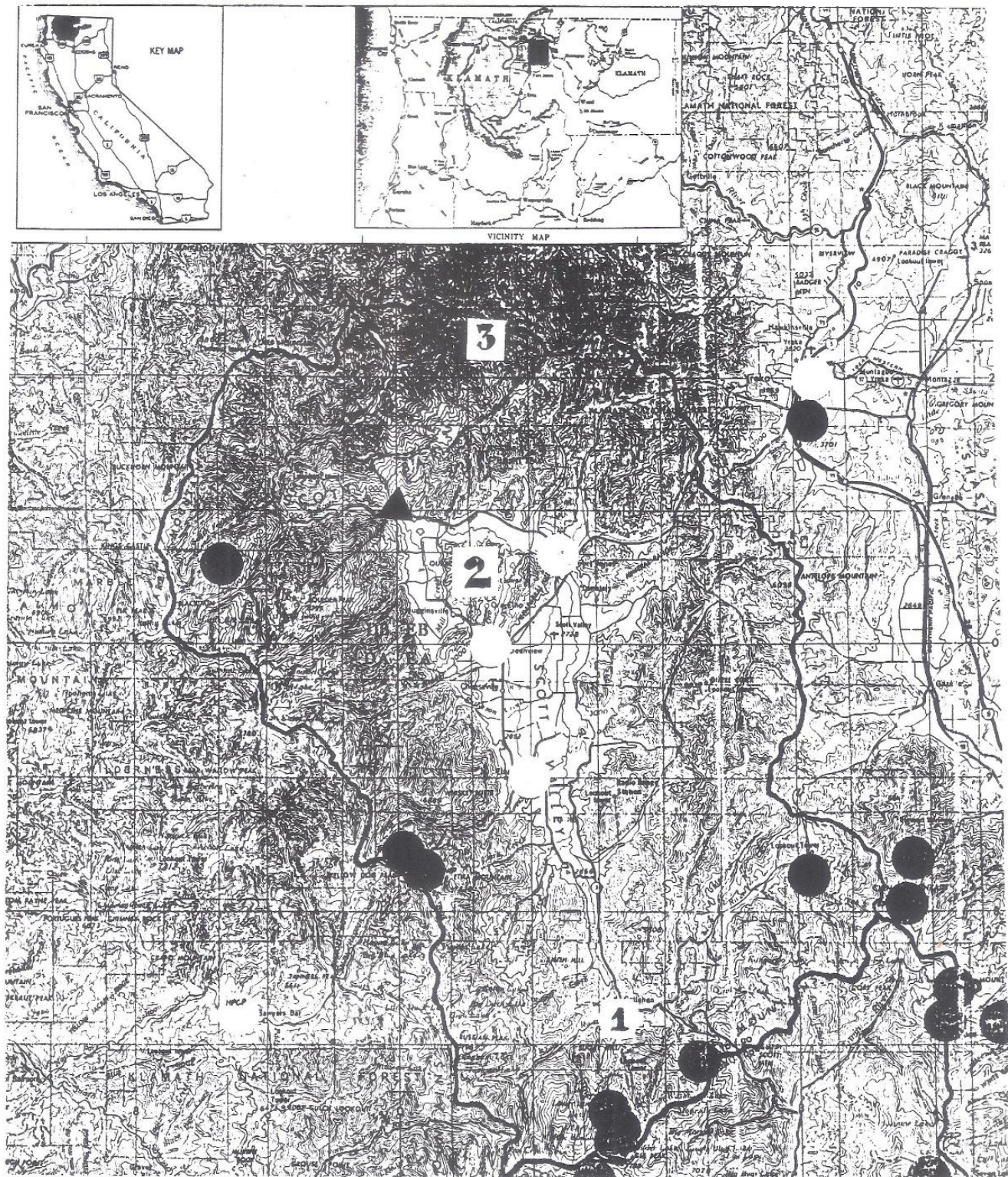


Figure 5.1 Scott Valley study area.

According to Suits (1986), diurnal fluctuations of SWE readings are a result of temperature induced effects, lose of contact between the sensor and the snow and sensitivity of the sensor to changing snow conditions. These fluctuations make a determination of the 3 hour incremental melt impossible. It is convenient therefore to use incremental daily SWE as a representative measure of the snow depth variations.

5.2.2. HYDROMETEOROLOGICAL DATA

Three remote automated weather stations (RAWS) in Scott Valley Basin measure hourly relative humidity, precipitation, air temperature wind speed and direction, and several parameters used to assess fire danger. These three stations are located at Collin's Baldy (1670), Quartz Hill (1200) and Callahan (500). Additionally, at Scott Mountain air temperature is measured and recorded every 3 hours.

5.2.3. SOLAR RADIATION

Total global solar radiation is monitored at Red Bluff by Pacific Gas and Electric company. A spectral piranometer measures total horizontal solar radiation yielding 30 minute average values. Fractional sky cover and cloud base elevation are recorded at Redding, Siskyou and Montague airports.

The short wave radiation data (sw) used was prepared by van der Heydt (1991) who calibrated a radiation model using Red Bluff solar radiation. The calibrated atmospheric transmissivity parameter was found to be 0.68. This is in agreement with Williams (1972). Subsequent adjustment to the basin was made possible by using Redding and Montague airport information of cloudiness. The albedo was computed by using an exponential decay function of albedo with time since the last snowfall (equation 2.6).

5.3. CASE 1: POINT LOCATION SIMULATION

The first test was directed toward the validation of the formulated methodology applied as a point location model. By setting the variances and

covariances to zero and considering $\langle \bar{T} \rangle$ and $\langle \bar{\rho} \rangle$ as point location variables, the result of the system will correspond to a point location solution.

The simulation period chosen is April, 6-19 of 1986 in which no snow accumulation occurred. The model was applied to the Scott Mountain site. For this particular location, most of the snowmelt occurred during April, 6 to 19. By April 19 snow depth had decreased from 39 cm to about 2 cm. The zero time for the simulation corresponds to April 6 at 4 AM. A 15 minute interval was used according to the data available, not requiring interpolation of the measurements.

The parameter values used in the model testing are detailed in the Appendix B. The input data of air temperature, relative humidity, wind, short wave incoming radiation and initial values are also plotted in the Appendix B.

5.3.1. SIMULATION RESULTS

In Figure 5.2, the values of snow temperature during the first 5 days of the simulation period, calculated by the model developed in this study are compared with the results predicted by Model L (van der Heydt, 1991). A classical periodic shaped curve was obtained as a result of the incoming energy fluctuations during the day-night cycle. Although there are some differences in curve shape and magnitudes of temperature at certain points in time, there is a significant agreement between two models.

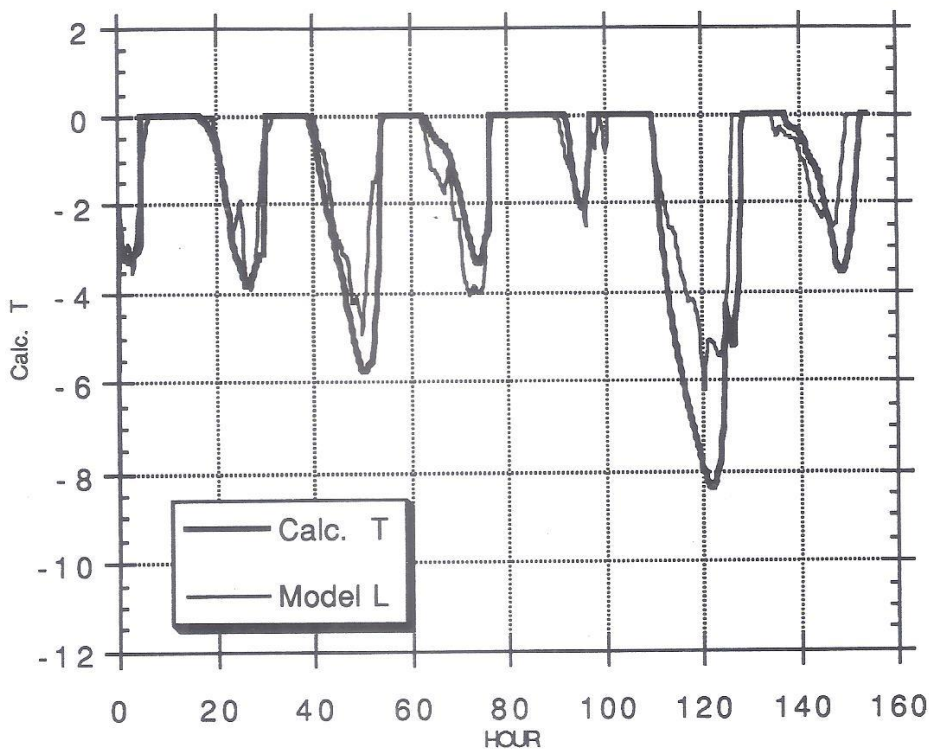


Figure 5.2 Surface snow temperature comparison.

In Figure 5.3, the snowmelt values, resulting from calculations performed by the model at 15' intervals, are shown. Figure 5.4 shows the comparison of daily cumulative snowmelt values. According to Figure 5.4 the simulation of the observed values at Scott Mountain site is satisfactory.

The discrepancies between the snowmelt calculated by the developed model and the van der Heydt predictions can be explained by several factors. In Model L equations are solved analytically, whereas in the spatial model a numerical solution is obtained (note that the spatially averaged equation system can not be solved analytically). This may be the reason for the slightly longer melting periods of Figure 5.2, that will contribute to higher snowmelt cumulative yields. During the melting periods, short wave radiation and turbulent transfer of heat to the atmosphere, dominate the energy balance. In

the turbulent transfer process, the values of the parameters involved may be different in the models compared, increasing the snowmelt calculated by the spatial model.

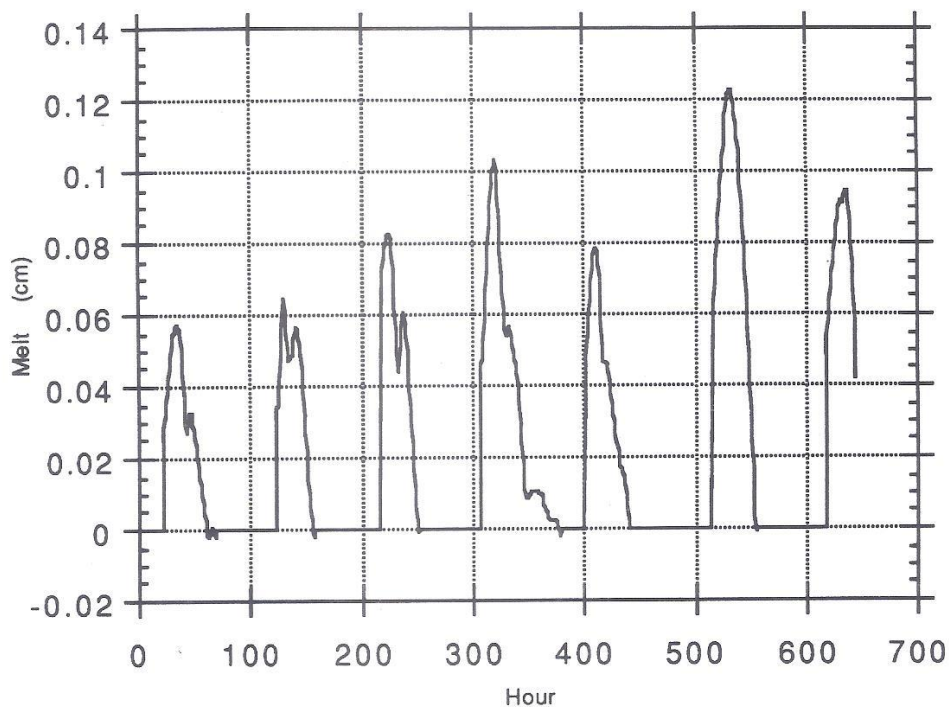


Figure 5.3 Calculated snow melt at 15 min. interval.

The general agreement among the two models and observed data confirm that the original point physics representation of the melting process is reasonably correct and the assumptions and simplifications made in the procedure are acceptable.

In summary, it can be said that based on the results obtained from the data available, the developed model performed satisfactorily as a point location simulation model.

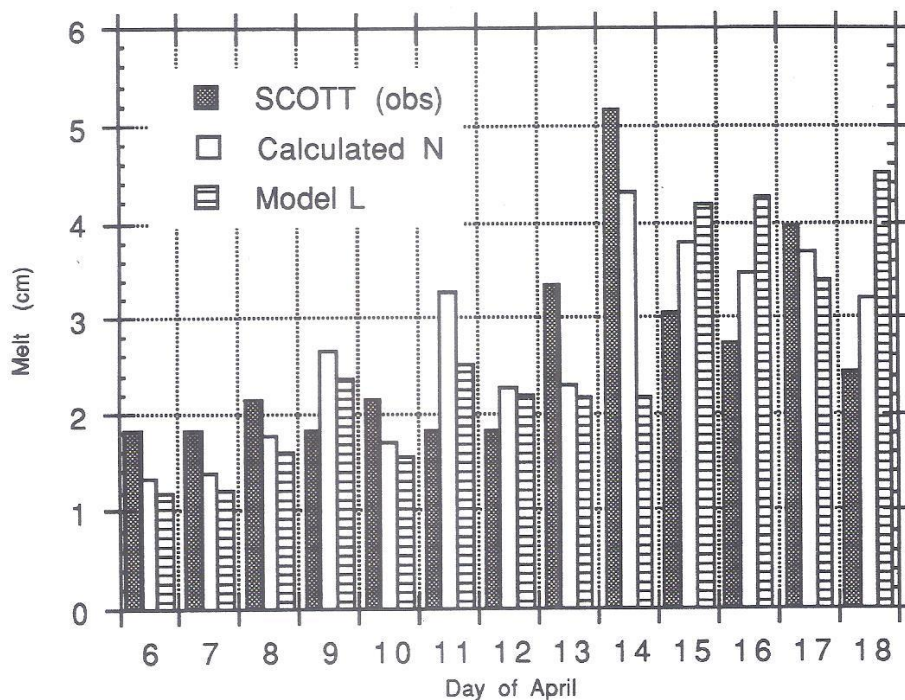


Figure 5.4 Comparison of snowmelt calculated by the developed model in its point location form (Calculated N), observed, and melt estimated by Model L.

5.4. CASE 2: THEORETICAL APPLICATION

To test the spatial model it is important to compare calculated areal mean snow temperature, snow temperature areal variance and mean snowmelt with corresponding observed quantities. However, only snowmelt is actually observed in the Scott Valley Basin. Consequently, a simulation of point location snow temperature was performed at three locations of Scott Basin by utilizing the model developed in this study (as a point location model). Meteorological data for air temperature, relative humidity, wind speed and solar radiation were available for three sites at Callahan, Collin's Baldy and Quartz Hill. The simulated snow temperature and snowmelt at these three locations were utilized to calculate the spatial arithmetic average of T and M, and the variance

of T . Although these values were simulated, we will call them hypothetically "observed" average T and M and "observed" variance of snow temperature.

On the other hand, the averaged values of air temperature, relative humidity, wind velocity and short wave radiation at these three locations were then used as input data to the spatial snowmelt model in order to estimate $\langle \bar{T} \rangle$, $\langle M \rangle$ and $\text{Var}(\bar{T})$. Finally, calculated spatial parameters and those "observed" ones were compared.

Figure 5.5 represent the model calculated snowmelt at Callahan, Collin's Baldy and Quartz Hill. The initial depth for the snow cover was assumed to be 39 cm for these 3 locations. The parameter values used for the calculations are similar to those presented in Appendix B. Similarly, the simulated snow temperature at these three locations, or "observed" snow temperatures are shown in Figure 5.6.

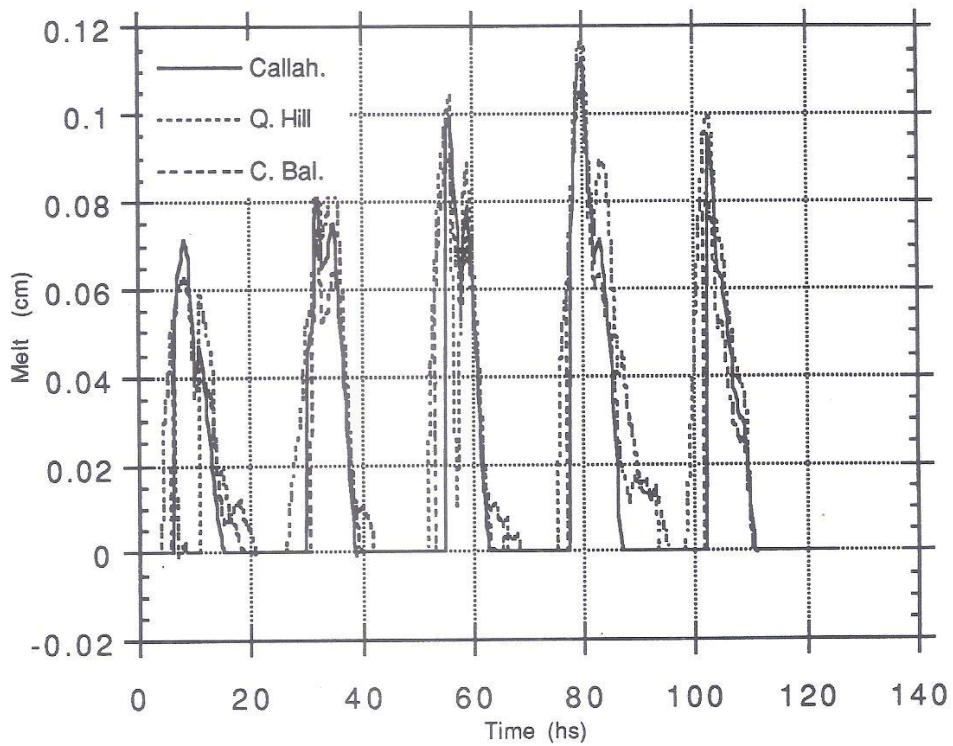


Figure 5.5 Snowmelt calculated by the point location form of the spatial model at 3 locations of Scott Valley Basin.

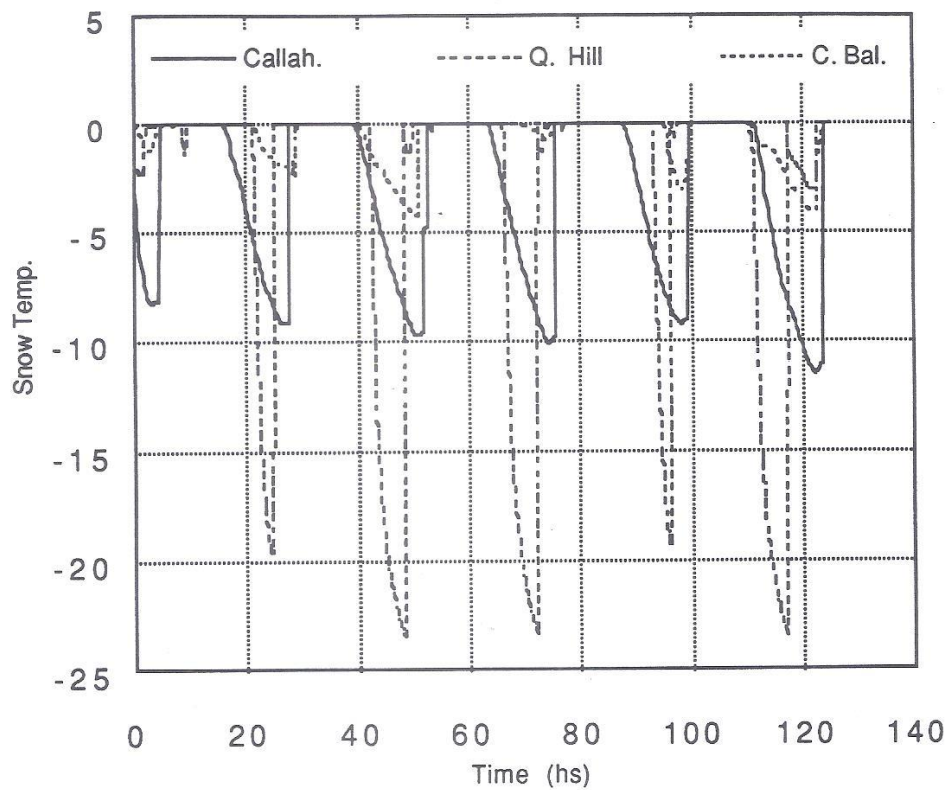


Figure 5.6 Snow temperature calculated at 3 locations of Scott Valley Basin.

In Figure 5.7, the areal mean value of snow temperature, $\langle \bar{T} \rangle$, obtained through the spatial model is compared with the "observed" temperature. Correspondingly, in Figure 5.8 calculated and "observed" snowmelt are compared. In both cases there is good agreement. There is no "calibration parameter" in the model. However, the initial values can be adjusted within a certain interval. In this case the initial conditions were:

$$\begin{aligned} \langle \bar{T} \rangle &= -2.0 \\ \text{Var}(\bar{T}) &= 4.0 \\ \langle \bar{\rho} \rangle &= 0.35 \\ \text{Var}(\bar{\rho}) &= 0.001 \\ \text{Cov}(\bar{\rho}, \bar{T}) &= 0.0 \end{aligned}$$

Analyzing the performance of the developed model, it was noticed that the effects of the initial values of $\langle \bar{T} \rangle$, $\text{Var}(\bar{T})$, $\langle \bar{\rho} \rangle$, $\text{Var}(\bar{\rho})$ and $\text{Cov}(\bar{\rho}, \bar{T})$ were very different. While the initial value of $\langle \bar{T} \rangle$ influenced the first daily cycle, the initial value of $\langle \bar{\rho} \rangle$ affected the whole calculation period. From Figure 5.9 it can be seen that $\langle \bar{\rho} \rangle$ does not have the repeating pattern shown by $\langle \bar{T} \rangle$ in Figure 5.7. On the contrary, the smooth decay of $\langle \bar{\rho} \rangle$ is mostly due to compacting through time. This affects the dynamics during all the period, which is in correspondence with the nature of snowmelting process. In Figure 5.9, the tiny deviations of $\langle \bar{\rho} \rangle$ from the main exponential tendency of the curve is due to variation in $\langle \bar{T} \rangle$ and can be barely noticed. The exponential dependence of $\langle \bar{\rho} \rangle$ on $\langle \bar{T} \rangle$ expressed in equation (3.37.d), is manifested when the same temperature persists for an extended period of time. The value of $\langle \bar{\rho} \rangle$ is also sensitive to $\text{Var}(\bar{\rho})$ that affects the rate at which $\langle \bar{\rho} \rangle$ changes. The tendency of $\text{Var}(\bar{\rho})$ is to decrease with time, indicating that the compacting effect tends to cause a more homogeneous snow cover density. The range of plausible values for $\text{Var}(\bar{\rho})$ is of the order of 0.001 gr/cm³ hr.

The temperature variance curves displayed in Figure 5. 10, show some differences in the magnitude of the peaks. The $\text{Var}(\bar{T})$ is very sensitive to the initial conditions and, perhaps, there exist different combinations of initial values that may yield a better fit. Another consideration is the number of points location from which the "observed" variance was estimated. Three sites is a low sample number. Also they may not be completely representative of the watershed or the area covered by the input data. However, the shape of both curves, tendency and location of the peaks are in agreement.

The covariance parameter has a fluctuating pattern which favors the determination of the initial value (Figure 5.12). A test run with the $\text{Cov}(\bar{\rho}, \bar{T})=0$ as initial value will show the magnitude and pattern from which a better initial value can be estimated. Although the values taken by the covariance are low in magnitude, they affect the dynamics. The covariance may be ignored in the perturbation procedure, approximating the snowmelt physics equations by only considering the variance terms. However, in that case (setting the $\text{Cov}(\bar{\rho}, \bar{T})=0$ and ignoring the equation for the covariance) it was seen that stability problems occur, causing the $\text{Var}(\bar{T})$ to take negative values which in turn leads to divergence problems.

The discrepancies observed between the curves in Figure 5.8 happen mainly at the beginning and end part of the melting cycle. The reason for this may be related to the assumption that melts occur only when $\langle \bar{T} \rangle = 0$. This is true at a point location scale but may not be true at areal scale. Some snowmelt can be expected even when $\langle \bar{T} \rangle$ is below freezing, especially when the mean temperature is close to the freezing temperature. This assumption could underestimate the cumulative snowmelt.

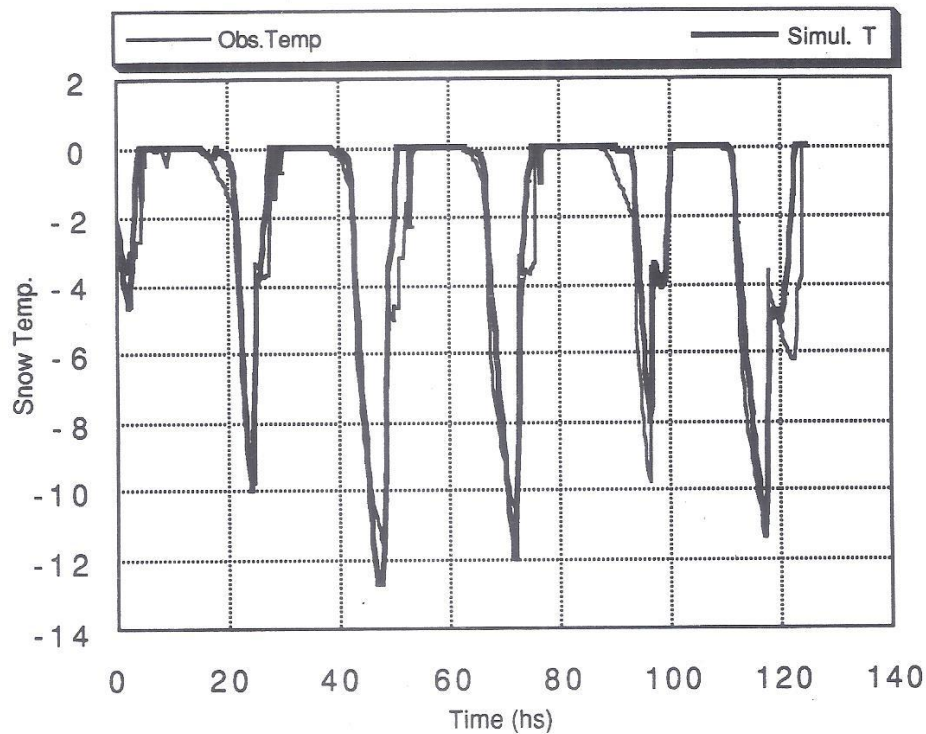


Figure 5.7 "Observed" versus calculated Spatial Snow Temperature

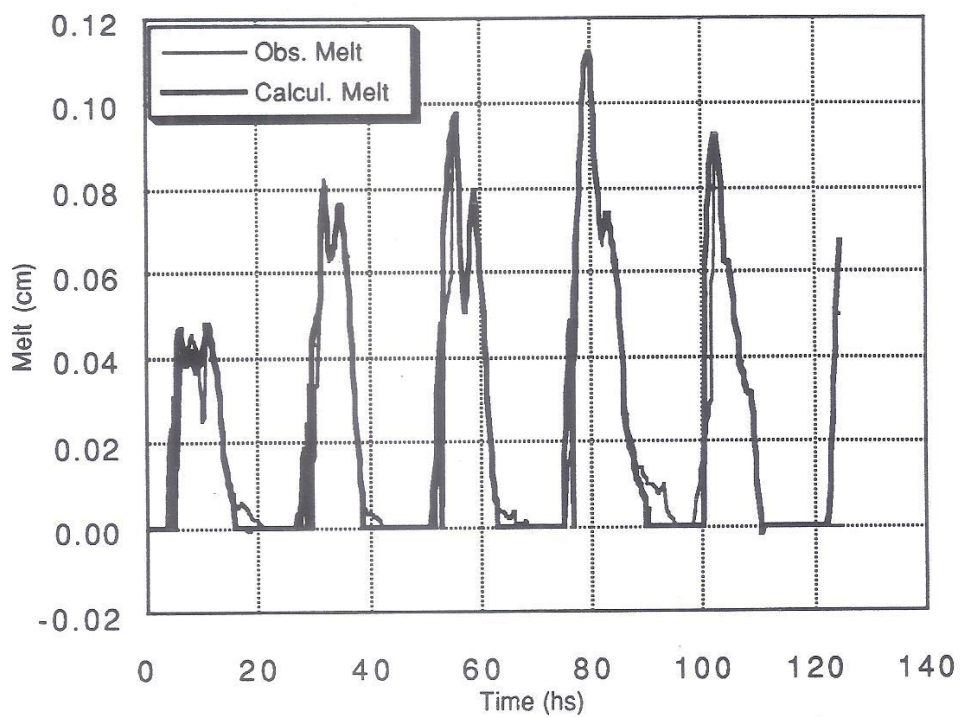


Figure 5.8 "Observed" (Obs. Melt) versus model calculated (Calcul. Melt) areal average snowmelt.

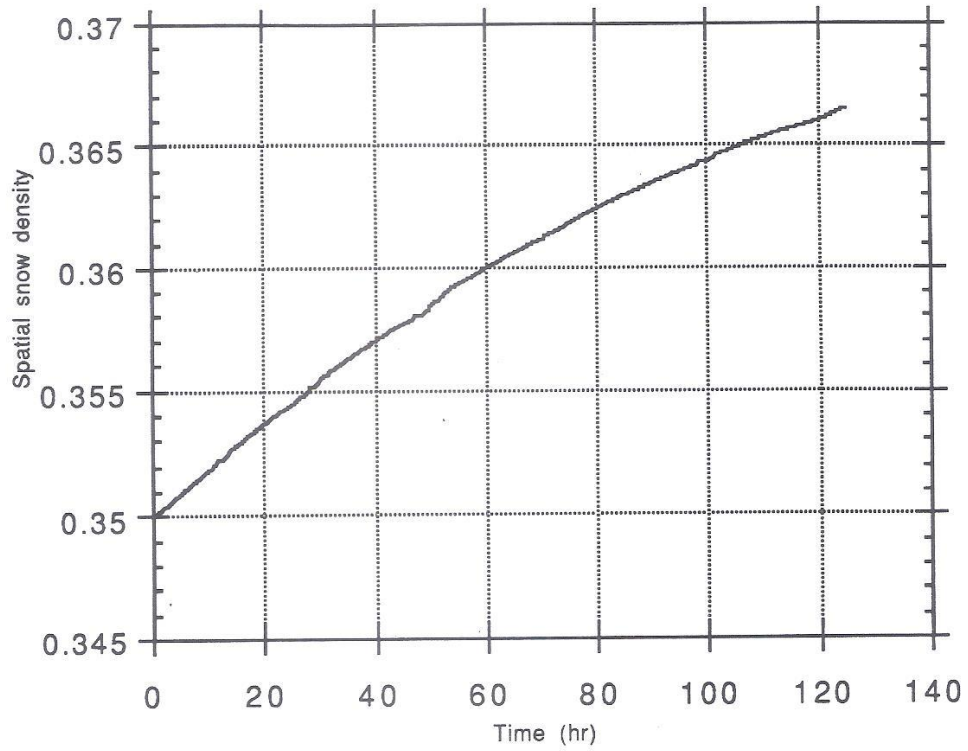


Figure 5.9 Model calculated Spatial snow density.

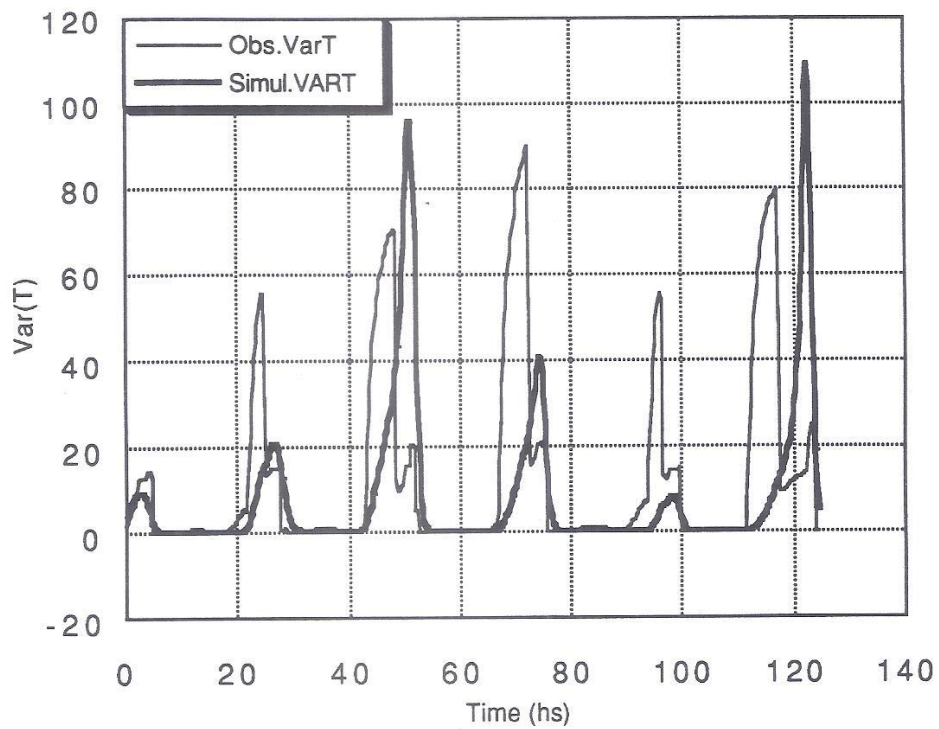


Figure 5.10 "Observed" (Obs. VarT) versus model calculated (Simul. VART) snow temperature areal variance.

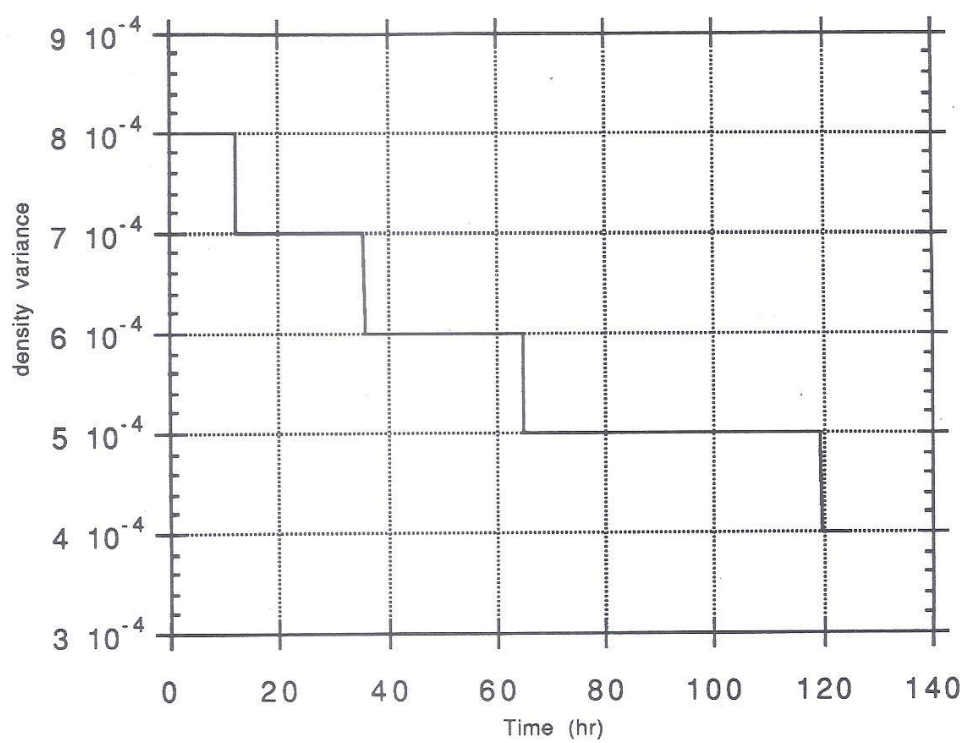


Figure 5.11 Calculated snow density areal variance.

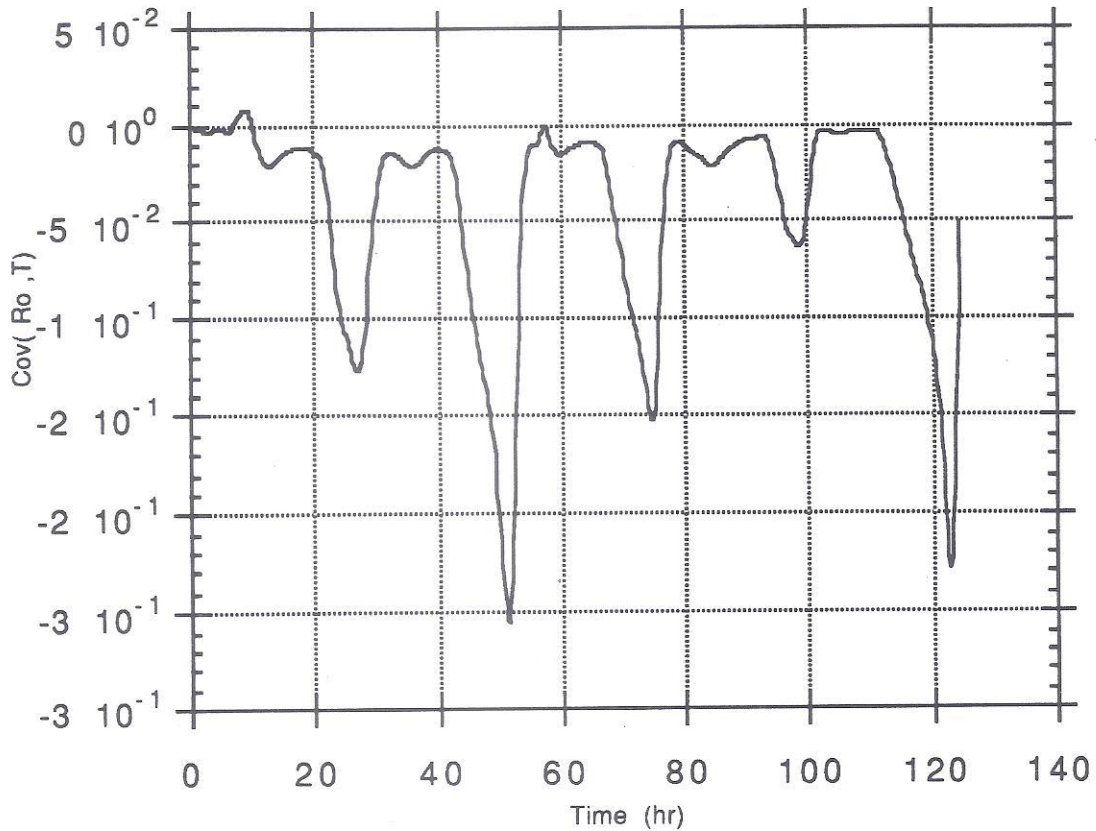


Figure 5.12 Calculated spatial covariance of snow density with snow temperature.

5.5. CASE 3: SPATIALLY AVERAGED ESTIMATIONS AT SCOTT VALLEY

A more realistic application was carried out in order to test the model performance. All the information available at Scott Basin area were used to compare observed areally averaged snowmelt with the areal mean snowmelt calculated by using the methodology developed in this study. The developed spatial model was loaded with averaged meteorological data of the basin and results were compared with areally averaged observed snowmelt of the area.

The calculation period used was again from April 6 at 4 AM to April 18 at 12 PM and the time interval was fixed to be 15 minutes. In Table 5.1, the

sources of the input data are indicated. And in Appendix C the input data series, used for the study period, are displayed graphically.

Averaged variable	Data source	Observations
Air Temperature Ta	Scott Mountain, C. Baldy, Callahan, Q. Hill	Readings at every 3 hr linear interp. at 15 min.
Relative Humidity RH	Scott Mountain, C. Baldy, Callahan, Q. Hill	
Short Wave Rad. sw	Red Bluff	Adjusted to Scott Valley Basin
Wind Speed	C. Baldy, Callahan, Q. Hill	
Snow water equiv. SWE	Scott Mountain, Peterson Q. Hill, M. Boulder	Negative readings eliminated Daily accum. used

Table 5.1. Scott Valley Basin data used in the model.

The variability of the observed areal average snowmelt can be noticed in Figure 5.13. Four out of five stations present similar values while Middle Boulder exceed the others significantly in magnitude. Given that we don't have any information on how representative these observation sites are of the Scott Valley Basin area, Middle Boulder was included in the averaging with the same weight as the other stations.

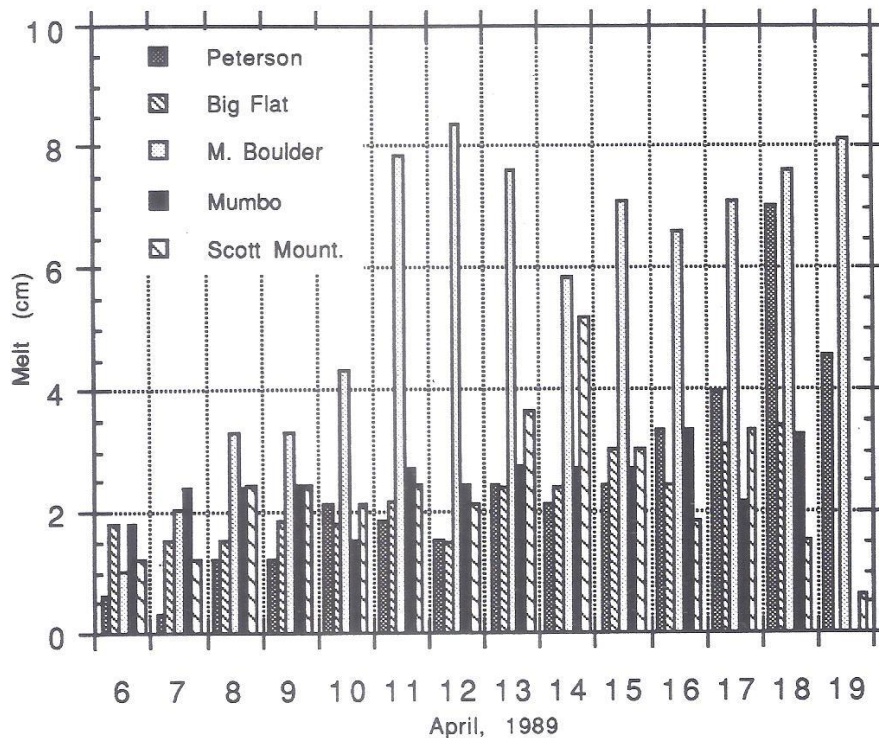


Figure 5.13 Measured snow melts at 5 stations in the study area.

5.5.1. RESULTS

Several runs were performed in order to find the best combination of initial values to fit the daily cumulative observed snowmelt. In the calibration process, emphasis was put on initial conditions rather than on the parameters values such as bulk turbulent transfer De and Dh , albedo coefficient, and snow water content Wo . Much can be said about the parameterization of the snowpack properties and the energy fluxes. The parameter values can always be improved, depending on the accuracy and density of the input data and observed output variables. This is not a particular problem of the developed model, but a common feature of any physics-based, depth averaged, energy budget snowmelt model. However, we will concentrate on the results related to the spatial features of the model, the central topic of this research.

On the other hand, more information about atmospheric conditions and snow cover state (reflectivity, grain size, thermal conductivity, etc.) is needed to physically base the estimation of these parameters. Consequently, the parameter values were taken from the literature.

During the calibration runs, it was observed that increasing the initial value of $\langle \bar{\rho} \rangle$ produces lower peaks in $\langle \bar{T} \rangle$ and $\text{Var}(\bar{T})$. An increase of density is associated with a quadratic increase of thermal conductivity. In a more conductive medium, a deeper snow layer becomes active keeping the fluctuations in temperature within a smaller range. As a consequence, can be expected a decrease in the $\text{Var}(\bar{T})$ when snow density decreases.

It was also observed that $\text{Var}(\bar{T})$ is very sensitive to initial values of $\text{Var}(\bar{\rho})$. Increasing $\text{Var}(\bar{\rho})$ by 0.001 results in high peaks of $\text{Var}(\bar{T})$. This effect again seems to be controlled by the relation between $\bar{\rho}$ and $\bar{\lambda}$, which turns out to be very important in the spatial dynamics. By adjusting the initial values it was possible to reproduce fairly well the observed snowmelt.

In Figure 5. 14, the calculated and observed areally averaged daily cumulative snowmelts are displayed. According to this figure there is a good agreement between calculated and observed daily melts. However, there is an underestimation of the calculated values. The observed melt during the study period sums to 49 cm whereas the calculated value is 46 cm. It is difficult to find a methodological explanation for the differences because several factors may be contributing :

- . The assumption stipulating that snowmelt occurs when $\langle T \rangle = 0^{\circ}\text{C}$ (explained in section 5.4)
- . Measurement errors. The variability of observed snowmelt is mainly given by one site (Middle Boulder) which may deviate the observed average melt upward beyond its real value.
- . Incorrect parameter values.

There is a similar tendency between incoming energy and daily melting. Figure 5.15 represents the total energy balance ($G_1 + sw$). It can be noticed that the positive net balance during this period yields an important quantities of snowmelt. Short wave radiation and air temperature during the period are the main contributing factors for the snowmelting. At the 9th simulation day (~190 hr) the snow temperature (Figure 5.16) is maintained at

0°C during the night. This is a particular long period where the snow stayed at the same temperature altering the compacting rate, and producing a visible effect in the snow density curve (Figure 5. 18).

The $\text{Var}(\bar{T})$ has a fluctuating behavior in correlation with the snow temperature as shown in Figure 5.17. According to Figure 5.17 it can be expected a higher degree of space homogeneity in the snow cover temperature at high levels of temperature than at low levels. In other words, maximum homogeneity can be achieved about noon time during the melting season. It can also be perceived that the peaks of $\text{Var}(\bar{T})$ diminish with time (Figure 5.17), which may be related to the variation of snow density. The increase of $\langle \bar{\rho} \rangle$ due to compacting is associated with a quadratic increase of $\langle \bar{\lambda} \rangle$ by equation (3.37.c) that produces smaller fluctuations in the $\text{Var}(\bar{T})$.

The behavior of CO ($\bar{\rho}, \bar{T}$) is dictated mostly by the spatial variation of temperature which is relatively larger with respect to the spatial variation of density. In Figure 5.20, a decay can be observed in the magnitude of the peaks analogous to the behavior of $\text{Var}(\bar{T})$.

According to Figure 5.14, the spatial model is capable of simulating the areal average snowmelt for the conditions presented in Scott Basin. Eventually, a better fit can be obtained by developing a parameter estimation scheme which will be based upon topography data, satellite information, wind profiles, stability parameters, vegetation, etc. However, the information available and used in this model are the usual data a hydrologist would have for any real application.

Additionally, a comparison of snowmelt resulting from the spatially averaged approach and from the point location approach was made. To accomplish this purpose, the same input data, used to calculate $\langle M \rangle$ were also applied to estimate M at a point location by considering the variance and covariance terms as zero. The point location approach represents the traditional way in which the snowmelt is estimated by using point location physical relationships under areally averaged inputs.

In Figure 5.21 observed, spatial model calculated and point-location model (with areally averaged inputs) calculated areal mean daily snowmelt values can be compared. The accumulated value for "point M" during the simulation period sums to 39 cm which is below the other two cumulative values (46 and 49). The dissimilar distribution of these daily values with time can be observed. Disagreements in calculated snowmelts by these two methods

are mainly due to differences in the calculated melting period during a day. The difference in melting period duration as a result of applying point location and spatial average methods is not easy to explain because this difference depends on the spatial variability of $\langle \bar{T} \rangle$ and $\langle \bar{\rho} \rangle$ throughout the period of simulation. In order to visualize the causes of these differences, an analysis of the energy equation is made in the next section.

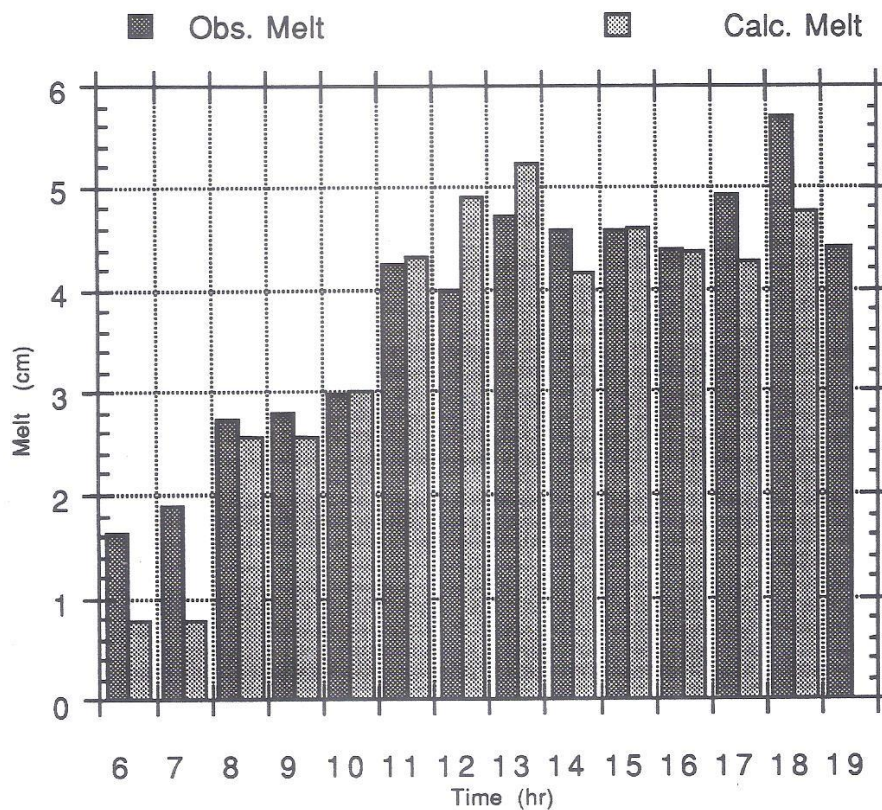


Figure 5.14 Comparison of measured averaged snowmelt (Obs. Melt) and model calculated areally averaged snowmelt (Calc. Melt).

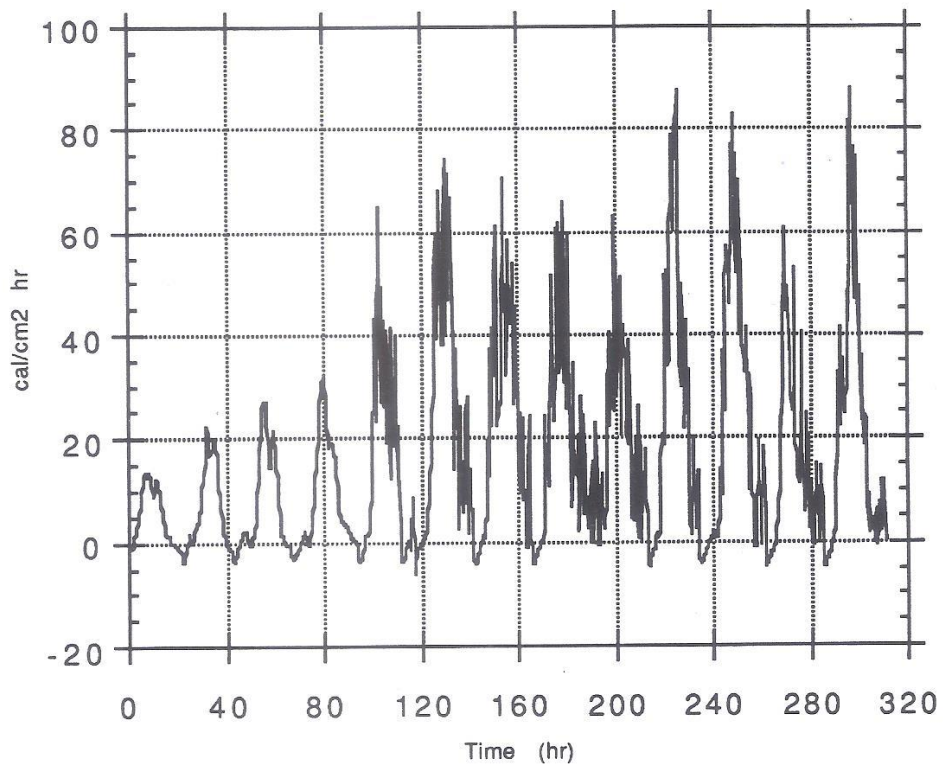


Figure 5.15 Net energy balance resulting from the averaged input data in Scott Valley Basin for the study period.

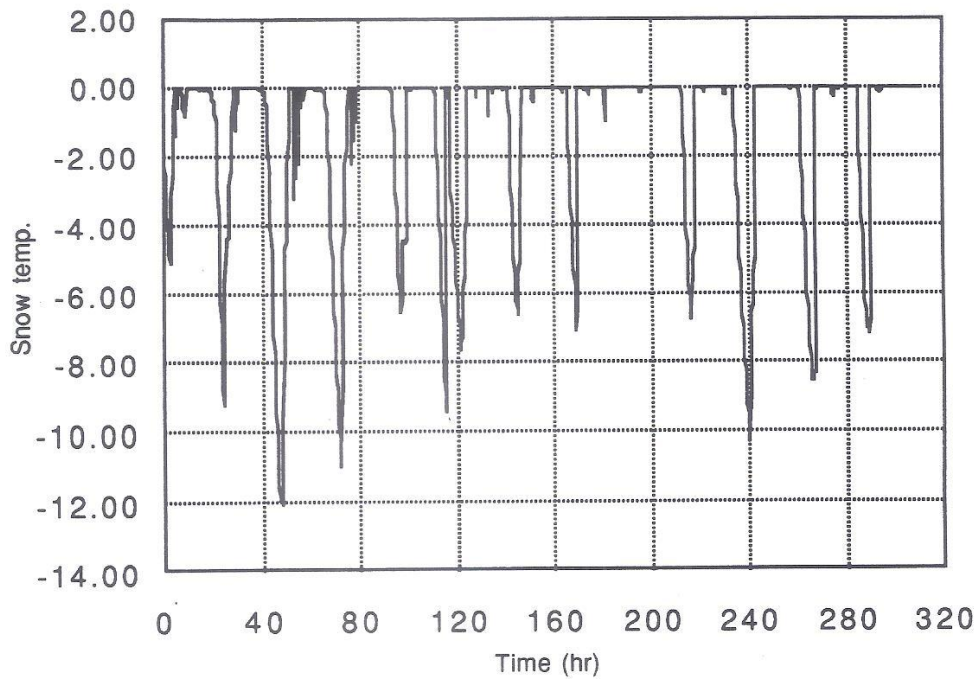


Figure 5.16 Areal average snow temperature for Scott Valley Basin.

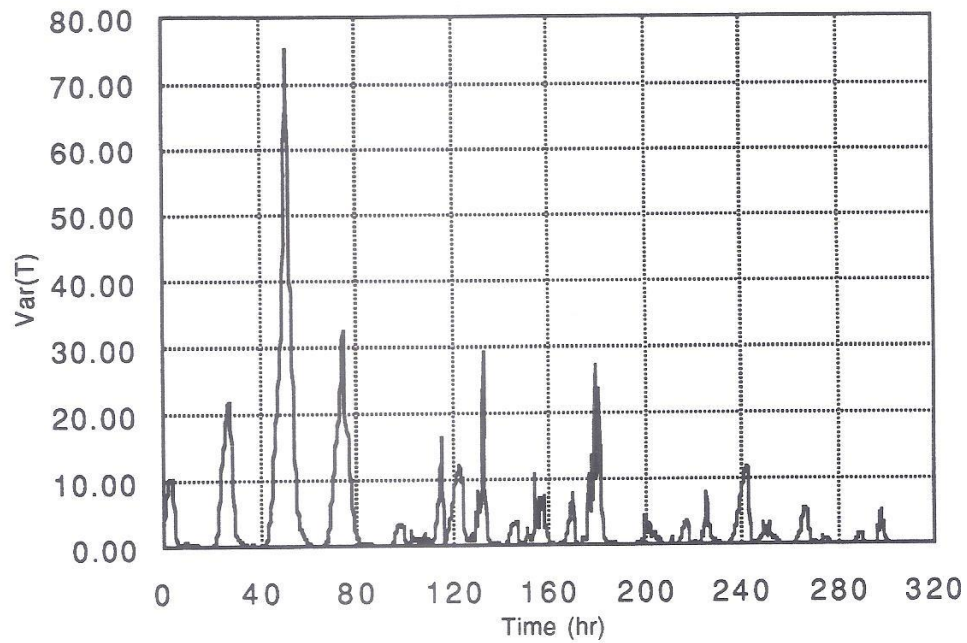


Figure 5.17 Areal averaged temperature variance for Scott Valley Basin.

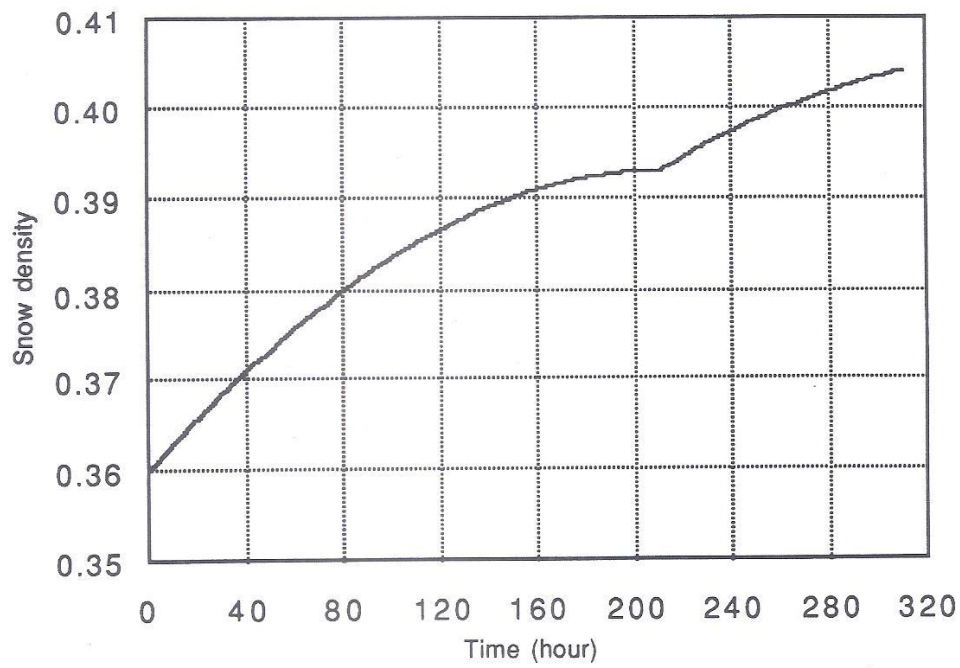


Figure 5.18 Arealley averaged snow density for Scott Valley Basin.

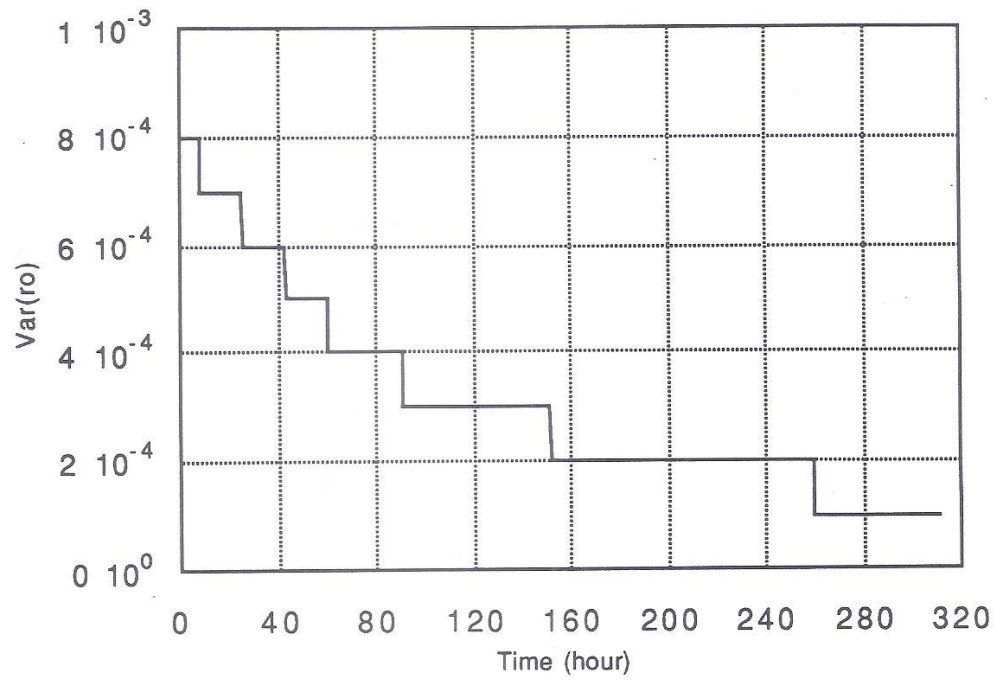


Figure 5.19 Snow density areal variance for Scott Valley Basin.

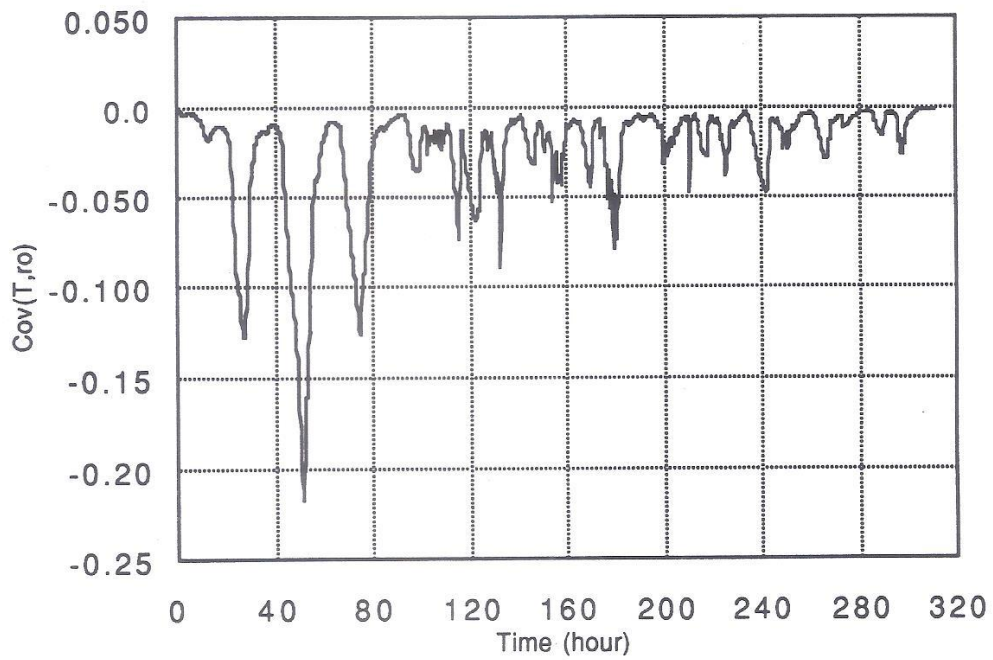


Figure 5.20 Areal covariance of snow temperature with density for Scott Valley Basin.

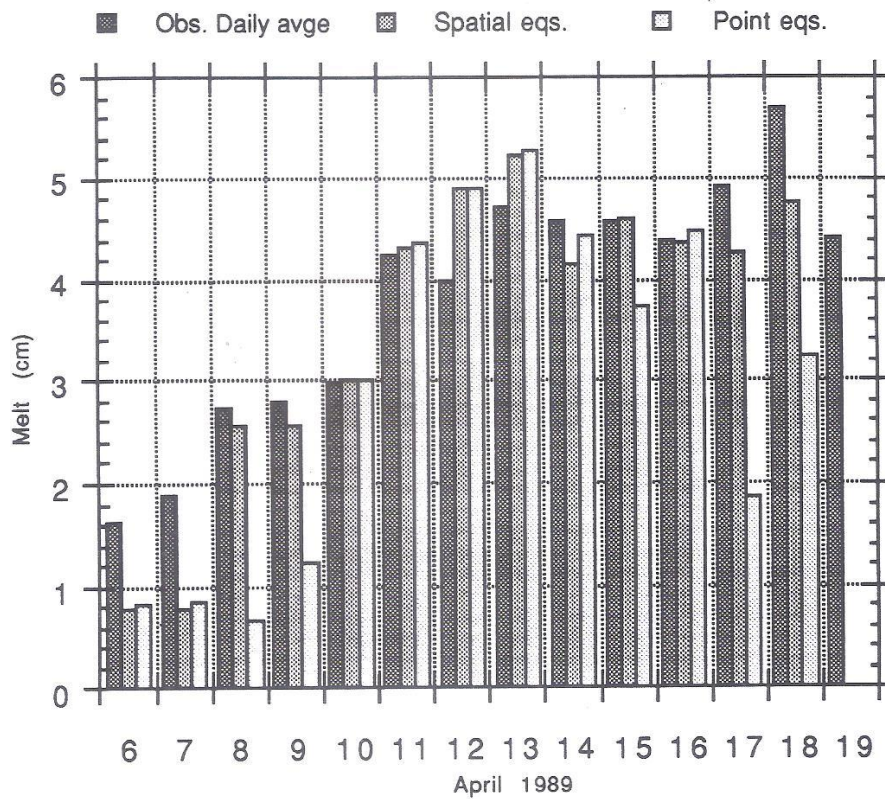


Figure 5.21 Comparison of measured areally averaged snowmelt and areal mean snowmelts calculated by spatial and point approaches.

5.5.1.1. CONTRIBUTION TO THE SPATIAL TEMPERATURE VARIATION

In order to understand the role of the spatial parameters in the average model, an analysis of equation (4.4) was made (see Appendix A). This energy equation estimates the mean snow cover temperature rate and also expresses the energy exchanged by the pack. The structure of equation (4.4) can be expressed as:

$$\frac{d\langle\bar{T}\rangle}{dt} = \text{Point Equat.} + \alpha \text{ Var}(\bar{T}) + \beta \text{ Var}(\bar{\rho}) + \delta \text{ Cov}(\bar{\rho}, \bar{T}) \quad (5.1)$$

The evaluation of each term of (5.1) was done during the running of the spatial model for the application to Scott Valley Basin. For the sake of clarity, the following analysis was done over the first 48 hours of the simulation period. Each term of (5.1) was expressed as a part of the total change of $\langle\bar{T}\rangle$ which occurred during the time interval (15 minutes).

In Figure 5.22 the areal mean snow temperature $\langle\bar{T}\rangle$ for the selected period of 48 hours is presented as a reference. Figure 5.23 shows the relative contribution (in absolute values) of the four terms of equation (5.1) to the change experienced in $\langle\bar{T}\rangle$ during the 48 hours period. These contribution are expressed as portions between 0 and 1 of $(d\langle\bar{T}\rangle/dt)$. At a first glance the importance of spatial variability in the snow cover dynamics can be seen. Note that the influences of first (point equations) and second ($\text{Var}(\bar{T})$) terms with respect to the $\text{Var}(\bar{\rho})$ and $\text{CO}(\bar{\rho}, \bar{T})$ terms, are greater.

According to Figures 5.22 and 5.23, when $\langle\bar{T}\rangle < 0$, the contribution of the term involving the $\text{Var}(\bar{T})$ is very important. However, when $\langle\bar{T}\rangle = 0$ the point location equation dynamics can explain most of the changes of $\langle\bar{T}\rangle$ (that is actually small). The transition from $\langle\bar{T}\rangle < 0$ to $\langle\bar{T}\rangle = 0$ appears to be influenced by the spatial variance. Therefore, one of the differences between the point location and spatial average approaches seems to be the lengthening and shortening of the melting period. This should give a different amount of snowmelting and/or a different distribution of this amount over time.

The relative contributions of $\text{Var}(\bar{\rho})$ and $\text{CO}(\bar{\rho}, \bar{T})$ are shown in Figure 5.25 and Figure 5.24, respectively. According to Figure 5.24, the influence of the spatial variability of $\bar{\rho}$ is maximum during the melting periods. $\text{Var}(\bar{\rho})$ fluctuates within a small range, showing two cycles during the day. When $\langle\bar{T}\rangle = 0$, the

variation of $\text{Var}(\bar{\rho})$ may be due to the changes in snow cover depth as a consequence of snowmelt that takes place at that temperature. When $\langle \bar{T} \rangle < 0$ during the night, fluctuation occurs due to the compacting of the snow cover controlled by the decreases in snow temperature.

From Figure 5.23 it can be concluded that the spatially averaged snowmelt dynamics is given by a different physical structure than the one described by the point location equations. Therefore, different results should be expected.

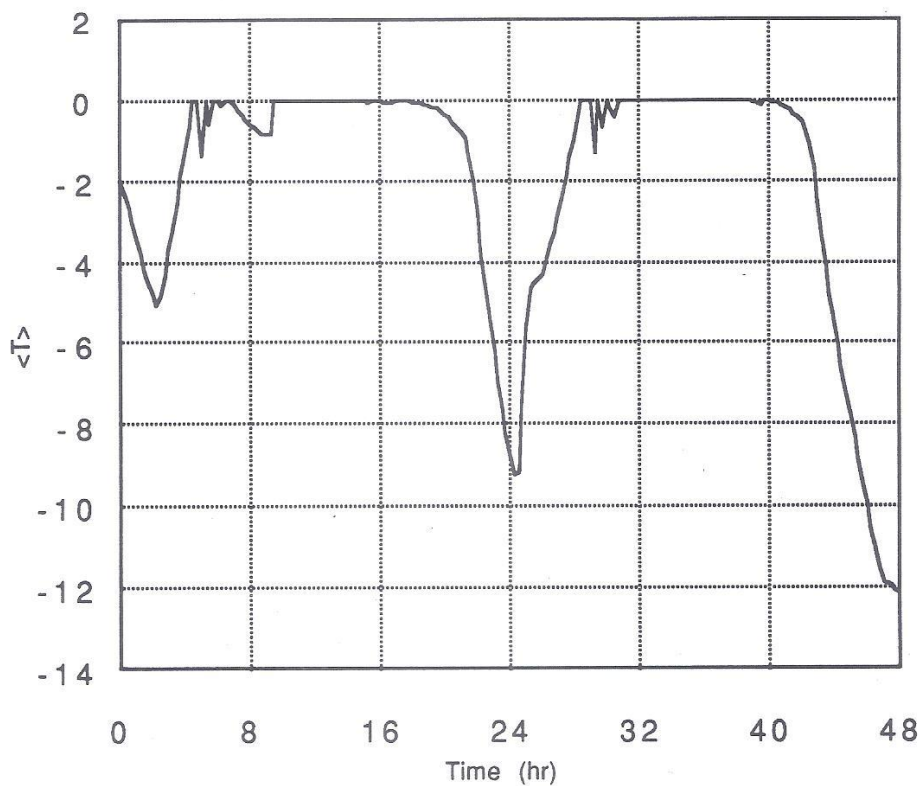


Figure 5.22 Calculated areal mean snow temperature for 48 hr period at Scott Valley watershed.

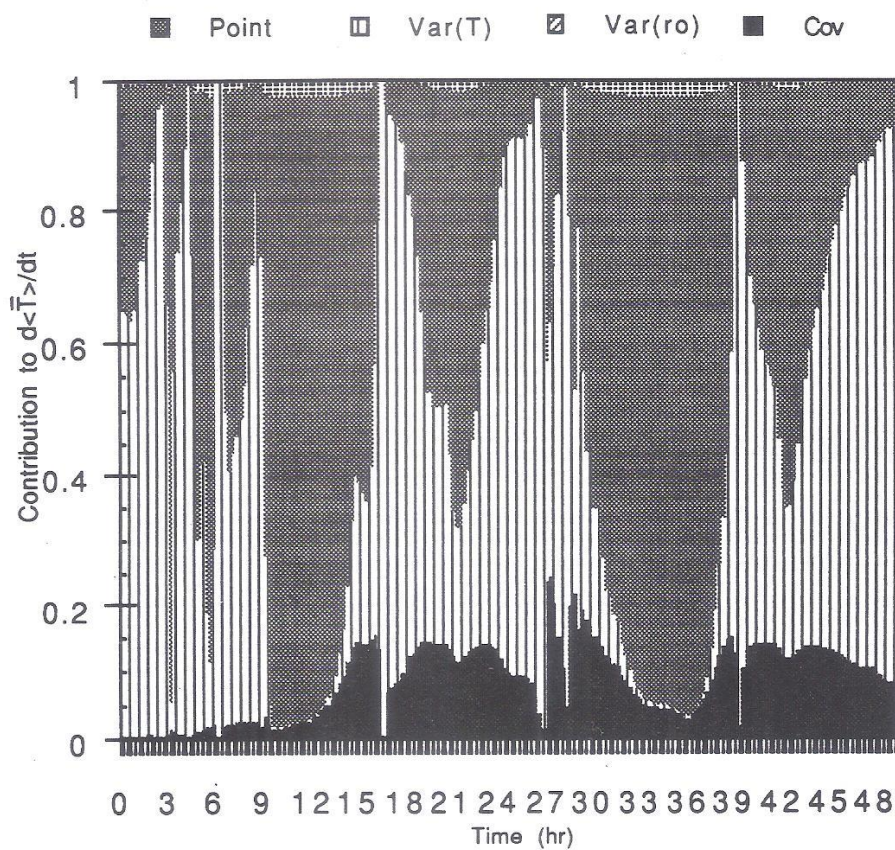


Figure 5.23 Relative contribution of terms in Eq. (5.1) to the spatial variation of the snow temperature

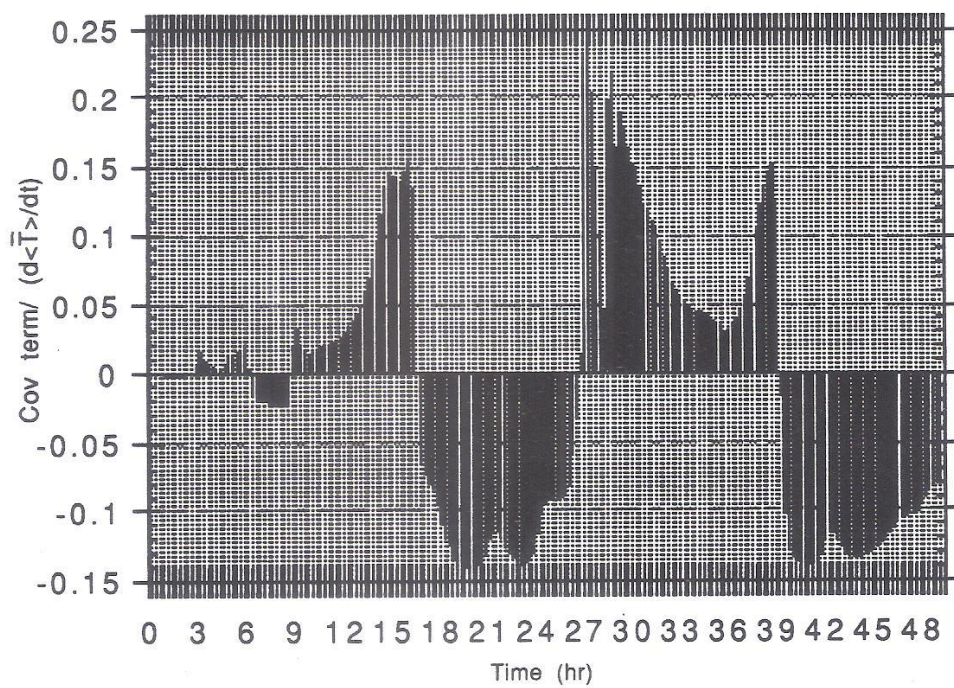


Figure 5.24 Contribution of the covariance term to the variation of snow temperature.

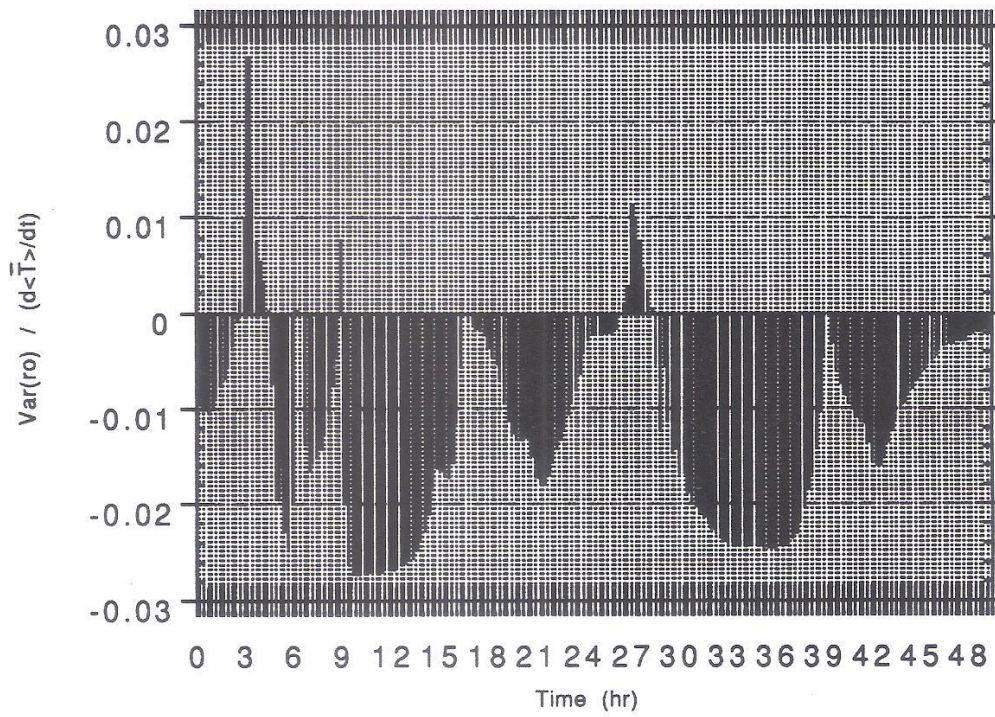


Figure 5.25 Contribution of the spatial variance of snow density term in Eq. (5.1) to the changes in $\langle T \rangle$.

CHAPTER VI.

6. CONCLUDING REMARKS

In this thesis a physics-based model of the snow cover is developed. The derived spatially averaged equations were based on the conservation of mass and energy at a point location. These equations relate the thermodynamic processes occurring in the snowpack with the energy fluxes exchanged with the surroundings. The spatially averaged equations were developed under the fundamental assumption that the snowmelt process is spatially ergodic over an area.

Each flux of the energy balance was estimated on the basis of the physics involved in each transfer mechanism. A linear expression for the energy balance was obtained as a function of the snow temperature. The input meteorological data required by the model for the energy budget estimation are: air temperature, relative humidity, wind velocity and short wave radiation.

In order to average the point location equations over the snow depth, a model for the snowpack was adopted. The main assumptions were: a) a linear relationship between snow temperature and freezing depth; and b) the snowpack includes two layers separated by the freezing depth. The upper layer is composed of dry snow whereas the lower layer holds a constant amount of water, W_0 . Using these assumptions, the point location equations were integrated over the snow depth using the Leibnitz rule of differentiation. An equation for the compacting effect of the pack was included in the depth-averaged equation system (DAE). The compacting or density variation of the snowpack was assumed to depend on the mechanical pressure and temperature variations of the snow.

The DAE system was then averaged over the snow cover area. The technique used in this averaging process relied on the Taylor series expansion of the DAE around the spatial mean snow temperature and spatial mean snow density. This technique is based upon the ergodicity of the spatial snowmelt process. Snow temperature and snow density were considered to be the better descriptors of snowmelt variability in space. A closed system of ordinary differential equations was obtained. These equations represent the thermodynamics processes occurring in the snow cover and are functions of

the first and second spatial moments of $\bar{\rho}$ and \bar{T} . The equation system was solved by using Runge- Kutta numerical technique.

Scott Valley Basin data was used in order to test the model. The spatial model results were compared with observed daily snowmelts. Based on the comparison, the model performed satisfactorily. It was capable of reproducing the observed snowmelt at a point location (Scott Mountain) and at the basin scale as well. At the basin scale, the areal average snowmelt calculated by the model was compared with the observed areal average snowmelt from 5 observation point locations.

The following conclusions and recommendations for future investigations may be stated:

1. The results of the spatial model developed in this study are in agreement with observed data. The magnitude and tendency of the measured daily snowmelt (basin averages) are reproduced satisfactorily by our spatial model. Additionally, the developed model performs well as a point location model when its results are compared with observed point location SWE data and with the results from another point location model. Therefore, the model performs well, independently of the scale of application, i.e., either point location scale and spatial areal scale.
2. There is evidence that the spatial model captured the spatial variability of the snow cover. Spatial snow temperature variance from the developed model agreed with the temperature variance estimated by point location simulations. The spatial model includes the spatial variability of snow temperature and snow density in the snow cover. This is an important departure from the traditional point location application. As a consequence, results obtained with the spatial average model differ from those obtained with the traditional point location model. Better concordance with areal observations is obtained with the spatial model.
3. The methodology which was used to develop a spatially averaged expression for snowmelt in this research can be applied to other physical processes involved in the hydrological sciences.

4. Although the results of the spatial model are in agreement with observed data, from a rigorous point of view, the model should also be tested over a wide range of snow cover and climate conditions. In addition, precise observed hourly SWE data is necessary for comparison with model results at time scale appropriate for the snowmelt dynamics. A large number of observation points that provide meteorological and snow cover data are essential for a conclusive validation of the approach. Intermediate scale of application between point location and basin areal scale is necessary to evaluate the independence of the model on the scale of the simulation.

5. The averaging procedure applied to the snowmelt processes allow for modifications in the method used to estimate the energy balance. There is a wide range of available energy budget techniques, depending on which components of the balance are measured directly and which empirical equations are used to estimate the others. Depending on the purpose of the application and on the available data, other techniques may be more adequate than the energy budget method included in the model developed in this research. For example, temperature index approach may be used in the model when only air temperature measurements are available. Additionally, satellite imagery and mesoscale climatic models can be very useful elements by providing spatial input for the model. The spatial approach could then be used in the analysis of snowmelt variations under the hypothesis of climate changes.

6. The movement of water within the snowpack is neglected in this model. The assumption of instantaneous release of water out of the pack is unrealistic. A spatial expression for the flow moving through the snow should be added to the model. The flow of water through the snow is subject to properties that depend on the metamorphic state of the snow. This makes it difficult to estimate the flows. However, this model makes it easier to solve the problem because it calculates a mean freezing depth which separates dry and wet snow layers. The freezing depth defines a boundary condition for the water that flows in the wet layer.

7. Future research is necessary to determine when, where, and how the snow cover area should be divided in order to make better use of the model.

Although the equations are expressed as functions of the spatial variability of the main physical properties of the snow cover, some differences in the characteristics of the area may justify subdivision of the study area. Seasonal and perennial snow covers are subject to different rates of compacting and different density-heat conductivity relationships. Climatic differences on the windward and leeward sides of a mountainous system should also be considered. Even short wave radiation captured by the snow may be very dissimilar from one snow cover area to another due to differences in albedo, exposition or vegetation. Therefore, it is important to establish a criterion for considering which characteristic should be preserved in a "homogeneous unit" of the snow cover area. Obviously, a division of the study area is also subject to the availability of data representative of each partition.

Nevertheless, with the same amount and quality of information, the spatial model provides better results than the traditional point approach.

REFERENCES

- Aese, J. K. and S. B. Idso, A Comparison of Two Formula Types for Calculating Long Wave Radiation from the Atmosphere, **Wat. Res. Research**, 14, pp. 623-625, 1978.
- Abbott, M., J. C. Bathurst, J. A. Cunge, P. E. O'Connell and J. Rasmussen, An Introduction to the European Hydrological System, "SHE", **Journal of Hydrology**, 87 pp 45-59, 1986.
- Akitaya, E., **IAHS- AISH**, Publication No 114, pp. 42-48, 1975.
- Anderson, E., A Point Energy and Mass Balance Model of a Snow Cover, **NOAA Technical Report NWS 19**, 150 pp., US Dept of Commerce, 1976
- Angstrom, A., Solar and Terrestrial Radiation, **Quarterly Journal of the Royal Meteorological Society**, 50, pp. 121-125, 1924.
- Bader, H., R. Haefeli, J. Bucher and others, Der Schnee und Seine Methamorphose, English Translation 14, Snow, and its Metamorphism in Snow, Ice and Permafrost Research Establishment, 313 pp., 1939.
- Bader, H., Sorge's Law of Densification of Snow on High Polar Glaciers, Res. Rep. No 2, **US Army Snow, Ice and Permafrost Res. Establ. Hanover**, New Hampshire, 1953.
- Bauwens, W., Snowmelt Models with Different Degree of Complexity Applied to Shallow and Short-Living snowpack in Lowland Basins, **Proc. of the 45th Eastern Snow Conf.** , Lake Placid, June 1988.
- Bloschl, G. and R. Kirnbauer, Point Snowmelt Models with Different Degrees of Complexity-Internal Processes, **Journal of Hydrology**, 129, pp 127-147, 1991.

Bloschl, G., R. Kirnbauer and D. Gutknecht, Distributed Snowmelt Simulations in an Alpine Catchment, 1. Model Evaluation on the Basis of Snow Cover Patterns, **Wat. Res. Research**, vol 27, N12, pp 3171-3179, (1991)

Bohren, C. F. and B. R. Barkstrom, Theory of Optical Properties of Snow, **Journal of Geophys. Res.**, Vol. 79, No 30, pp. 4527-4535, 1974.

Brunt, D., Physical and Dynamical Meteorology, **Cambridge University Press**, Cambridge, Mass., 1952.

Brutsaert, W., On a Derivable Formula for Long-wave from Clear Skies, **Water Res. Res.**, Vol 11, pp. 742-744, 1975.

Businger, J. A., J. C. Wyngaard, Y. Izumi and E. F. Bradley, Flux-Profile Relationships in the Atmospheric Surface Layer, **J. Atmos. Sci.**, Vol. 28, pp. 181-189, 1971.

Chen, C. L., and T. V. Chow, Formulation of Mathematical Watershed Model, **Journal of Engineering**, ASCE, Vol 97, N EM3, pp 809-828, 1971.

Choudhury, B J., Passive Microwave Remote Sensing Contribution to Hydrological Variables, in **Land Surface-Atmosphere Interaction for Climate Modelling**, edited by Eric Wood, Kluwer Academic Publisher, 1991.

Colbeck, C., Grain and Bond Growth in Wet Snow, in **Snow Mechanics**, IAHS Publ. 114, pp. 51-61, 1975.

Colbeck, S. C., A theory of Water Percolation in Snow, **Journal of Glaciol.**, 11(63), pp 369-385, 1972.

Colbeck, S. C., Classification of Seasonal Snow Cover Crystals, **Wat. Resour. Res.**, 22, pp. 59S- 70S, 1986.

Colbeck, S. C., Grain and Bond Growth in wet Snow, in **Snow Mechanics**, IAHS Publ. 114, pp 51-61, 1975.

Colbeck, S. C., The Vapor Diffusion Coefficient for Snow, **Water Resour. Res.**, Vol 29, No 1, pp. 109-115, 1993.

Davies, J. A., and S. B. Idso, Estimating the Surface Radiation Balance and its Components, in **Modification of the Aerial Environment of Plants**, edited by Gerber and Barfield, ASAE Monograph 2, pp. 183-210, 1979.

de Quervain, M. R., Snow Structure, Heat and Mass Flux Through Snow, Proceeding of Banff Symposium, **Intern. Assoc. Hydrologic Sci. Publ.** No 107, Vol. 1, pp. 203-226, 1973.

DeVries, J. and C. Franke, Evaporation from Snow Fields, Estimation of Potential for Control, Final Report for Hatch Project 3055, Water Science and Engineering Paper 3014, 88 pp., University of California, Davis, 1988.

Dorsey, N. E., Properties of Ordinary Water Substances, Van Nostrand-Reinhold, Princeton, New Jersey, 1940.

Dozier, J., A Solar Radiation Model for a Snow Surface in Mountainous Terrain, Proc. **Modeling Snow Cover Runoff**, edited by Colbeck and Ray, US Army Cold Reg. Res. Lab., Hanover, N.H., pp144-153, 1979.

Dozier, J., et al., Snow Deposition, Melt, Runoff, and Chemistry in a small Alpine Watershed, Emerald Lake Basin, Sequoia National Park, Final Report Contract A3-106-32, 156 pp., **California Air Resources Board**, Sacramento, CA, 1987.

Dozier, J., Recent Research in Snow Hydrology, **Review of Geophysics**, Vol 25, N 2, PP 153-161, 1987.

Dunne, T., A. G. Price and S. C. Colbeck, The Generation of Runoff from Sub-Antartic Snowpack, **Wat. Res. Research** 12(4), pp 677-685, 1976.

Garnier, B. J. and A. Ohmura, The Evaluation of Surface Variations in Solar Radiation Income, **Solar Energy**, Vol. 13, pp. 21-34, 1970.

Geiger, R., *Das Klima der Bodennahen Luftschicht*, English translation by Scripta Technica Inc., **Harvard Univ. Press**, 1961.

Giddings, J. C. and E. La Chapelle, **Journal of Geoph. Resources**, Vol 66, pp. 181-189, 1962.

Hobbs, P. V. and L. F. Radke, **Journal of Glaciology**, 6, 879-891, 1967.

Hobbs, P. V., and B. J. Masson, **Philos. Mag.** [8] 9, 181-197, 1964.

Kojima, K. and H. Motoyama, Melting and Heat Exchange at the Bottom of a Snow Cover, **Ann. of Glaciol.** 6, pp. 276-277, 1985.

Kojima, K., *Densification of Seasonal Snow Cover in Physics of Snow and Ice*, **Proceeding of Int. Conf. on Low Temperature Science**, vol 1, part 2, Sapporo, Japan, 1967.

Kondo J. and T. Yamazaki, A Prediction Model for Snowmelt, Snow Surface Temperature and Freezing Depth Using a Heat Balance Method, **Journal of Applied Meteorology**, 29, pp. 375-384, 1990.

Kondratyev, K., *Radiation in the Atmosphere*, **Int. Geophys. Ser.**, Vol. 12, Academic Press, NY, 1969.

Kutchment, L. S., V. N. Demidov and Y. G. Motovilov, *River Runoff Formation, Physically Based Models*, Nauka, Moskva, 1983.

Kuz'min, P. P.(1961), *Melting of the Snow Cover*, **Gidrometeorol. Izd. Leningrad.**, Translation TT71-50095. Israel Program of Scientific Translation, (1972).

Langham, E. J., *Advanced Concepts and Techniques in the Study of Snow and Ice Resources*, edited by Santeford and Smith, **Nat. Acad. of Sci.**, Wash. DC, pp. 67-75, 1981.

List R. J., Smithsonian Meteorological Tables, **The Smithsonian Institute**, Wash. DC, 1968.

Male, D. H. and D. M. Gray, Snowcover Ablation and Runoff, **Handbook of Snow**, pp 360-436, 1981.

Male, D. H., The Seasonal Snowcover, **Dynamics of Snow and Ice Masses** edited by S. Colbeck, pp 305-395, 1980.

Manz D. H., Interaction of Solar Radiation with Snow, M. Sc. Thesis, Dept. Agr. Eng., Univ. Sask., Saskatoon, 1974.

Martinec, J. and A. Rango, Parameter Values for Snowmelt Runoff Modeling, **U.S. Army, CRREL**, Hannover, NH, pp 269-278, 1986.

Mellor, M., Engineering Properties of the Snow, **Journal of Glaciology**, 19, (81) pp. 15-66, 1977.

Mellor, M., **IAHS-AISH Publ.** No 114, pp. 251-291, 1975.

Mellor, M., Some Optical Properties of Snow, International Symposium on Scientific Aspects of Snow and nIce Avalanches, **Inter. Assoc. Sci. Hydrology Publ.**, 69, pp. 128-140, 1964.

Monin, A. S. and A. M. Obukhov, Basic Laws for Turbulent Mixing in the Ground Layer of the Atmosphere, Trudy 151, **Akad. Nauk. SSSR Geofiz. Inst.**, pp. 163-187, 1954.

Morris, E. M., and J. Godfrey, The European Hydrological System Snow Routine , in **Proceeding: Modeling of Snow Cover Runoff**, edited by C. Colbeck and M. Ray, US Army, CRREL, Hanover, NH., pp 269-278, 1975.

Morris, E. M., Sensitivity of the European Hydrological System Snow Model, in Hydrological Aspects of Alpine and High Mountain Areas, edited by J. W. Glen, IAHS Publ. 138, pp. 221-231, **International Association Hydrologic Science**, Wallingford, UK, 1982.

Morris, E. M., Snow and Ice in **Hydrological Forecasting** edited by M. Anderson and T. P. Burt, pp. 154-182, 1985.

Morris, E. M., Modelling the Flows of Mass and Energy within a Snowpack for Hydrological Forecasting, **Annals of Glaciology**, 4, International Glaciological Society, U.K., 1983.

Motovilov, Yu G., A Model for Snow Cover Formation, in **Modeling Snow Processes** edited by E. M. Morris, IAHS Publ. No. 155, 1986.

Munn, R. E., Descriptive Micrometeorology, **Academic Press**, NY, (1966)

Murdock, J., Perturbation Theory and Methods, Willey Interscience, 1991.

Obleid, Ch. and B. Rosse, Mathematical Models of Melting Snowpack at an Index Plot, **Journal of Hydrol**, 32(1977), pp 139-163, 1977.

Obleid, Ch. and H. Harder, **Modeling Snow Cover Runoff**, edited by Colbeck and Ray, US Army Cold Reg. Res. Lab., Hanover, N.H., pp. 179-204, 1979.

Oke, T. R. and F. G. Hannell, Variation of Temperature within a Soil, **Weather**, Vol. 21, 21-8, 1966.

Paltridge, G. W., and C. M. Platt, Radiative Processes in Meteorology and Climatology, 318 pp. **Elsevier**, Amsterdam, 1976.

Perla, R., Temperature Gradient and Equitemperature Metamorphism of Dry Snow, Paper presented at **Deuxieme Rencontre Internationale sur la Nieve et les Avalanches**, Grenoble, France, 1978.

Prandtl, L., Meteorologische Anwendung der Stromungslehre, **Beitr. Phys. D. Freien Atmos.**, Vol. 19, pp. 188-202, 1932.

Smith, J. L., Hydrology of Warm Snowpacks and Their Effects Upon Water Delivery...Some New Concepts, in **Advances Concepts and Techniques in the Study of Snow and Ice Resources**, compiled by H. S. Santeford and J. L. Smith, National Academy of Sciences, Was. pp. 76-98, 1974.

Suckling, P. W. and J. E. Hay, A Cloud Layer-Sunshine Model for Estimating Direct, Diffuse and Total Solar Radiation, **Atmosphere**, Vol. 5, pp. 194-207, 1976.

Suits, R. D., California Snow Sensor Performance, Master's Thesis, Department of Civil Eng., Univ. of California, Davis, 1986.

Swinbank, W. C., A Comparison Between Predictions of Dimensionless Analysis for the Constant-Flux Layer and Observation in Unstable Conditions, **Q. J. R. Meteor. Soc.**, Vol. 94, pp. 460-467, 1963.

Unsworth, M. H. and J. L. Moneith, Long-wave Radiation at the Ground and Angular Distribution of Incoming Radiation, **Q. J. R. Meteorological Society**, 101, pp. 13-24, 1975.

van der Heydt, L., Application of a Point Energy Balance Model of a Snow Cover, M. Sc. Dissertation, Department of Civil Eng., University of California, Davis, 1991.

Wankiewicz, A., A Review of Water Movement in Snow, edited by S. C. Colbeck and M. Ray, Proceeding of Meeting, NH, U. S. Army CRREL, pp 222-252, 1978.

Williams, L. D., Application of Computed Global Radiation for Areas of High Relief, **Journal of Applied Meteorology**, 11, pp 526-533, 1972.

Wood, E., **Land Surface-Atmosphere Interaction for Climate Modelling**, edited by Eric Wood, Kluwer Academic Publisher, 1991.

World Meteorological Organization, Intercomparison of Models of Snowmelt Runoff, **WMO Operational Hydrology**, Rep. 23 Publ. 646, Geneva, 1986.

Yen, Y. C., Effective Thermal Conductivity of Ventilated Snow, **Journal of Geophysics Res.**, 67, pp 1091-1098, 1962.

Yosida Z., and Colleages, Physical Studies on Deposited Snow. I. Thermal Properties, **Contribution from the Institute of Low Temperature Science**, No 7, Sapporo, Japan, pp. 19-74, 1955.

Zuzel, J. and L. Cox, Relative Importance of Meteorological Variables in Snowmelt, **Wat. Res. Research**, Vol 11, N 1, 1975.

Appendix A.

The derivatives of $a_{(T,p)}$, $b_{(T,p)}$ and $c_{(T,p)}$ with respect to T and p as defined in Chapter III were substituted in equations (4.7) , (4.8) , (4.12) , (4.13), (4.18) , (4.20) . The expressions obtained are displayed in the following page. This formulation may be simplified by algebra manipulations. However, it is presented in a way that can be related to the structure of the expressions developed in Chapter IV. For the sake of clarity some abbreviations were adopted:

$$cd1 = 2 A \bar{T} c1 + B \bar{T}^2 c1 - A c2$$

$$\lambda = (k1 + k2 \bar{\rho}_s^2)$$

$$c1 = \text{specific heat of ice (Cp)}$$

$$c2 = W_o L_f$$

$$\begin{aligned}
d\langle T \rangle / dt &= \frac{(A + B T)^2 (A + B T + sw)}{2 cd1 \lambda \rho_s} + \\
0.5 \text{Var}(\rho_s) &\left(\frac{k2 (A + B T)^2 (A + B T + sw)}{cd1 \rho_s \lambda^2} + \right. \\
&\frac{4 \rho_s k2^2 (A + B T)^2 (A + B T + sw)}{cd1 \lambda^3} + \\
&\left. \frac{(A + B T)^2 (A + B T + sw)}{cd1 \lambda \rho_s^3} \right) + \\
\text{cov}(T, \rho_s) &\left(\frac{B k2 (A + B T)^2}{cd1 \lambda^2} - \frac{B (A + B T)^2}{2 cd1 \lambda \rho_s^2} - \right. \\
&\frac{2 B k2 (A + B T) (A + B T + sw)}{cd1 \lambda^2} - \frac{B (A + B T) (A + B T + sw)}{cd1 \lambda \rho_s^2} + \\
&\frac{k2 (A + B T)^2 (2 A c1 + 2 B T c1) (A + B T + sw)}{cd1^2 \lambda^2} + \\
&\frac{(A + B T)^2 (2 A c1 + 2 B T c1) (A + B T + sw)}{2 \lambda cd1^2 \rho_s^2} + \\
0.5 \text{Var}(T) &\left(\frac{2 B^2 (A + B T)}{cd1 \lambda \rho_s} - \frac{B (A + B T)^2 (2 A c1 + 2 B T c1)}{\lambda \rho_s cd1^2} + \right. \\
&\frac{B^2 (A + B T + sw)}{cd1 \lambda \rho_s} - \frac{B c1 (A + B T)^2 (A + B T + sw)}{\lambda \rho_s cd1^2} + \\
&\frac{(A + B T)^2 (2 A c1 + 2 B T c1)^2 (A + B T + sw)}{\lambda \rho_s cd1^3} - \\
&\left. \frac{2 B (A + B T) (2 A c1 + 2 B T c1) (A + B T + sw)}{\lambda \rho_s cd1^2} \right)
\end{aligned}$$

$$\begin{aligned}
 d \text{Var}(T)/dt = & - \text{cov}(T, \rho_s) \left(\frac{(A + B T)^2 (k_1 + 3 k_2 \rho_s^2) (A + B T + sw)}{cd_1 \lambda^2 \rho_s^2} \right) - \\
 & \text{Var}(T) (A + B T) \left(\frac{2 A B c_2 sw + 3 B c_2 A^2 + 2 c_1 sw A^2}{(\lambda \rho_s cd_1^2)} + \right. \\
 & \left. \frac{2 c_1 A^3 + 3 A T c_2 B^2 - 3 A c_1 B^2 T^2}{(\lambda \rho_s cd_1^2)} - \right. \\
 & \left. \frac{c_1 B^3 T^3}{(\lambda \rho_s cd_1^2)} \right)
 \end{aligned}$$

$$\begin{aligned}
 d \langle \bar{\rho}_s \rangle / dt = & \text{Var}(\rho_s) \left(\frac{0.667 D \text{EXP}(-(T c \rho_s) - k_0 \rho_s)}{nu} - \right. \\
 & \left. \frac{1.33 D k_0 \rho_s \text{EXP}(-(T c \rho_s) - k_0 \rho_s)}{nu} \right) + \\
 & \frac{2 D \text{EXP}(-(T c \rho_s) - k_0 \rho_s) \rho_s^2}{3 nu} + \\
 & \text{Var}(T) \frac{0.33 D \text{EXP}(-(T c \rho_s) - k_0 \rho_s) c \rho_s^2 \rho_s^2}{nu} + \\
 & \text{Var}(\rho_s) \frac{0.33 D \text{EXP}(-(T c \rho_s) - k_0 \rho_s) k_0^2 \rho_s^2}{nu} - \\
 & \text{cov}(T \rho_s) \frac{2 D c \rho_s \rho_s \text{EXP}(-(T c \rho_s) - k_0 \rho_s) (2 - k_0 \rho_s)}{3 nu}
 \end{aligned}$$

$$d \text{Var}(\bar{\rho}_s)/dt = \text{cov}(T, \rho_s) \frac{-4 D c \rho_s \text{EXP}(-(T c \rho_s) - k_0 \rho_s) \rho_s^2}{3 \text{nu}} +$$

$$\text{Var}(\rho_s) \frac{4 D \rho_s \text{EXP}(-(T c \rho_s) - k_0 \rho_s) (2 - k_0 \rho_s)}{3 \text{nu}}$$

$$d \text{Cov}/dt = \text{Var}(T) \frac{-2 D c \rho_s \text{EXP}(-(T c \rho_s) - k_0 \rho_s) \rho_s^2}{3 \text{nu}} +$$

$$\text{Var}(\rho_s) \left(- \frac{k_2 (A + B T)^2 (A + B T + \text{sw})}{c d_1 \lambda^2} - \frac{(A + B T)^2 (A + B T + \text{sw})}{2 c d_1 \lambda \rho_s^2} \right) +$$

$$\text{cov}(T, \rho_s) \left(\frac{4 D \rho_s \text{EXP}(-(T c \rho_s) - k_0 \rho_s)}{3 \text{nu}} -$$

$$\frac{2 D k_0 \text{EXP}(-(T c \rho_s) - k_0 \rho_s) \rho_s^2}{3 \text{nu}} + \frac{B (A + B T)^2}{2 c d_1 \lambda \rho_s} +$$

$$\frac{B (A + B T) (A + B T + \text{sw})}{c d_1 \lambda \rho_s} -$$

$$\frac{(A + B T)^2 (2 A c_1 + 2 B T c_1) (A + B T + \text{sw})}{2 \lambda \rho_s c d_1^2})$$

$$\begin{aligned} \langle Z \rangle &= \text{Var}(\rho_s) \frac{2 \cdot T \cdot k_2}{A + B T} + \frac{2 T (k_1 + k_2 r_o)}{A + B T} + \\ \text{cov} &\left(\frac{-4 B T k_2 r_o}{(A + B T)^2} + \frac{4 k_2 r_o}{A + B T} \right) + \\ 0.5 \text{Var}(T) &\left(\frac{4 B T^2 (k_1 + k_2 r_o^2)}{(A + B T)^3} - \frac{4 B (k_1 + k_2 r_o^2)}{(A + B T)^2} \right) \end{aligned}$$

When the freezing depth takes minimum or maximum value allowable, the mean snow temperature is calculated from (4.20) as we mentioned in Chapter IV. In order to use Newton's method the derivative of $\langle Z \rangle$ with respect to T must be specified:

$$\begin{aligned} \frac{d\langle Z \rangle}{dT} &= \frac{-2 \cdot B T \text{Var}(\rho_s) k_2}{(A + B T)^2} + \frac{2 \cdot \text{Var}(\rho_s) k_2}{A + B T} - \frac{2 B T (k_1 + k_2 r_o)}{(A + B T)^2} + \\ &\frac{2 (k_1 + k_2 r_o^2)}{A + B T} + \text{cov} \left(\frac{8 B^2 T k_2 r_o}{(A + B T)} - \frac{8 B k_2 r_o}{(A + B T)^2} \right) + \\ 0.5 \text{Var}(T) &\left(\frac{-12 B^3 T (k_1 + k_2 r_o^2)}{(A + B T)^4} + \frac{12 B^2 (k_1 + k_2 r_o^2)}{(A + B T)^3} \right) \end{aligned}$$

APPENDIX B

PARAMETER VALUES

The value given to the parameters of the model was related to the conditions existing in Scott Mountain during the period April, 6-19.

1- Emissivity of the snow surface, $\epsilon_s = 0.99$

2- Water content of snow at 0^0 C , $W_0 = 0.10$. This value is suggested by Kondo and Yamazaki (1990).

3- Bulk coefficient for turbulent transfer, $D_h = 0.0030$ and $D_e = 0.0015$ (Gray and Male, 1981)

4- Effective thermal conductivity coefficient, $k_1 = 0.25$ and $k_2 = 25$., values corresponding to De Vaux equation (units: cal/cm h K).

5- Densification coefficient, $\eta_0 = 20 \text{ cm h}$ and $k_0 = 21 \text{ cm}^3/\text{g}$ (Anderson, 1976)

INITIAL VALUES

$$T = -10 \text{ C}$$

$$\text{Var}(T) = 0$$

$$\rho_s = 0.38 \text{ g/cm}^3$$

$$\text{Var}(\rho_s) = 0$$

$$\text{Cov}(\rho_s, T) = 0$$

$$D = 39 \text{ cm}$$

INPUT DATA

The observed data of air temperature, relative humidity, wind speed and incoming solar radiation are presented in the following graphs. Time is expressed in hours since April 6, 1988 at 4 AM.

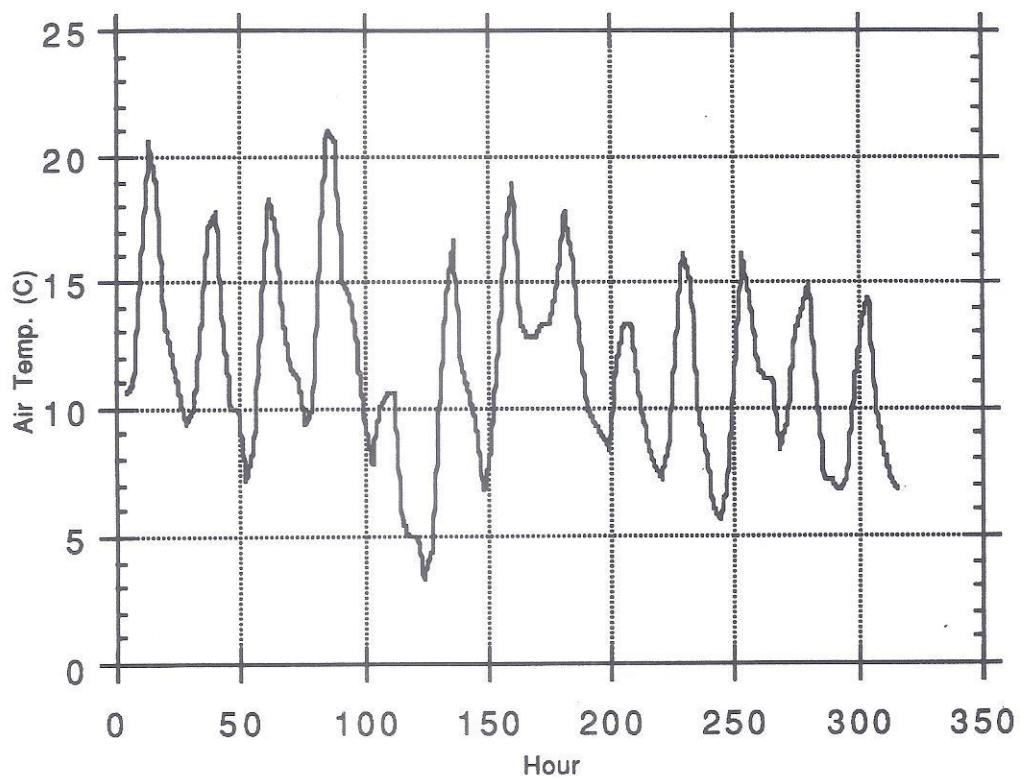


Figure B.1 Scott Mountain observed air temperature.

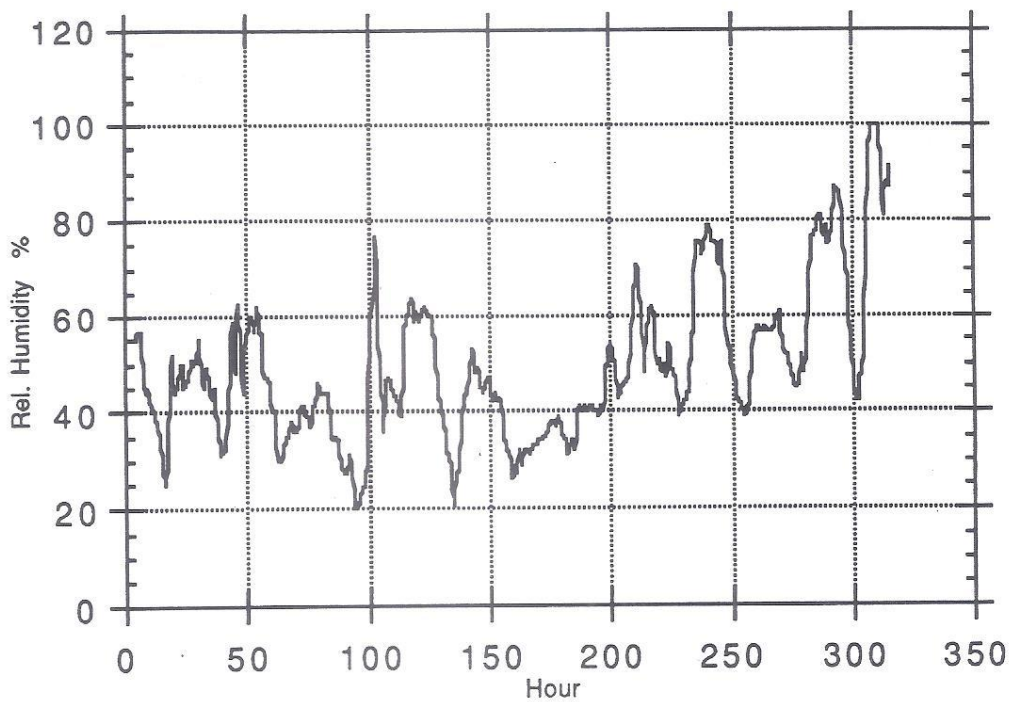


Figure B.2 Relative Humidity used for snowmelt calculation at Scott Mountain, from observation at Collin's Baldy.

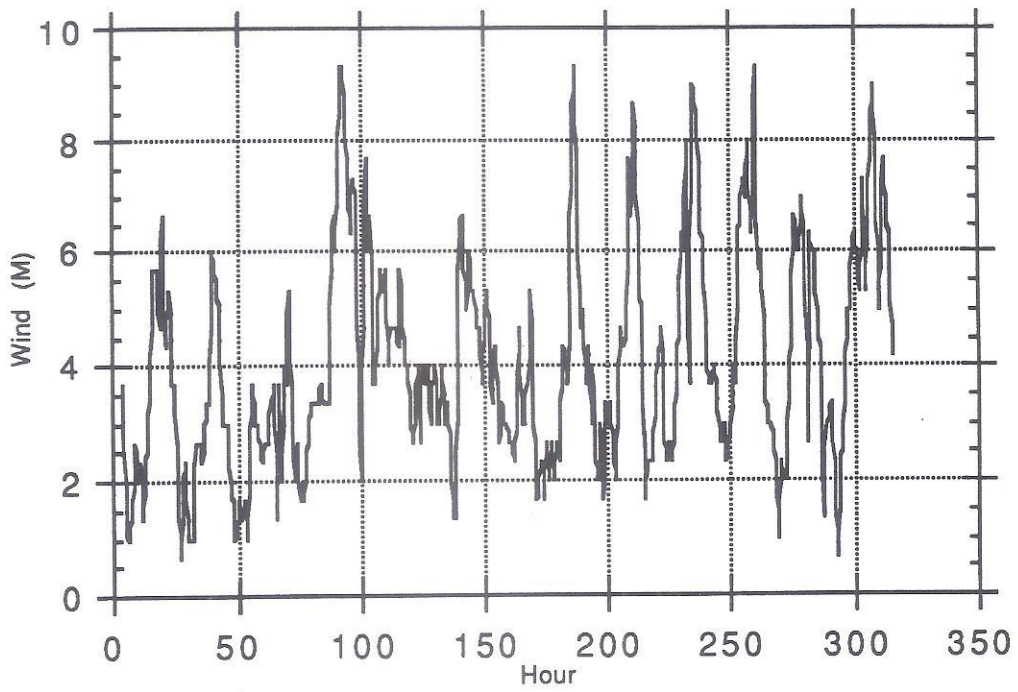


Figure B.3 Hourly average wind speed of values observed at Collin's Baldy, Callahan, and Quartz Hill

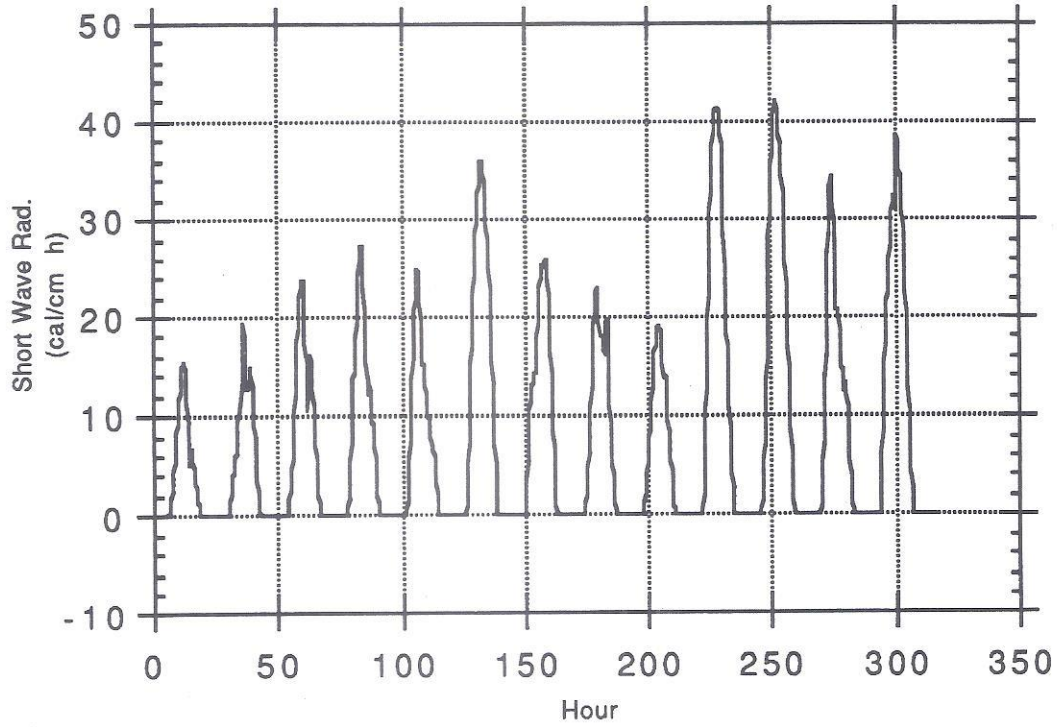


Figure B.4 Short wave incoming radiation based on Red Bluff observations.

APPENDIX C

Figures C.1 and C.2 shows the air temperature and relative humidity used in the Scott Basin snowmelt simulation (case 3). The data of solar radiation and wind speed are the same used in the theoretical case 2, and are displayed in Figure B.4 and B.3 of Appendix B.

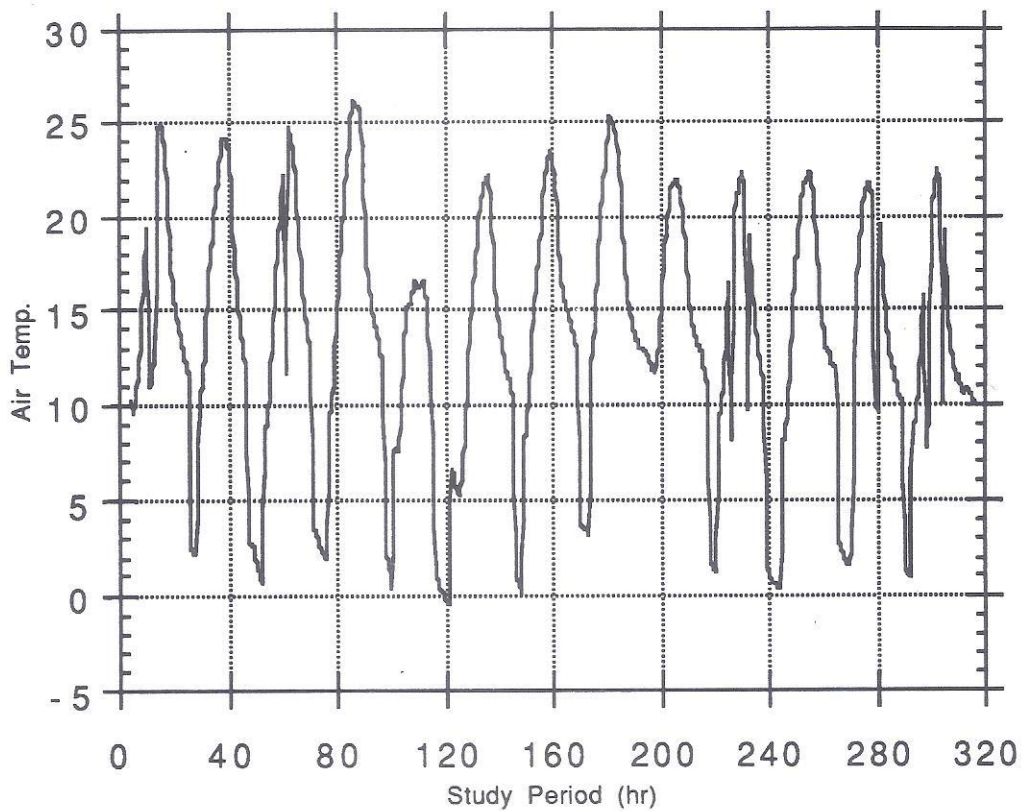


Figure C.1 Averaged air temperature from observations at Callahan, Collin's Balby, Quartz Hill and Scott Mountain, during April 6-19, 1989.

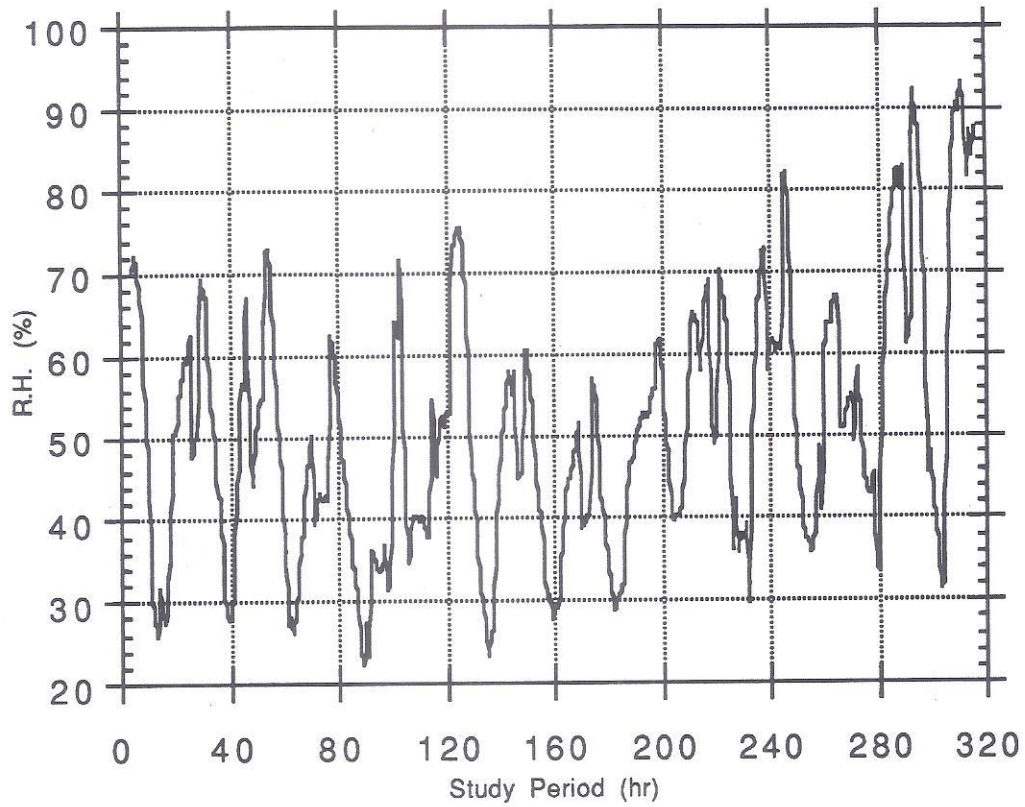


Figure C.2 Averaged relative humidity from observations at Callahan, Collin's Balby, Quartz Hill and Scott Mountain, during April 6-19, 1989.